The Pennsylvania State University

The Graduate School

College of Engineering

# APPLICATIONS OF ASYMMETRIC NANOTEXTURED PARYLENE SURFACE USING ITS WETTING AND TRANSPORT PROPERTIES

A Dissertation in

Engineering Science and Mechanics

by

Koray Sekeroglu



Submitted in Partial Fulfillment

of the Requirements

for the Degree of

Doctor of Philosophy

December 2013

The dissertation of Koray Sekeroglu was reviewed and approved* by the following

Melik C. Demirel
Professor of Engineering Science and Mechanics
Dissertation Adviser
Chair of Committee

Osama O. Awadelkarim
Professor of Engineering Science and Mechanics

Sulin Zhang
Associate Professor of Engineering Science and Mechanics

Aman Haque
Professor of Mechanical and Nuclear Engineering

Judith A. Todd
Professor of Engineering Science and Mechanics
P. B. Breneman Department Head

*Signatures are on file in the Graduate School.

# Abstract

In this thesis, basic digital fluidics devices were introduced using polymeric nanorods (nano-PPX) inspired from nature. Natural inspiration ignited this research by observing butterfly wings, water strider legs, rye grass leaves, and their asymmetric functions. Nano-PPX rods, manufactured by an oblique angle polymerization (OAP) method, are asymmetrically aligned structures that have unidirectional wetting properties. Nano-PPX demonstrates similar functions to the directional textured surfaces of animals and plants in terms of wetting, adhesion, and transport. The water pin-release mechanism on the asymmetric nano-PPX surface with adhesion function provides a great transport property. How the asymmetry causes transport is discussed in terms of hysteresis and interface contact of water droplets. In this study, the transport property of nano-PPX rods is used to guide droplets as well as transporting cargo such as microgels. With the addition of tracks on the nano-PPX rods, the surfaces were transformed into basic digital fluidics devices. The track-assisted nano-PPX has been employed to applications (i.e. sorting, mixing, and carrying cargo particles). Thus, digital fluidics devices fabricated on nano-PPX surface is a promising pathway to assemble microgels in the field of bioengineering.

The characterization of the nano textured surface was completed using methods such as Scanning Electron Microscopy, Atomic Force Microscopy, Contact Angle Goniometry, and Fourier Transform Infra-Red Spectroscopy. These methods helped to understand the physical and chemical properties of nano-PPX. Parameters such as advancing and receding contact angles, nanorod tilt angle, and critical drop volumes were utilized to investigate the anisotropic wetting properties of nano-PPX surface. This investigation explained the directional wetting behavior of the surface as well as approaching new design parameters for adjusting surface

properties. The nanorod tilt angle was a key parameter, thus changing the angle provided the surface with essential wetting properties. This adjustment on the nano-PPX surface exhibited excellent control on water droplet transport as well as guided the droplets from desired points to targets. The results demonstrated that it is possible to create railroad-like paths to manipulate the droplet movements by deforming the nano-PPX surface. Controlling physical properties of the surface granted the inspiration for fabricating basic fluidic devices to sort and mix droplets. These devices are promising for assembly purposes in terms of using microgels in engineering applications (i.e. building blocks for bioengineering). The surface has potential for further development to achieve the directed assembly of microgels into close proximity.

# Table of Contents

# List of figures

# Acknowledgements

I would like to express my deepest appreciation to my advisor, Prof. Melik C. Demirel, for his patience, guidance, and never ending advice during my doctoral studies at The Pennsylvania State University. His motivation and discipline on scientific research will always be a guide for my future career. I am grateful to Dr. Matthew J. Hancock for his essential effort and critics on our research publications and theory discussions. I am indebted to Dr. Niranjan Malvadkar for his insightful advice and endless help with the laboratory experiments.

I would like to thank the committee members, Prof. Osama AwadelKarim, Prof. Sulin Zhang, and Prof. Aman Haque for their valuable reviews and time to improve my thesis. Productive time spent with our research group members will always stay as a memory. Hence, I would like to thank Miguel Santiago Cordoba, Abdon Pena Francesca, Dr. Yusuf Nur and former group members Adem Ozcelik and Dr. Gokhan Demirel for their collaborations.

My wife, my daughter and all my family members deserve my deep appreciation for their endless support, patience, and encouragement during my studies. I would like to acknowledge the financial support from Ministry of Education in Turkey (MEB) and The Pennsylvania State University for making research possible.

# Chapter1. Thesis Overview

## 1.1. Introduction

Biomimicry is to imitate naturally existing materials with their exact forms and functions. From macro to nano scale, the functions of natural materials create promising pathways to establish commercial devices and applications[1]. For instance, hydrophobic and directional nano structures manufactured artificially for self-cleaning applications bioinspired from lotus leaves[2] and butterfly wings[3], are only a few materials out of a myriad of examples in nature. This research begins with natural inspiration and ends with bioinspired simple digital fluidics devices.

The chart in Figure 1-1 explains the path followed throughout the thesis. The path starts with observation in nature. Nature has already built materials in optimized working conditions. We are inspired by nature due to the amazing functionality of materials that help the world population live well. After characterization, making the same materials synthetically (Biomimetics) is one of the inception points of Material Science. The produced synthetic structures from macro to nano scale are tested to demonstrate whether they perform the actual function of natural materials. If the function of the synthetic material is successful, then the work continues on making new devices for application. These devices are used in engineering and medical fields to discover solutions in order to benefit and improve health.

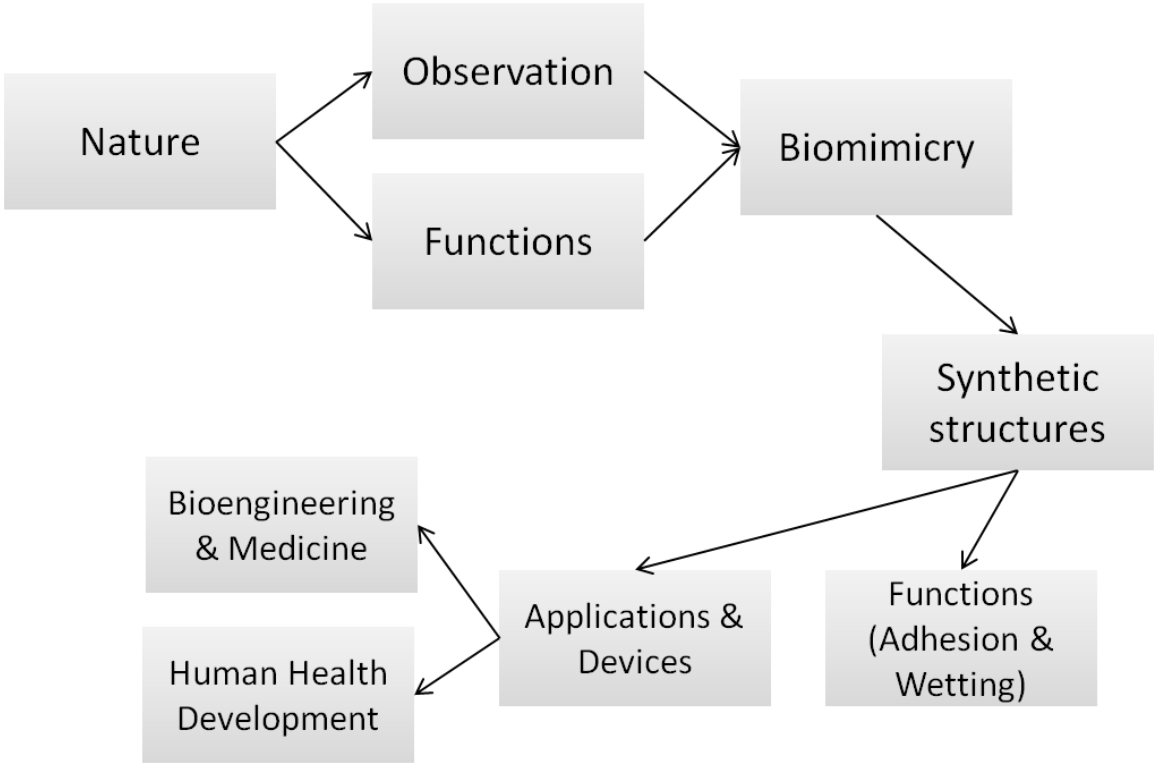


**Figure 1-1.** The thesis path

The scientific question asked in this thesis is “Does asymmetry cause transport”? In other words, this study will investigate the hypothesis which is whether asymmetry in nanoscale provides droplet transport. The importance of studying the nanoscale roughness is due to certain conditions. Nanoscale roughness requires lower energy for transport. Nanoscale surfaces should allow smaller water droplets to be transported as well as keeping droplets in minimum deformation. Biomimicking the natural nanoscale roughness is expected to preserve the wetting and transport functions on the synthetic surfaces.

Biomimicry in nanoscale is achieved by two approaches. One is producing the same structure observed in nature, where the synthesized material preserves its function (e.g., self-cleaning windows inspired by the Lotus leaf[4,5]). The second one is carried out by synthesizing a new material from the observed natural material. In this case, the functions are not exactly preserved, but the application serves the same purpose (e.g., planes inspired by birds).

## 1.2. Anisotropy and Directionality

The direction of asymmetric structures on material surfaces determines their anisotropic physical properties. The anisotropy of the material and its system are identified by various factors. These anisotropic factors are divided into five types, which include structure and geometry, external forces, surface conditions, physical property, and body motion/deformation[6]. Structure and geometry play an important role in anisotropic structures. Glotzer *et al*., reported the significance of anisotropic structures, which include colloidal molecules, geometric shaped blocks, rods, ellipsoids, and patterned particles, in terms of the ability of assembling these building blocks into a complex construction[7]. Daniel *et al*., investigated the importance of external forces applied to a water droplet on a hydrophobic surface. The external force created by applying asymmetric lateral vibrations of the surface caused a unidirectional droplet propulsion[8]. Surface conditions may provide the system with anisotropy even though the material is isotropic[6]. For instance, Malvadkar *et al*., and Sekeroglu *et al*., reported that textured surfaces transport water droplets by vertical vibrations[9,10]. Textured surfaces also spread liquids along the surfaces with no external forces applied[11]. If force is applied to a

material, the response of the material can change at different planes. In other words, if the modulus of the material has internal asymmetry, this may cause anisotropic movements[6]. Lastly, Purcell reported that an anisotropic object with two hinges can be designed to swim in viscous fluid creating asymmetric motions[12].

## 1.3. Directional Surfaces in Nature

Directional surfaces exist in animal and plant kingdoms on micro-scale and nano-scale surfaces. These textured architectures play an essential role for the survival against predators and causes in nature. The directional limbs on water striders[13–16] are built to stay on water and they are able to provide rapid propulsion during a predator attack. Butterflies[3,9,17,18] use their directional textured wings to keep their bodies from getting wet with a pinning-release mechanism. Beetles[19] have directional bristles on their limbs that attach on leaves preventing them from becoming bait. Plants[20–22] use their directional textured surfaces to trap pollen and insects as well as ridding excess water from their leaves. Geckos[23–25] demonstrate an incredible adhesion feature on vertical surfaces using their directional textured feet. They are able to attach and detach their limbs even on smooth surfaces such as glass. Spiders[26] produce an abundant amount of silk and exhibit a water collecting mechanism by a directional ratcheting system.

These textured surfaces such as setae, hairs, bristles, and ratchets obtain their directional features from asymmetric micro and nanostructures. Inspired from these directional structures, engineers have developed numerous amounts of synthetic functional materials. These materials have a variety of functions such as transporting droplets and gels, spreading liquids, stochastic or directed assembly of materials, and creating directional

friction and adhesion. Since the physicochemical properties of these materials are tunable, scientists have managed to produce advanced functional devices using the changeable surface properties. These devices have already been used in a variety of applications in fields such as bioengineering, medicine, and bionanotechnology.

## 1.4. Directional Surfaces in the Animal Kingdom: Dry & Wet Adhesion

Two kinds of adhesion mechanisms of directional surfaces are observed in nature: dry adhesion and wet adhesion. The dry adhesion mechanism broadly exists in the animal kingdom. Some beetles eject a special form of fluid out of their limbs to obtain wet adhesion on surfaces. The beetle, *hemisphaerota cyanea*,[19] activates his tarsal adhesion mechanism to protect his body against predators. Almost 60,000 single bristles are directionally lined up in order to to adhere on smooth and rough substrates. The beetle employs his bristles to defend himself by resisting forces up to 60 times its body weight for about 2 minutes during a predator attack[19].

Hierarchical directional structures observed on gecko feet are formed by single seta hairs. Autumn *et al*., reported the direct adhesive force measurement of a single gecko seta for the first time[25]. Autumn *et al*., discovered that a seta holds on surfaces by Van der Waals forces. The combination of these small forces by approximately half-a-million setae provides the gecko to adhere on any vertical surface[25]. While the gecko easily attaches on surfaces, the detachment happens at a critical angle with a lower force than adhesion due to directionality of the hierarchical structures[24]. The gecko is an animal with the unique

feature which is the ability to adhere to dry and wet surfaces. Stark *et al.*, indicated that gecko feet exhibit significant adhesion when in contact with wet surfaces[27]. Gamble *et al*., mentioned a hypothesis that geckos may have faced the loss of adhesive toepads throughout the evolutionary process. They introduced an investigation about the phylogeny of geckos to reveal the frequency of loss/gain periods of the adhesion feature in the morphologic evolution of the toepads[28].

A common example for wet adhesion is spider silk collecting water droplets through the ratchets[26]. These directional ratchets are made of nanofibers. The directional nanofibers structures are called spindle-knots, where the water drops are collected. The collection of water droplets is powered by gradients in surface energy and Laplace pressure[6,26]. As the condensation occurs, droplets get bigger at the spindle-knots that are easily observed on spider webs by the naked-eye.

Another example for wet adhesion is droplet behavior on butterfly wings. Butterfly wings[3] consist of overlapping aligned nanostripes that are superhydrophobic. A droplet tends to roll off the wing away from the body instead of hitting the body. The water droplet is pinned towards the body but released away from the body. This pinning-release mechanism keeps the butterfly safe during natural causes such as rain and dew.

Similar to water droplets on ratchets, water insects such as water striders[14,15] have directional hairs that are able to stay on water. The hairs at the limbs repel the water strongly due to the surface roughness and the air trapped in between the hairs. This natural construction gives a great ability to the water strider to protect itself from

predators. On the other hand, water striders have a waxy disposal that turns their hydrophobic body into a hydrophilic state, which is useful for leaving eggs inside water.

## 1.5. Directional Surfaces in the Plant Kingdom: Dry & Wet Adhesion

The pitcher plant[21] is the most significant example of directional textured surfaces in the plant kingdom. It has directional ratchets that help to seize insects that are forced to go inside the plant for digestion. The crucial mechanism is provided by anisotropic surface roughness and lubrication on the plant[21,29]. A variety of grass species have directional awns. They employ their directional features to bury and self-seed in the ground. Their directional movement is powered by environment humidity change[30]. Rice leaves[4] and ryegrass leaves[22] are other examples for directional surface roughness in the plant kingdom. Similar to the butterfly, these leaves contain directional textured features on the surface. Water drops shed off the leaves leaving clean leaves behind. These kinds of surfaces have inspired self-propelled and self-cleaning systems in research and industrial areas.

## 1.6. Engineered Synthetic Directional Surfaces

Directional surfaces with micro and nano features have been produced and inspired by nature. Bioinspired surfaces carry out similar textures to their origins. These directional textures have various kinds such as posts, pillars, hairs, rods, lines, ratchets, and fibers in micro and nano scales. These structures can be fabricated using four common methods, including template-free, template assisted, lithography and self-assembly[6]. These methods produce rigid structures (e.g., nano-PPX[31,32]), stimuli-responsive structures (e.g.,

Cilia-like PDMS micro pillars under magnetic field[33]), and self-adapting structures (e.g., superparamagnetic particles assembled using magnetic field[34]), presented in Figure 1-2.

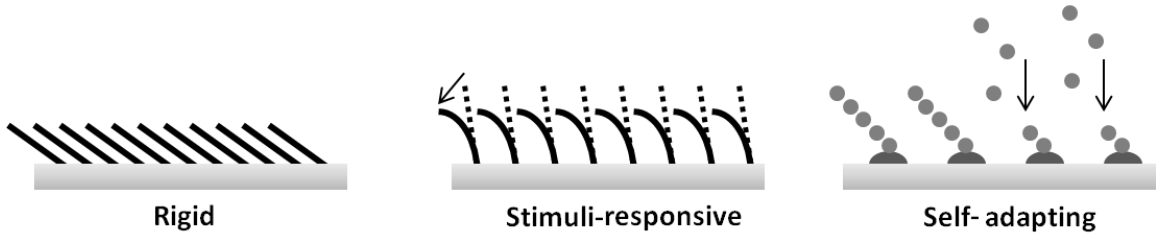


**Figure 1-2.** Directional structures fabricated by template-free, template-assisted, lithography and self assembly methods[35].

Biomimetics is the imitation of natural structures and their functions. The purpose of creating these structures is to benefit from their essential functions. The aim is to replicate functions such as water repellency[36,37], water spreading[11], droplet transports[9,10,38,39], and adhesion[40,41] in devices used in many fields[6].

A number of research groups have created directional surfaces to perform the droplet transport function. First directional droplet transport was achieved by Sandre *et al*., using directional saw-tooth like structures with an applied electric field[42]. Shastry *et al*., and Duncombe *et al*., have created microposts aligned in asymmetric patterns[43,44]. These substrates are able to transport water droplets by mechanical vibrations and electrical oscillations. Linke *et al*., and Lagubeau *et al*., managed to transport droplets and ice on a hot surface with a directional topography. The vapor that gathers underneath the water droplet provides levitation, known as the Leidenfrost effect[45]. Also, the directional ratchets implement directional droplet propulsion[46,47].

Directional wet adhesion is an essential property occurring on synthetically anisotropic surfaces in nano and micro scales. Water droplet retention forces are much greater in nano textured structures than in micro textured structures[6,9]. Demirel *et al*., and Cetinkaya *et al*., reported a unidirectional surface, an array of poly-chloro-p-xylylene nanorods (also known as Parylene, PPX-Cl), that is both hydrophobic and water adhesive. This wet adhesion of the PPX nanorods surface is powered by a ratchet mechanism[31,41,48]. This ratchet mechanism has pinning and release functions. If the substrate is held 90 degrees perpendicular to the ground, the pinning direction will hold a droplet at a critical volume whereas the same amount of water droplet will slide off the release direction. This water droplet behavior is naturally observed in butterfly wings[3] and ryegrass leaves[22]. Sphor *et al*., manufactured a similar directional surface to PPX nanorods using an ion track etching method on polycarbonate substrates followed by hydrophobicity treatment[49].

The liquid spreading function in hydrophilic nanoscale surfaces have been investigated by a number of researchers. This function may be utilized in microfluidic devices, liquid cooling, functional coating, and lubrication applications. Jokinen *et al*., have managed to demonstrate directional wetting on asymmetric SU-8 microstructured pillars[50]. Kim *et al*., manufactured stooped polymeric nanohairs using replica molding and e-beam radiation. They investigated the unidirectional wetting and spreading behavior of water droplets on these slanted nanohairs[51,52]. Chu *et al*., has controlled liquid spreading on nanostructured hydrophilic surfaces. These polymer coated nanopillars at different angles demonstrate an increasing wetting behavior in terms of unidirectional spreading[11].

The gecko's feet demonstrate an essential hierarchical structure that is the initial inspiration for synthetic directional structures for dry adhesion[23,24,53]. These engineering artificial gecko-like structures are used as adhesives in biomedical and robotics fields. Lee *et al*., has demonstrated gecko-like structures fabricated by tilting polypropylene microfibers for directionality and adhesion purposes[54]. The same group also fabricated high density polyethylene lamellar nanofibers arrays with increased adhesion properties[53]. Parness *et al*., created wedge-shaped structures in micro size as a bio-inspired dry adhesive using the dual-angle lithography process[55]. So *et al*., investigated the mechanical anisotropy of nano-PPX rods, produced by the oblique angle deposition method, by performing frictional adhesion experiments[56]. Recently, Jeong *et al*., has fabricated polymeric nanohairs by molding. These slanted hierarchical nanohairs manufactured by simple molding and partial UV curing methods exhibited an excellent dry adhesion similarly to the gecko foot pad[57].

## 1.7. Research Objectives

The inspiration of this thesis was a significant paper published by Boduroglu *et al*., on controlling the adhesion and wetting properties of nano-PPX surfaces[41]. In this paper, it was mentioned that controlling the hydrophobicity and water adhesion of the film surface can lead to coatings similar to natural self-cleaning surfaces. Water droplets on self-cleaning surfaces are transported from one point to another. During this transport, the shape of water droplets has minimal deformation. In other words, the beginning static contact angle of the water droplet remains the same as the end of the transport. Also, several water droplet transport mechanism were reported on micro surfaces[43,46,58] but the

challenge was having a surface that can provide smaller roughness which requires lower vibrational energy for droplet transport. These surfaces will easily transport droplets with small deformation at low frequencies that controls droplets movements. Therefore, water droplet transport on a nano-PPX surface seemed to be feasible due to the wetting and adhesion properties. Directional transport of water droplets on a nano-PPX surface, similar to a self-cleaning surface, can open a pathway to transporting cargo such as microgels in bioengineering and medical fields.

The aims of this thesis include;

i. To investigate directional wetting for transport in microscale.
ii. To manage to directionally move droplets on the nano-PPX surface with minimal drop deformation using frequency vibrations.
iii. To control the velocity and droplet volumes as a function vibrational frequencies as well as transporting soft cargo materials in the droplets.
iv. To manage track fabrication on nano-PPX to eliminate curved surfaces
v. To create more efficient transport pathways on the nano-PPX surface to provide point-to-point delivery of water droplets, specifically to create basic inexpensive devices as a biomedical application.

## 1.8. Thesis Organization

Chapter 2 initially focuses on the manufacturing details of nano-PPX film. Further, characterization methods such as scanning electron microscopy (SEM), atomic force microscopy (AFM), contact angle goniometry (CAG) and Fourier transform infrared spectroscopy (FTIR) are mentioned in terms of their benefit and analysis to explain the nano-PPX surface and its physical and chemical properties. Cross sectional SEM analysis reveals the nano-PPX angle, the diameter and the length of the nanorods as well as the spacing between two single nano-PPX rods. AFM method demonstrates the roughness and the porosity of the nano-PPX surface with high resolution. If the nano-PPX surface is modified, an AFM analysis can easily compares the roughness change. For a quick surface analysis, an AFM is preferred over an SEM due to the easy sample preparation and no vacuum requirement convenience. A CAG is employed to measure static, advanced and receding water contact angles on nano-PPX surfaces for wetting, adhesion, and Co calculations. An FTIR analysis was performed to basically examine the surface chemistry of nano-PPX using bond vibration spectrums.

Chapter 3 mainly discusses directional micro-nano structures observed in nature. These directional structures, which include butterfly wings, water strider limbs, gecko feet, and ryegrass leaves, have essential properties such as directional wetting and transport. This chapter also mentions how PPX nanorods are employed to have similar wetting and transport properties to naturally existing creatures. Further, directional transport is explained and experimented in terms of frequency dependence and droplet speed. Critical drop volumes were analyzed on nano-PPX surface by observing the advanced and

receding contact angle to explain the anisotropic wetting behavior. The pin-release mechanism existing on the nano-PPX surface is very similar to butterfly wings. Moreover, the chapter discusses the unidirectional drop motion on a nano-PPX coated half-pipe surface with control experiments. The directional droplet transport was also used to carry a soft cargo material (e.g. microgel). Water droplets with and without cargo materials were compared in terms of transport at specific vibrational frequencies.

Chapter 4 focuses on investigating the theory behind the directional wetting and transport on PPX nanorods in terms of understanding how the mechanism works. This chapter suggests models of water droplets on nano-PPX rods investigating the advancing and receding contact angles for pin and release directions. Parameters such as advancing, receding contact angles, nanorod diameter, nanorod tilt angle, lateral and longitudinal nanorod spacing are discussed in terms of their affect on retention forces and their explicit equations. Comparison of theoretical model and experimental results are discussed to design new surfaces with enhanced anisotropic wetting behavior for future applications in bioengineering, surface coating and anti-fouling fields.

Chapter 5 starts with background information on the directional water transport mechanisms found in nature and produced synthetically in lab-scale. It explains why nano-PPX is a useful platform for various applications such as droplet transport as well as merging/assembling microgels. Furthermore, the chapter focuses on how to create tracks on nano-PPX surfaces in terms of adjusting nanorod angles by mechanical shear. The new nano-PPX surface with formed tracks exhibits a different wetting behavior than the regular nano-PPX surface in terms of critical drop volume and advancing-receding

contact angles in the pin-release mechanism. The anisotropic wetting function and forming tracks on the nano textured surface are combined into several device applications. These applications are presented in the form of basic inexpensive digital fluidics devices. The aims of these devices are sorting and mixing droplets from initial points to desired targets.

Chapter 6 presents the summary of the thesis with all conclusions that are reached as well as indicating future work.

## References

[1] B. Bhushan, Philosophical Transactions of the Royal Society A-Mathematical Physical And Engineering Sciences **367**, 1445 (2009).

[2] L. Feng, S. Li, Y. Li, H. Li, L. Zhang, J. Zhai, Y. Song, B. Liu, L. Jiang, and D. Zhu, Advanced Materials **14**, 1857 (2002).

[3] Y.M. Zheng, X.F. Gao, and L. Jiang, Soft Matter **3**, 178 (2007).

[4] T.L. Sun, L. Feng, X.F. Gao, and L. Jiang, Accounts of Chemical Research **38**, 644 (2005).

[5] F.G. Wang, S.Y. Song, and J.Y. Zhang, Chemical Communications 4239 (2009).

[6] M.J. Hancock, K. Sekeroglu, and M.C. Demirel, Advanced Materials **22**, 2223 (2012).

[7] S.C. Glotzer and M.J. Solomon, Nature Materials **6**, 557 (2007).

[8] J.E. Longley, E. Dooley, D.M. Givler, W.J. Napier, M.K. Chaudhury, and S. Daniel, Langmuir **28**, 13912 (2012).

[9] N.A. Malvadkar, M.J. Hancock, K. Sekeroglu, W.J. Dressick, and M.C. Demirel, Nature Materials **9**, 1023 (2010).

[10] K. Sekeroglu, U.A. Gurkan, U. Demirci, and M.C. Demirel, Applied Physics Letters **99**, 63703 (2011).

[11] K.-H. Chu, R. Xiao, and E.N. Wang, Nature Materials **9**, 413 (2010).

[12] E.M. Purcell, American Journal of Physics **45**, 3 (1977).

[13] D.L. Hu, B. Chan, and J.W.M. Bush, Nature **424**, 663 (2003).

[14] X. Gao and L. Jiang, Nature **432**, 36 (2004).

[15] P.J. Wei, S.C. Chen, and J.F. Lin, Langmuir **25**, 1526 (2009).

[16] N.M. Andersen and J.T. Polhemus, in *Marine Insects* (North Holland Publ. Co., 1976), pp. 187–224.

[17] Y. Zheng, X. Gao, and L. Jiang, Soft Matter **3**, 178 (2007).

[18] H. Kusumaatmaja and J.M. Yeomans, Soft Matter **5**, 2704 (2009).

[19] T. Eisner and D.J. Aneshansley, Proceedings of the National Academy of Sciences USA **97**, 6568 (2000).

[20] B. Oelschlagel, S. Gorb, S. Wanke, and C. Neinhuis, New Phytologist **184**, 988 (2009).

[21] H.F. Bohn and W. Federle, Proceedings of the National Academy of Sciences USA **101**, 14138 (2004).

[22] P. Guo, Y. Zheng, C. Liu, J. Ju, and L. Jiang, Soft Matter **8**, 1770 (2012).

[23] N.S. Pesika, H.B. Zeng, K. Kristiansen, B.X. Zhao, Y. Tian, K. Autumn, and J. Israelachvili, Journal of Physics: Condensed Matter **21**, 464132 (2009).

[24] K. Autumn, A. Dittmore, D. Santos, M. Spenko, and M. Cutkosky, Journal of Experimental Biology **209**, 3569 (2006).

[25] K. Autumn, M. Sitti, Y.C.A. Liang, A.M. Peattie, W.R. Hansen, S. Sponberg, T.W. Kenny, R. Fearing, J.N. Israelachvili, and R.J. Full, Proceedings of the National Academy of Sciences USA **99**, 12252 (2002).

[26] Y. Zheng, H. Bai, Z. Huang, X. Tian, F.-Q. Nie, Y. Zhao, J. Zhai, and L. Jiang, Nature **463**, 640 (2010).

[27] A.Y. Stark, I. Badge, N.A. Wucinich, T.W. Sullivan, P.H. Niewiarowski, and A. Dhinojwala, Proceedings of the National Academy of Sciences **110**, 6340 (2013).

[28] T. Gamble, E. Greenbaum, T.R. Jackman, A.P. Russell, and A.M. Bauer, PLoS ONE **7**, (2012).

[29] T.-S. Wong, S.H. Kang, S.K.Y. Tang, E.J. Smythe, B.D. Hatton, A. Grinthal, and J. Aizenberg, Nature **477**, 443 (2011).

[30] I.M. Kulić, M. Mani, H. Mohrbach, R. Thaokar, and L. Mahadevan, Proceedings of the Royal Society B: Biological Sciences **276**, 2243 (2009).

[31] M.C. Demirel, S. Boduroglu, M. Cetinkaya, and A. Lakhtakia, Langmuir **23**, 5861 (2007).

[32] M.C. Demirel, Colloids and Surfaces A: Physicochemical and Engineering Aspects **321**, 121 (2008).

[33] B.A. Evans, A.R. Shields, R.L. Carroll, S. Washburn, M.R. Falvo, and R. Superfine, Nano Letters **7**, 1428 (2007).

[34] M. Vilfan, A. Potočnik, B. Kavčič, N. Osterman, I. Poberaj, A. Vilfan, and D. Babič, Proceedings of the National Academy of Sciences **107**, 1844 (2010).

[35] M.J. Hancock and M.C. Demirel, MRS Bulletin **38**, (2013).

[36] M. Callies and D. Quéré, Soft Matter **1**, 55 (2005).

[37] X.-Q. Feng, X. Gao, Z. Wu, L. Jiang, and Q.-S. Zheng, Langmuir **23**, 4892 (2007).

[38] T.A. Duncombe, E.Y. Erdem, A. Shastry, R. Baskaran, and K.F. Boehringer, Advanced Materials **24**, 1545 (2012).

[39] S. Mettu and M.K. Chaudhury, Langmuir **27**, 10327 (2011).

[40] G.E. Fogg, Faraday Discussions of the Chemical Society **3**, 162 (1948).

[41] S. Boduroglu, M. Cetinkaya, W.J. Dressick, A. Singh, and M.C. Demirel, Langmuir **23**, 11391 (2007).

[42] O. Sandre, L. Gorre-Talini, A. Ajdari, J. Prost, and P. Silberzan, Physical Review E **60**, 2964 (1999).

[43] A. Shastry, M.J. Case, and K.F. Böhringer, Langmuir **22**, 6161 (2006).

[44] T.A. Duncombe, J.F. Parsons, and K.F. Böhringer, Langmuir **28**, 13765 (2012).

[45] J.G. Leidenfrost, *De Aquae Communis Nonnullis Qualitatibus Tractatus* (Duisburg, 1756).

[46] H. Linke, B.J. Alemán, L.D. Melling, M.J. Taormina, M.J. Francis, C.C. Dow-Hygelund, V. Narayanan, R.P. Taylor, and A. Stout, Physical Review Letters **96**, 154502 (2006).

[47] G. Lagubeau, M. Le Merrer, C. Clanet, and D. Quéré, Nature Physics **7**, 395 (2011).

[48] M. Cetinkaya, N. Malvadkar, and M.C. Demirel, Journal of Polymer Science Part B-Polymer Physics **46**, 640 (2008).

[49] R. Spohr, G. Sharma, P. Forsberg, M. Karlsson, A. Hallén, and L. Westerberg, Langmuir **26**, 6790 (2010).

[50] V. Jokinen, M. Leinikka, and S. Franssila, Advanced Materials **21**, 4835 (2009).

[51] T.-I. Kim and K.Y. Suh, Soft Matter **5**, 4131 (2009).

[52] M.K. Kwak, H.-E. Jeong, T.-I. Kim, H. Yoon, and K.Y. Suh, Soft Matter **6**, 1849 (2010).

[53] J. Lee, B. Bush, R. Maboudian, and R.S. Fearing, Langmuir The Acs Journal Of Surfaces And Colloids **25**, 12449 (2009).

[54] J. Lee, R.S. Fearing, and K. Komvopoulos, Applied Physics Letters **93**, 191910 (2008).

[55] A. Parness, D. Soto, N. Esparza, N. Gravish, M. Wilkinson, K. Autumn, and M. Cutkosky, Journal of The Royal Society Interface **6**, 1223 (2009).

[56] E. So, M.C. Demirel, and K.J. Wahl, Journal of Physics D: Applied Physics **43**, 45403 (2010).

[57] H.E. Jeong, J.-K. Lee, H.N. Kim, S.H. Moon, and K.Y. Suh, Proceedings of the National Academy of Sciences USA **106**, 5639 (2009).

[58] J. Zhang, Z. Cheng, Y. Zheng, and L. Jiang, Applied Physics Letters **94**, 144104 (2009).

# Chapter2. Materials and Methods

## 2.1. PPX Deposition Types

The parylene deposition process[1] outputs four different structures. These are bulk parylene (also called planar-PPX), helical shaped PPX, concave shaped PPX, and columnar PPX (also called nano-PPX)[2]. Figure 2-1 is the schematic representation of all the PPX types in terms of their final structure depending on their deposition methods.

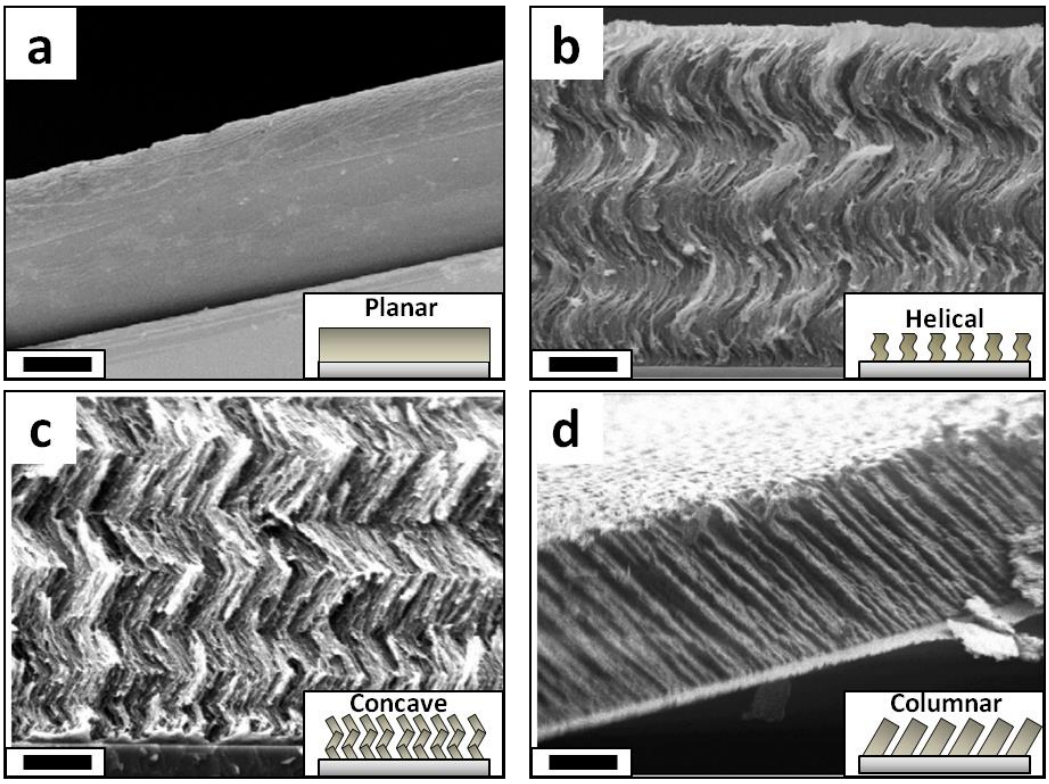


**Figure 2-1.** PPX structure types: a. planar PPX b. helical PPX, concave PPX, and columnar PPX. SEM images are reproduced with permission from Demirel, *Colloids and Surfaces A* **321**, 121-124 (2008) DOI: 10.1016/j.colsurfa.2008.02.028, Copyright 2008 Elsevier.

Planar-PPX (also called thin film parylene) has no texture, which is used in many commercial coating applications for isolation, hydrophobicity, and protection[3]. Planar-PPX may be deposited on any solid surface as a conformal coating. Its deposition thickness is proportional to the amount of dimer introduced before the process.

Columnar PPX (nano-PPX) is deposited with an oblique angle method[4]. The deposition angle is $10^o$. This type of PPX has been used throughout this research and in this thesis. Concave and helical PPX structures are also formed when substrate is placed with the oblique angle method. Yet rotation of the substrate takes place during the deposition process. For helical deposition, the substrate is fully rotated with 1 rpm speed, resulting in a helix structured PPX. For concave deposition, the substrate is rotated $180^o$ in a clockwise direction, then $180^o$ rotated to a counter clockwise direction, or vice versa, at 1rpm speed. The resulting structures are similar to concave shapes[2].

Cetinkaya *et al*., reported that during nano-PPX deposition, the height difference of the growing structures creates a geometric shadowing effect. The mechanism of nano formation during the growth process depends on a power-law, expressed by $d = ch^p$ (where $d$ is the diameter of columns, $h$ is the height of columns, and $c$ and $p$ are constants). The shadowing happens when the columns reach ~ 50 nm in height. Also, the columns expand in width until the film thickness reaches ~ 1 μm[4]. Fortin *et al.*, indicated that physisorption and chemisorption take place during the parylene deposition process. According to their chemisorption model, the growth rate can be predicted as a function of pressure and temperature[5].

## 2.2. Nano-PPX Preparation

All the depositions used in the experiments were performed by a modified parylene deposition unit LABCOATER 2 PDS 2012 (Specialty Coating Systems). The modification was made by adding a nozzle and an angled substrate holder for oblique angled deposition[2,4]. This deposition unit is capable of depositing parylene dimer under *vacuo* onto various substrates such as glass, silicon wafer, polymer surfaces, and metals. The unit contains three main parts, a vaporizer, a furnace, and a deposition chamber (Figure 2-2). A complete deposition process takes 2.5 hours including heating the furnace, heating the vaporizer, polymerization, and cooling all the parts, respectively.

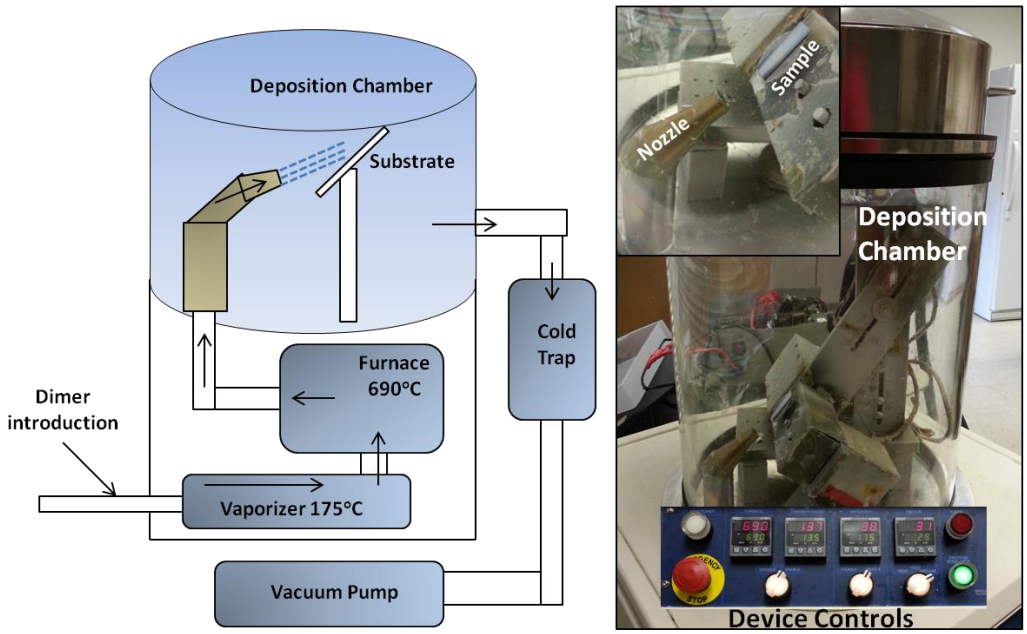


**Figure 2-2.** Schematic and real image of parylene deposition device. Arrows display the paths of the dimer such as going into the vaporizer, furnace, nozzle, bombarding onto the surface, and excess monomers collected by cold trap, respectively.

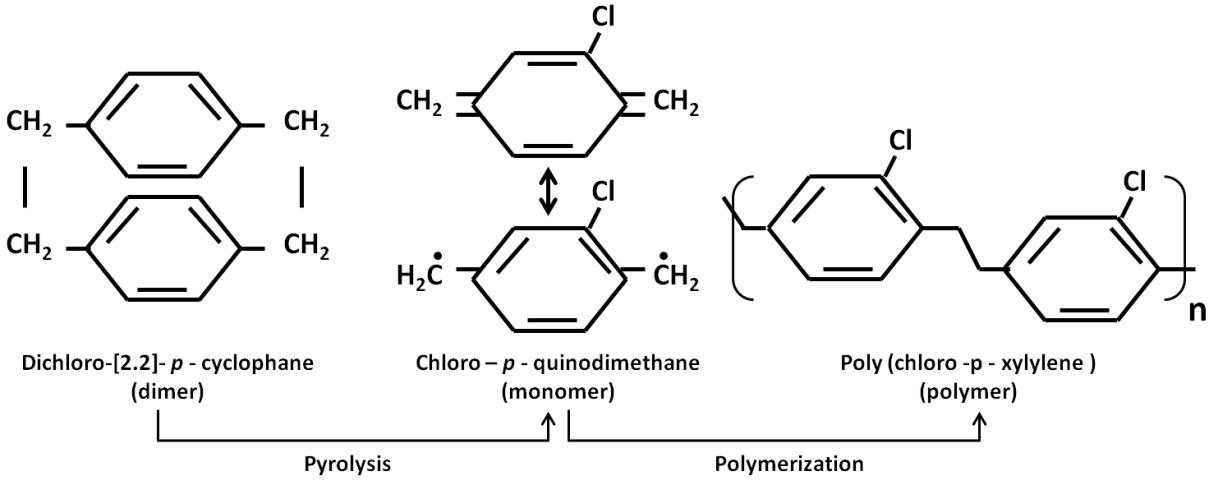


**Figure 2-3.** Parylene deposition process, Pyrolysis (Monomerization of the dimer), Deposition (Polymerization of hot monomers when they hit the surface of the substrate)

The deposition is performed in several steps. The first step is introducing the paracyclophane dimer to the vaporizer. Then, the deposition system goes under vacuum and the furnace is heated gradually ($10^{o}$C/min). When the furnace reaches $690^{o}$C and the vacuum is down to 10 torr, the vaporizer starts to be heated. The parylene dimer evaporates in the vaporizer at $175^{o}$C and flows into the hot furnace. Pyrolysis takes place when the dimer meets the hot furnace, breaking into monomers. Finally, these hot monomers go through the nozzle bombarding the cold surface and polymerize on the substrate. After the system is cooled down and vents, the sample can be collected. The resulting columnar parylene structures are called nano-PPX (Figure 2-4).

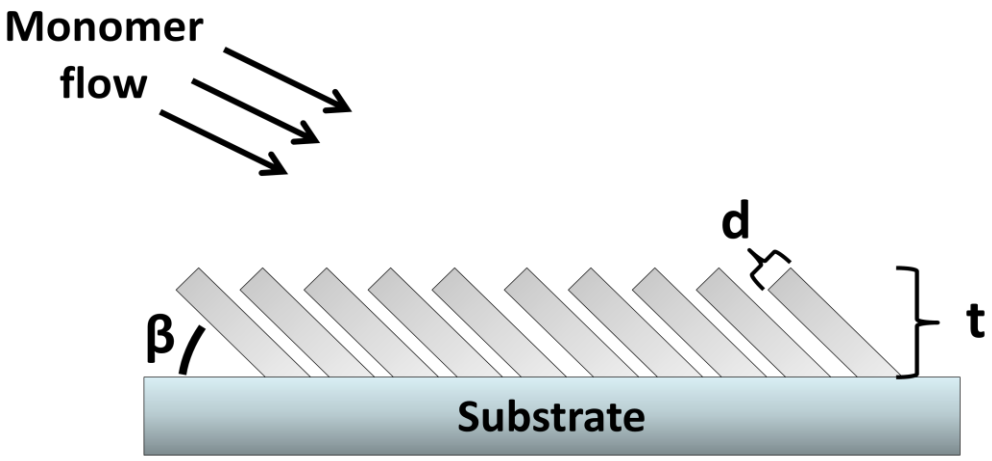


**Figure 2-4.** Schematic of nano-PPX film on substrate after a complete deposition (β = nano-PPX angle, t = nanofilm thickness, d = nanorod diameter)

Several methods were used to characterize and analyze the fundamental properties of nano-PPX. Scanning Electron Microscopy (SEM) was used to image the cross sectional and the top views of all nano-PPX samples. Atomic Force Microscopy (AFM) was used to observe the topographic changes for the nano-PPX and tilted nano-PPX samples. Contact Angle Ganiometry (CAG) was employed to investigate the static contact angle, advancing, and receding contact angles of critical droplet volumes. Fourier Transform Infra-Red Spectrocopy data was collected to show that changing the nano-PPX rod angle on the substrate does not change the surface properties.

## 2.3. Scanning Electron Microscopy

Scanning Electron Microscopy is a well-known technique that is employed to observe materials in high magnification by focused electron bombardment towards surfaces.

Many SEM devices are able to display images at nano scales. Philips XL30 ESEM Scanning Electron Microscope was used for all the SEM images shown throughout the thesis.

The sample preparation is a very essential procedure in order to obtain well-expressed pictures during SEM runs. Samples were placed on an SEM stub using carbon tape and tweezers. Flat SEM stubs were used for top view images and perpendicular plane SEM stubs were used for cross sectional images. Nano-PPX coated samples were cut in liquid nitrogen using a glass cutter for cross-sectional images in SEM. Since nano-PPX is an elastic polymer, cutting the cross section in air will cause excessive bending and necking so that images will not represent the actual cross section of nano-PPX. Figure 2-5 represents a cross sectional image of a nano-PPX surface.

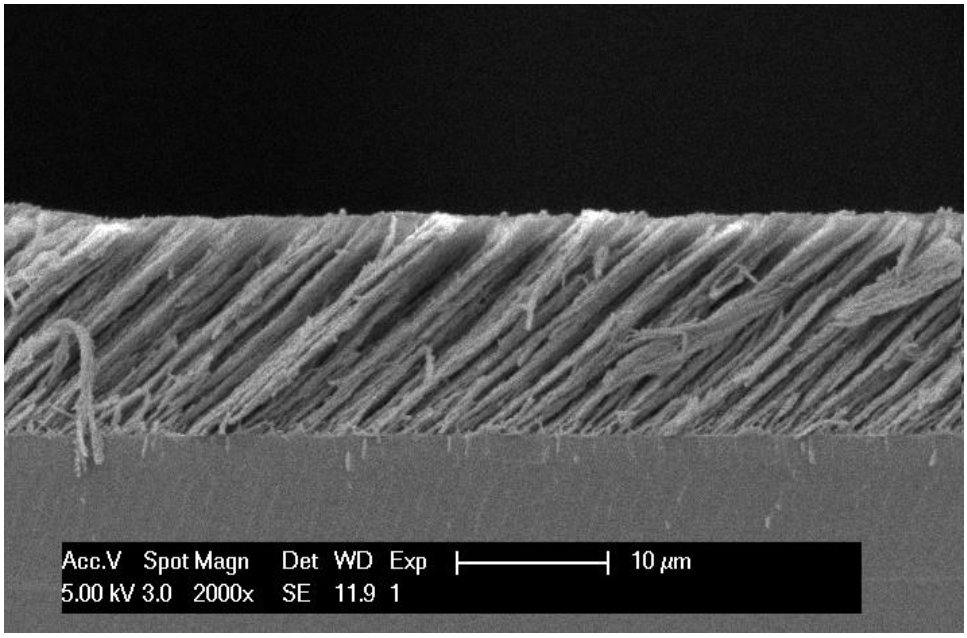


**Figure 2-5.** SEM image of nano-PPX with a 45 degree angle

Polymers face a charging problem when high voltage is applied during the SEM process, which prevents users from obtaining clear images. This problem is solved by coating a thin film layer of gold, platinum, or iridium. All the samples were coated with a 5-10nm thick gold using a plasma vapor deposition device before each SEM analysis. The coated gold layer has an insignificant thickness and does not cause manipulation since nano-PPX rods have 200 nm diameters.

## 2.4. Atomic Force Microscopy

Atomic Force Microscopy (AFM) is a common technique that investigates topographical features of surfaces. AFM does not demonstrate an image as well as a real SEM image, yet AFM easily reaches nanometer scale without having high vacuum conditions. The AFM cantilever has a nano-tip, mostly made of silicon or carbide, which scans the surface with two common techniques such as tapping mode and contact mode. A contact mode AFM device (Veeco – NanoScope E Scanning Probe Microscope Controller) was used for all the AFM images shown throughout the thesis. Figure 2-6 represents an AFM image of nano-PPX surface and its deflection. The ridges in the AFM image are bundling due to capillary forces.

Nano-PPX samples were cut into small pieces and placed on AFM flat stubs. The nano-PPX film surface is adhesive; therefore the AFM cantilever tip may be affected by sticking on the surface. Gold coated nano-PPX surfaces show better image results, providing a non-sticky surface for AFM cantilever tip.

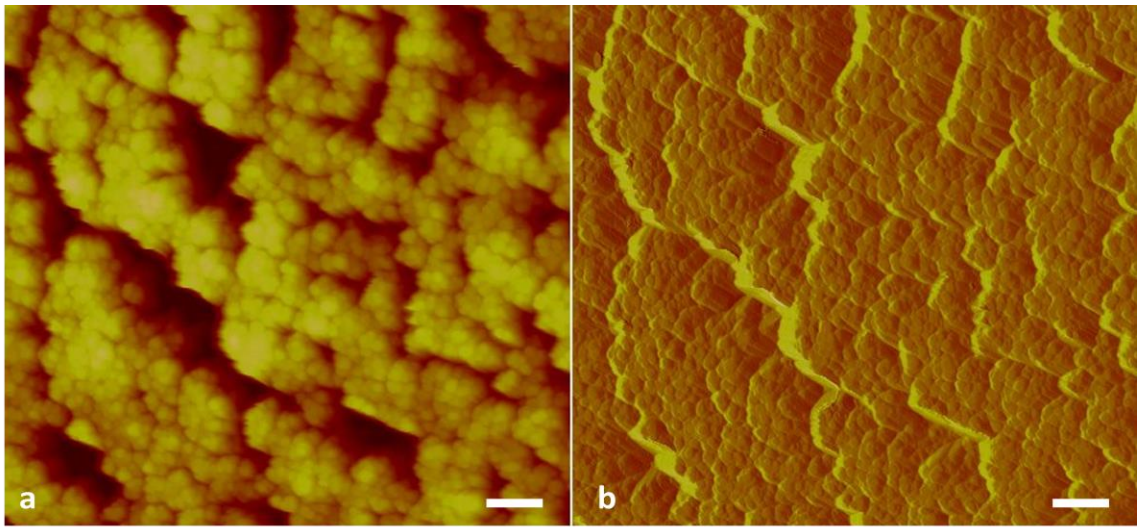


**Figure 2-6.** Topographic AFM images of nano-PPX (Scale: 1µm) b. Deflection image (Scale: 1µm)

## 2.5. Contact Angle Goniometry

Contact Angle Goniometry (CAG) is a device which measures water/liquid contact angles on flat and tilted surfaces using the aid of multiple devices such as a camera, an automated stage, and a volume controlled syringe. A CAG device (DFTA 1000) was used with the First Ten Angstroms software.

In some cases such as tilted surfaces or very large drops (i.e., critical drop volumes), only one side of the three-phase edge is seen. Thus, the software may not be able to measure the contact angle. Figure 2-7 demonstrates the important lines to measure for the water contact angle on nano-PPX surfaces. The base line (straight line) is drawn between the droplet and its reflection on the substrate. The curvature line (dashed line) is drawn

around the water droplet. An extra straight line is drawn where the base and curvature lines intersect. The angle between the baseline and the extra straight line represent the water contact angle.

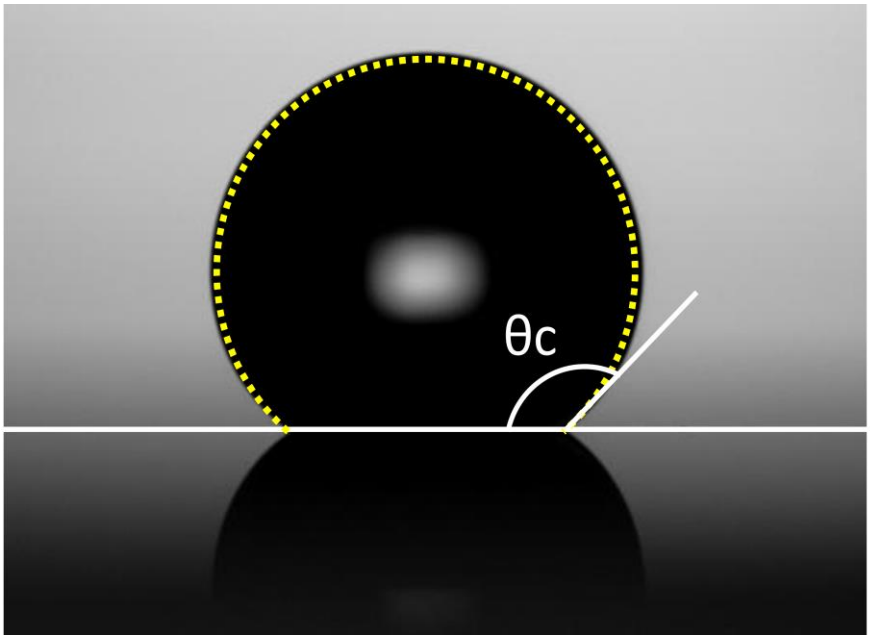


**Figure 2-7.** Contact angle measurement method using border lines

## 2.6. Fourier Transform Infrared Spectroscopy

Fourier Transform Infrared Spectroscopy (FTIR) is a common spectroscopy technique that defines existing bonds on a surface. An FTIR device takes measurements by vibrating bonds by infrared radiation, collecting the data in the defined spectrum, and converting this data into an absorption or transmission plot by mathematical calculations. After the spectrum is obtained, the peaks are identified using the peak library database.

The advantage of FTIR is the ability to find the changes to the surface in terms of new chemical bonds.

## 2.7. Surface Profilometry

Profilometry measurements were performed by using a profilometry device, TENCOR Alpha-Step 500. This device is able to measure nano-PPX film thickness with a diamond stylus tip. Before measurements, a true scratch was made on the nano-PPX surface so that the stylus can scan the area and show the topographic difference between the surface of the nano-PPX and the base substrate. The scanning parameters included a diamond stylus force of 1mg, scan speed of 20µm/s, and sampling rate of 100 Hz. As a result, the nano-PPX thickness was found at approximately 10-20 µm, which matches the cross sectional analysis of the SEM method.

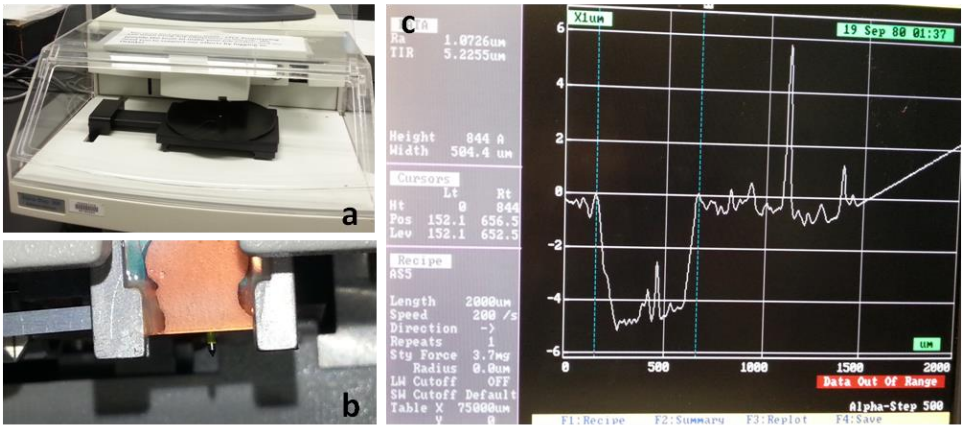


**Figure 2-8.** a. Surface profilometer device, b. Stylus tip, c. A thickness measurement of a nano-PPX surface where plot between the dashed lines is the true scratch on the surface and the height difference between the top and the bottom valley is the thickness of the nano-PPX coating.

## 2.8. Mechanical Oscillator

The PASCO SF 9324 mechanical vibration device was used for all the droplet transport experiments. This device provides frequencies as low as 1 Hz with constant low amplitudes. An amplitude of 0.585 mm was applied for all of the experiments. Nano-PPX surfaces were glued horizontally on the mechanical oscillator.

## 2.9. Video Recording and Image Analysis

All the videos and images were recorded using a digital video camcorder SONY DCRTRV-50. Velocity estimation of water droplets were done by Windows Movie Maker and Image J software.

## 2.10. Microgel Preparation

Microgels were used as cargo materials, which were carried with microliter water droplets on nano-PPX surfaces[6]. Figure 2-9.a shows a schematic representation of the microgel cross-linking setup assisted by photomask and UV light. Figure 2-9.b shows an optical image of microgels. A pre-polymer solution was prepared by mixing 20% poly(ethylene glycol) methacrylate (PEGMA, Sigma) in Dulbecco's phosphate buffer saline (DPBS). This mixture was added to a photo initiator (2-hydroxy-4-(2-hydroxy-ethoxy)-2-methyl-propiophenone (98%, Sigma). The photo initiator was dissolved in the pre-polymer solution using a vortex mixer for 15 minutes. The final solution was placed in between a glass slide and a cover slip by adjusting the height with glass spacers. A photomask was placed on top of the cover slip, where the actual printed side of the photomask is closer to the pre-polymer solution Figure 2-9.c. Having the photomask very

close to the pre-polymer solution prevents the UV light from being scattered during the exposure. UV light (UVP B-100A, wavelength: 365 nm) was exposed on the pre-polymer solution through the photomask for approximately 3 minutes. During the exposure, the UV light and the microgel cross-linking setup were kept in a dark box with a ventilation system. The cover slip was slowly removed off the microgels. The surface was washed with ultrapure water to another container and the microgels were collected using a micro pipette.

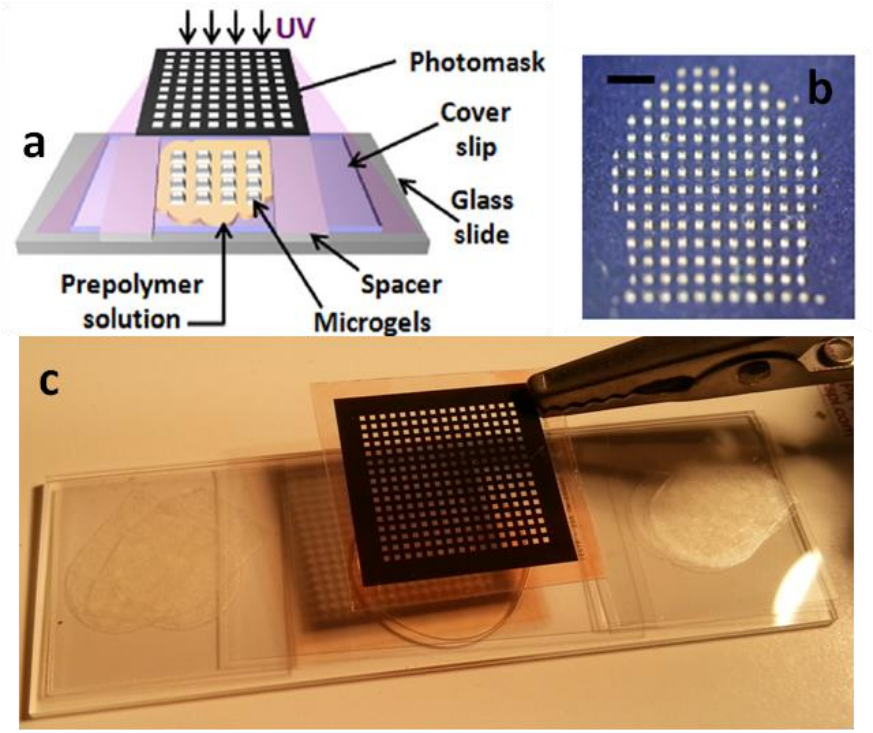


**Figure 2-9.** a. Schematic of microgel fabrication setup using a photomask and UV light, b. Produced microgels (Scale bar: 1mm), c. Real image of microgel fabrication setup. Figures a and b were reproduced with permission from Sekeroglu *et al., Applied Physics Letters* **99**, 063703 (2011) DOI: doi:10.1063/1.3625430. Copyright 2011 American Institute of Physics[6].

## References

[1] M.C. Demirel, S. Boduroglu, M. Cetinkaya, and A. Lakhtakia, Langmuir **23**, 5861 (2007).

[2] M.C. Demirel, Colloids and Surfaces A: Physicochemical and Engineering Aspects **321**, 121 (2008).

[3] N.A. Malvadkar, K. Sekeroglu, W.J. Dressick, and M.C. Demirel, Langmuir **26**, 4382 (2010).

[4] M. Cetinkaya, N. Malvadkar, and M.C. Demirel, Journal of Polymer Science Part B-Polymer Physics **46**, 640 (2008).

[5] J.B. Fortin and T.-M. Lu, Chemistry of Materials **14**, 1945 (2002).

[6] K. Sekeroglu, U.A. Gurkan, U. Demirci, and M.C. Demirel, Applied Physics Letters **99**, 63703 (2011).

# Chapter3. Directional Wetting and Transport

## 3.1. Introduction

The directionality of nanostructures may be considered a physical property of aligned similar structures. Directional nanofilms and nanofibers are well displayed in nature. Butterfly wings[1], water strider legs[2], adhesive gecko feet[3], grass seed, and ryegrass leaves are such great examples from animals and plants. Furthermore, droplet transport mechanisms exist in animal and plant kingdoms. Butterflies directing/shedding water droplets off their wings and ryegrass leaves releasing water droplets unidirectionally are common examples. Inspired from nature, these creatures' limbs/parts have been produced synthetically in lab scale, also known as biomimicry.

The micro-thick directional film that is formed by poly(chloro-p-xylylene) nanorods is an engineered ratchet surface. These ratchets can transport droplets unidirectionally, similar to butterfly wings and ryegrass leaves. The mechanism is built with a pin-release mechanism that guides water droplets directionally. We fabricated these anisotropic polymeric nanorods using oblique angle polymerization technique in *vacuo*. The resulting surface is used to transport water droplets via vertical vibrations of nanofilm coated half-pipes and glass slides at various frequencies. The polymeric surface ratchets are able to move cargo such as microgels, fabricated by photolithography, and encapsulated in water droplets.

## 3.2. Wetting States

Wetting is the ability of a liquid coming in contact with a solid. During the wetting process, liquid spreads on the solid surface competing with air[4]. Therefore, droplets on surfaces have three interfaces: solid-liquid, solid-vapor, and liquid-vapor. Thomas Young was the first scientist to determine these three interfaces in terms of calculating the energy between solid and liquid at a surface[5]. The equation he proposed was:

$$\gamma_{LV}\, cos\theta = \gamma_{SV} - \gamma_{SL} \qquad \text{Eq. 3-1}$$

The interfacial energies such as $\gamma_{LV}$, $\gamma_{SV}$, and $\gamma_{SL}$ are liquid-vapor, solid-vapor, solid-liquid, respectively. They exist at the edge of a liquid drop in contact with solid and air. Figure 3-1 represents the three-phase boundary for interfacial energies.

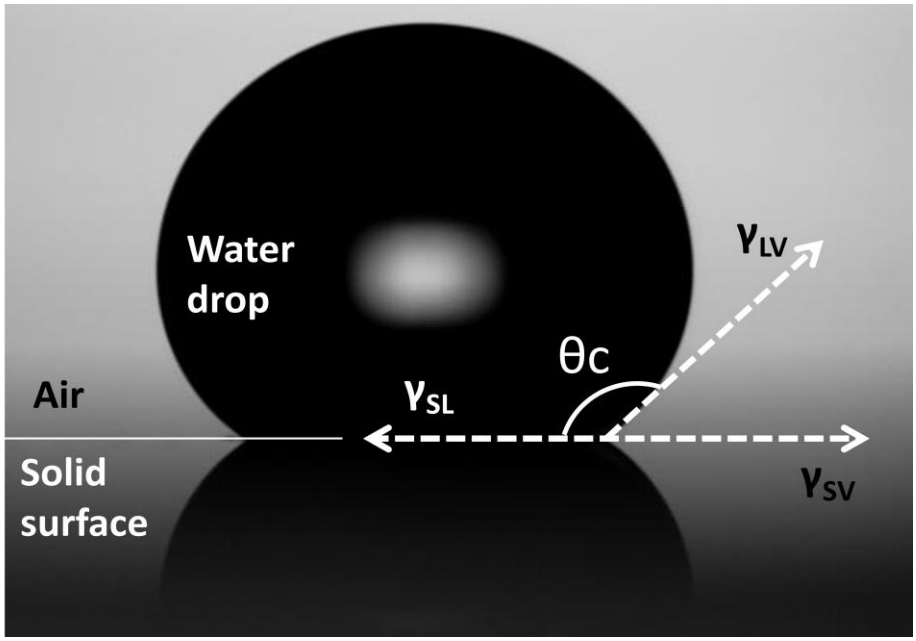


**Figure 3-1**. Air, solid, and liquid interfaces with water contact angle.

The angle between the $\gamma_{LV}$ and $\gamma_{SL}$ is called the contact angle ($\theta$)[5,6]. The contact angle determines how much the solid surface is wetted by the liquid. A contact angle also exhibits the hydrophilicity ($0 < \theta < 90$), hydrophobicity ($0 < \theta < 150$), and the superhydrophobicity ($120 < \theta < 180$) of the surface. Nano-PPX is considered to be in the hydrophobic region, where its surface exhibits a ~120$^{o}$ static contact angle.

There are two common wetting condition models for hydrophobic surfaces that have roughness (i.e., nano-texture, nano-PPX); they include the Wenzel state[7] and the Cassie state[8,9] (also known as Cassie-Baxter), illustrated in Figure 3-2.

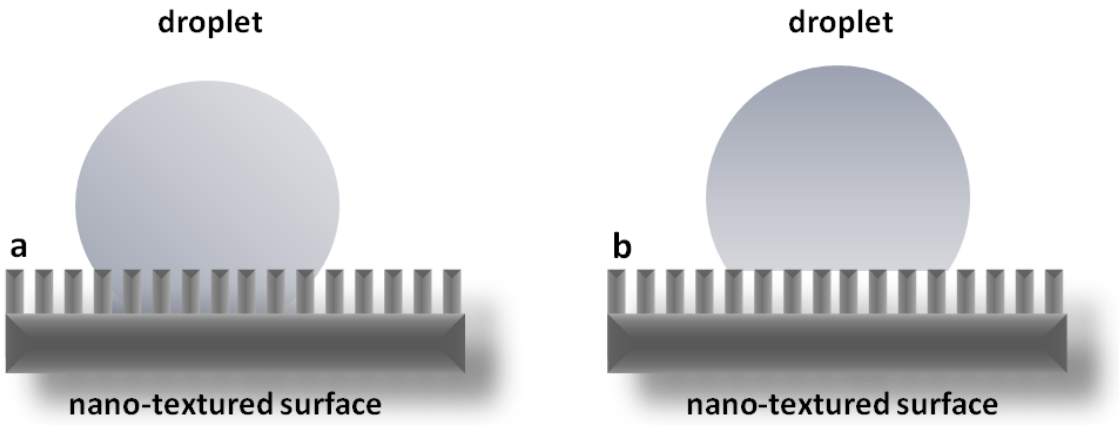


**Figure 3-2**. a. Wenzel Model[7], b. Cassie-Baxter Model[8,9]

If the water drop penetrates in the nano-textured surface, the Wenzel model is considered. On the other hand, if air is trapped in between the water and the solid (nano-textured surface), it is represented by the Cassie-Baxter model[4].

There is also an intermediate state where the water droplet could switch between Wenzel and Cassie states. The water droplet may start with the Cassie state, slowly fill and penetrate inside the nano roughness, and stay at the Wenzel state. This normally happens if the adhesive forces are nearly equal to the hysteresis of water.

## 3.3. Wetting Behavior of Nano-PPX

Water droplets on nano-PPX surfaces mainly exhibit the intermediate state (between Cassie and Wenzel). It is suggested that this behavior is provoked by van der Waals and/or capillary forces acting at the three-phase regions of nano-PPX structures[10].

Nano-PPX exhibits an anisotropic wetting behavior due to the directional geometry of the nano pillars on the substrate. This non-wetting nano surface can hold water droplets up to 10-40 µl even at vertical and inverted positions. Figure 3-3 demonstrates that many water droplets can be pinned on the nano-PPX surface at vertical (substrate is $90^o$ to the ground) positions. The droplets can be placed on the surface while the nano-PPX rods are pointing upward direction, against the ground.

The vertical position, where nanorods pointing down (release position), always carries less amounts of maximum water droplet volume than the vertical position with nanorods pointing up (pin position). This pin-release mechanism demonstrates that the anisotropic wetting behavior is related to the nanorod orientation[11].

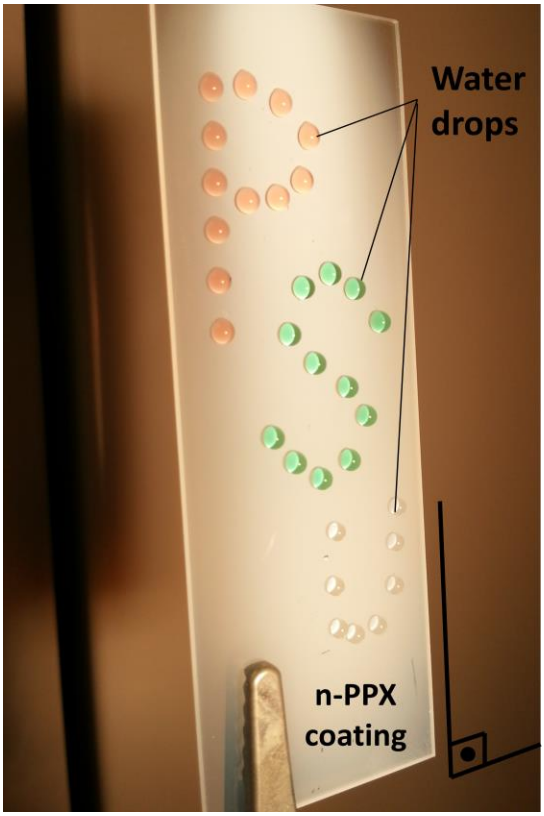


**Figure 3-3**. Water droplets pinned on the vertical nano-PPX coated glass substrate.

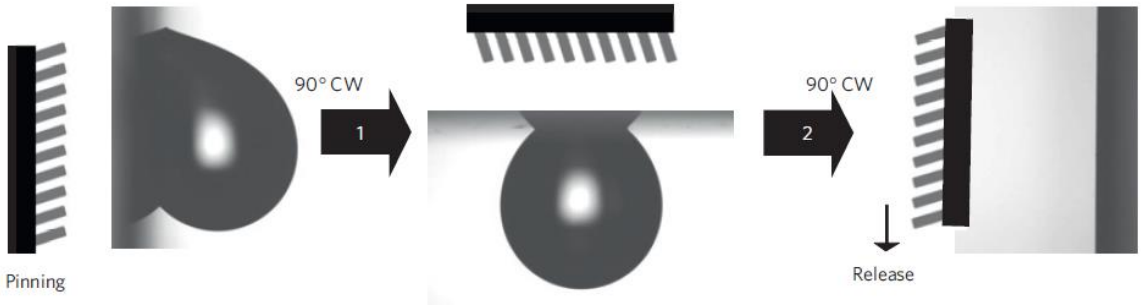


**Figure 3-4.** Three conditions of water on nano-PPX rods, pinned, inverted, and released. Reproduced with permission from Malvadkar *et al.*, *Nature materials* **12**, 1023-1028 (2010) DOI: 10.1038/NMAT2864. Copyright 2010 Macmillan Publishers Limited[11].

## 3.4. Contact Angle Hysteresis

Water droplets may adhere to surfaces that exhibit high contact angles. For instance, butterfly wings, which are superhydrophobic surfaces with contact angles above $150^{o}$, are able to hold water droplets vertically[1]. Nanostructures such as pores and rods can have high contact angles as well as having water adhesion[12,13]. This adhesion on the textured surfaces depends on the pinning of the asperities[14]. During adhesion and pinning, a water droplet is applied a force, which creates a difference in the contact angles. This difference is called contact angle hysteresis with advanced and receding contact angles at solid, liquid, and gas (SLG) interface[15–17]. Figure 3-5 shows the advancing ($\theta a$) and the receding ($\theta r$) contact angles on the nano-PPX surface that has a tilt angle ($\alpha$).

In case of contact angle hysteresis, retention force ($F_r$) occurs as a consequence. This force presents the adhesion force causing the droplets stick to surface[18,19]. It can be calculated by the following equation:

$$FF_r = k\gamma R(cos\Theta_r - \Theta_a) \qquad \text{Eq. 3-2}$$

where k is a pre-factor that is a specific contact line shape, 2R is the drop width, $\Theta_r$ is the receding angle, and $\Theta_a$ is the advanced angle. Contact angle hysteresis may be affected by surface roughness, defects, contamination, and solutes in liquids.

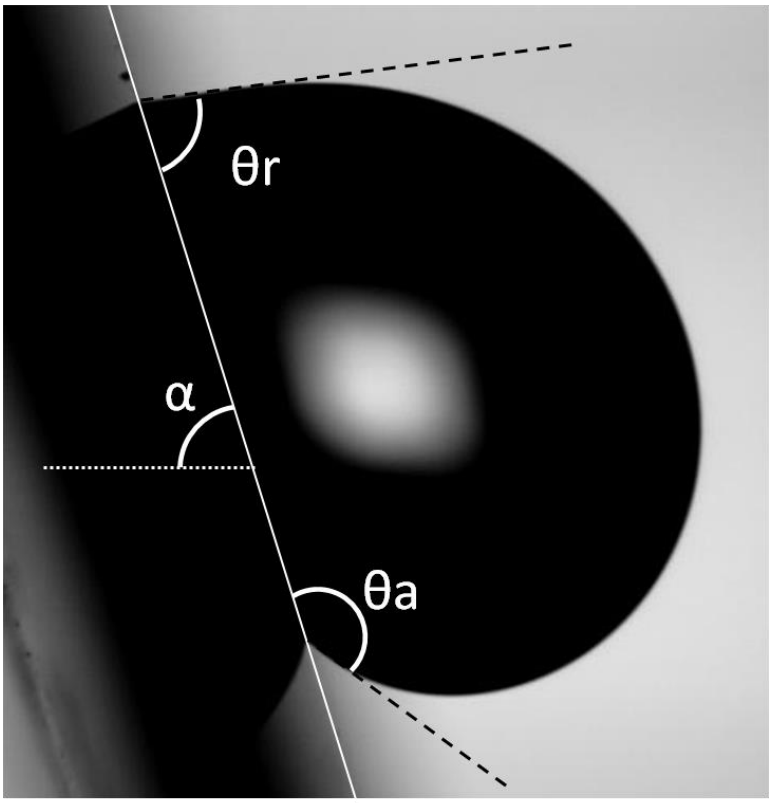


**Figure 3-5.** Sessile drop on nano-PPX surface tilted with an angle ($\alpha$). Advancing and receding contact angles are displayed at the SLG interfaces.

The static load-bearing capability and the stability of a water droplet determine the amount of maximum water droplets that adheres to the inverted nano-PPX surface. The static load-bearing capability number for nano-PPX surface can be approximately calculated with $\sim N\ \pi\ \gamma\ d$, where N is the number of nanorods per unit area (40,000,000/mm$^2$), $\gamma$ is water surface tension, and $d$ is the diameter of nanorods (150-200 nm). The calculated surface tension force for nano-PPX surface is very large, 1N/mm$^2$. Surfaces with smaller asperities are expected to hold bigger water droplets due to N being proportional to $1/d^2$. Consequently, the static load-bearing capacity is inversely proportional to the diameter of nano-PPX rods. Yet, the static load-bearing capability is

decreased due to different conditions exhibited by meniscus stability[20] and contact line[21] at the drop perimeter.

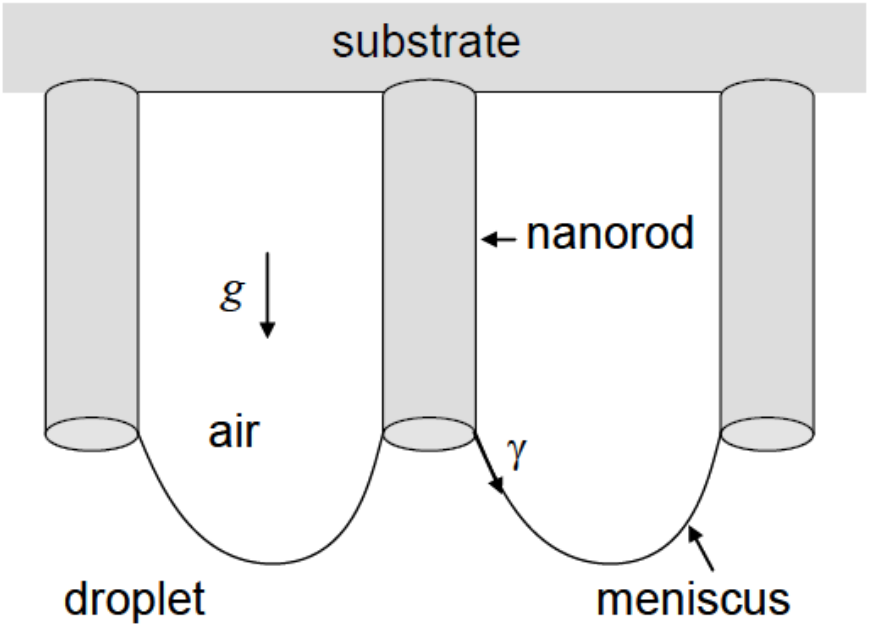


**Figure 3-6.** Droplet-meniscus. Reproduced with permission from Malvadkar *et al.*, *Nature materials* **12**, 1023-1028 (2010) DOI: 10.1038/NMAT2864. Copyright 2010 Macmillan Publishers Limited[11].

Nano-PPX rods are able to hold sessile droplets in the Cassie state on their hydrophobic and adhesive surface. Interregional areas of the hydrophobic nanorods are still penetrated by water with a certain pressure. This pressure can be calculated by γ / nanorod spacing[6]. Critical drop volume (*V*) is the amount of water droplet that can adhere to the nano-PPX surface at a certain angle (α) of the substrate. This represents the anisotropic wetting behavior of a nano-PPX surface, compared with its isotropic directions. The gravitational force has an effect on droplets that are placed on inclined surfaces. This force may be

represented as $F_g = \rho V g sin\alpha$ ($V$: critical drop volume, ρ: water density, g: gravitational force), which is at the opposite direction with retention force ($F_r$). Anisotropic and isotropic wetting data is presented in Figure 3-7. The nano-PPX coated substrate was tilted at angles (α) from 45 to 80 degrees.

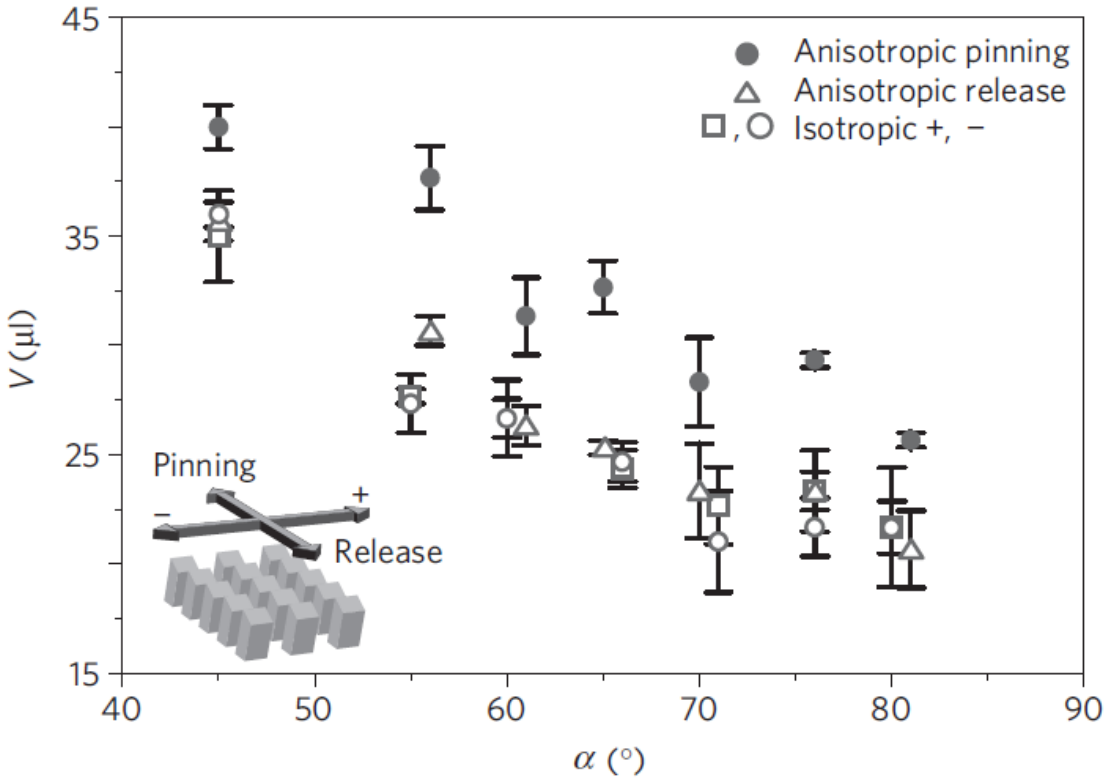


**Figure 3-7.** Critical drop volumes of anisotropic pinning, anisotropic release, and isotropic directions as a function of substrate angle, (inset: pinning, release, +, and – directions). Reproduced with permission from Malvadkar *et al., Nature materials* **12**, 1023-1028 (2010) DOI: 10.1038/NMAT2864. Copyright 2010 Macmillan Publishers Limited[11].

Water droplets were added on the nano-PPX rods with a micro pipette at once. Critical volumes of droplets were found for each angle with all directions such as anisotropic pinning ($V_{PIN}$), anisotropic release ($V_{REL}$), isotropic plus ($V_{ISO+}$), and isotropic minus ($V_{ISO-}$). Critical volume is determined where the gravitational force and retention force are equal, in other words, water droplets have the potential to slide off the surface.

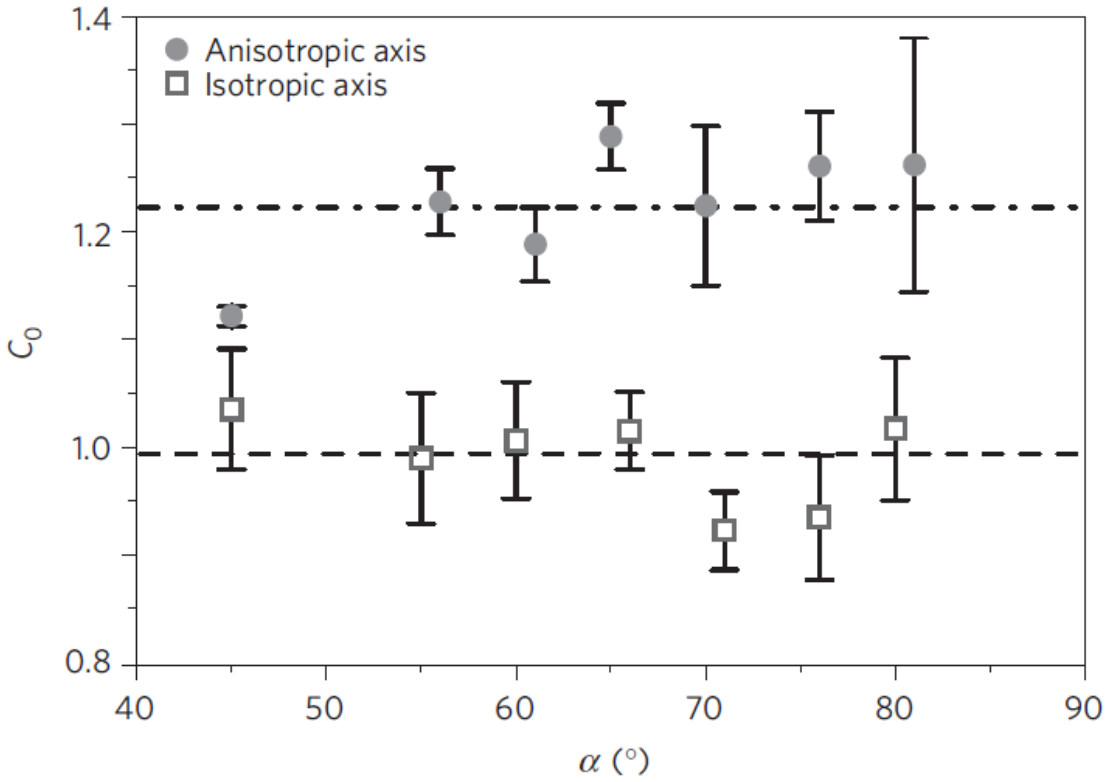


**Figure 3-8.** $V_{PIN}/V_{REL}$ and $V_{ISO+}$ / $V_{ISO-}$ ratios as a function of substrate angle. Reproduced with permission from Malvadkar *et al.*, *Nature materials* **12**, 1023-1028 (2010) DOI: 10.1038/NMAT2864. Copyright 2010 Macmillan Publishers Limited[11].

Figure 3-8 demonstrates that the critical drop volumes at anisotropic pinning case seem to hold more water volumes than the anisotropic release and isotropic cases. Isotropic + and isotropic – conditions have similar results due to having the same geometry in terms of nano-PPX arrays in + and – directions.

In Figure 3-8, the ratio of anisotropic axis volumes ($V_{PIN}/V_{REL}$) displays an average of 1.22 and the ratio isotropic axis volumes ($V_{PIN}/V_{REL}$) shows an average of 0.99. This exhibits that a significant wetting anisotropy is observed for the anisotropic axis of nano-PPX rods. On the contrary, no wetting anisotropy is observed for the isotropic axis.

A quick calculation of the retention force using$F_r = \rho V g sin\alpha$ demonstrates that the difference between the retention forces of pinning and release directions can reach up to 80 μN, which is much greater than the reported values in previous studies for synthetically produced anisotropic surfaces[22].

Figure 3-9 shows the schematic representation of the experimental setup for droplet movements in nano-PPX coated and uncoated half-pipe samples. Both half pipes were attached to the same substrate, which is placed on a mechanical oscillator. The mechanical oscillator provides the surfaces with random vertical vibrations at low amplitudes (~0.5 mm). The uncoated half-pipe was observed as a control experiment.

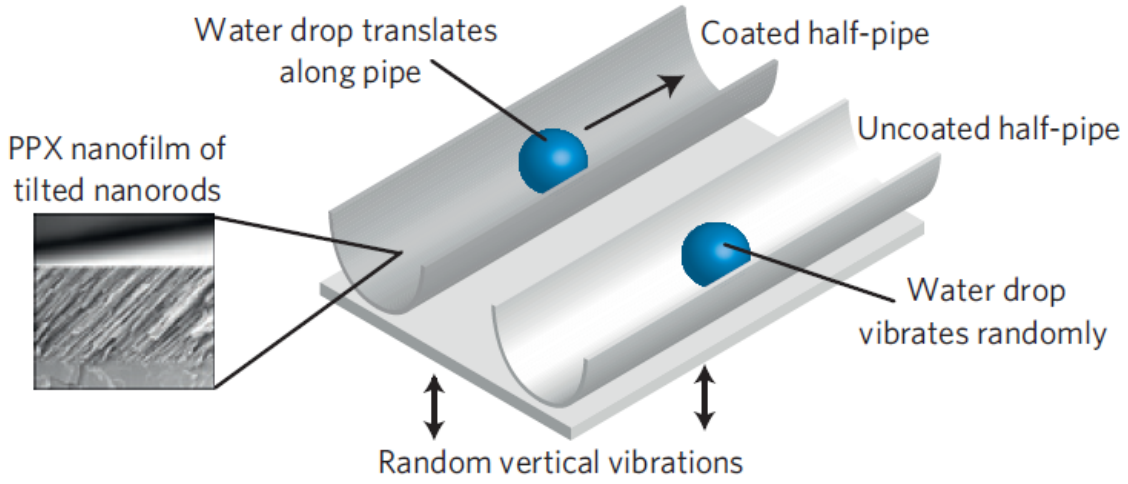


**Figure 3-9.** Experimental setup of water droplet propulsion on nano-PPX coated half-pipe. Reproduced with permission from Malvadkar *et al.*, *Nature materials* **12**, 1023-1028 (2010) DOI: 10.1038/NMAT2864. Copyright 2010 Macmillan Publishers Limited[11].

5 µL drops were placed into half-pipes, shown in Figure 3-10. When vertical vibrations were applied the water droplet on the nano-PPX coated half-pipe immediately started to move, whereas the water droplet on the uncoated half-pipe only vibrated at the same spot.

This experiment exhibited that unidirectional transport of micro liter water droplet can be achieved on a nano scale surface.

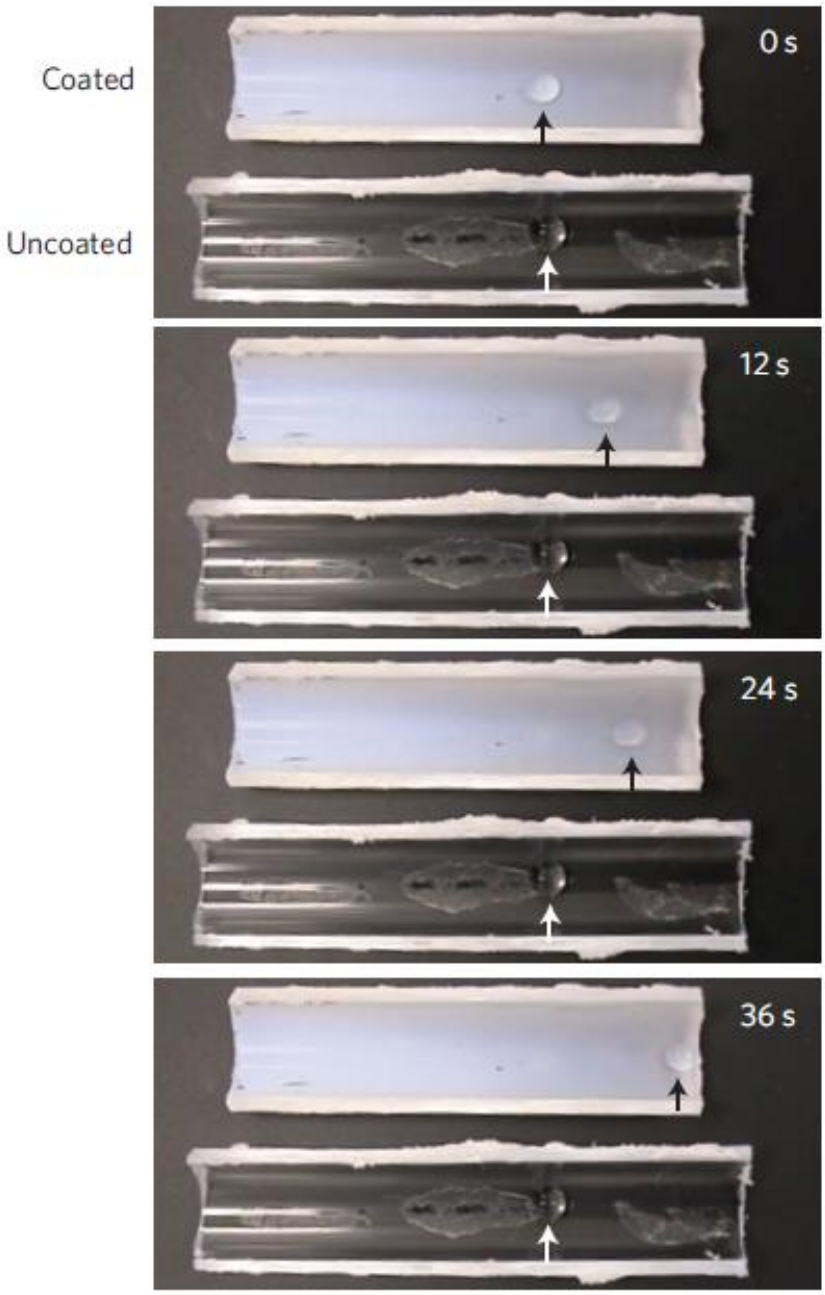


**Figure 3-10.** Droplet motion observation on nano-PPX coated and uncoated (control) half-pipes in time-lapse. Reproduced with permission from Malvadkar *et al.*, *Nature materials* **12**, 1023-1028 (2010) DOI: 10.1038/NMAT2864. Copyright 2010 Macmillan Publishers Limited[11].

## 3.5. Directional Droplet Transport

The anisotropic nano-scale roughness of the nano-PPX rods is the key feature to the directional droplet transport mechanism. The nano-PPX surface features are hydrophobic and adhesive. The propulsion of micro-liter water droplets in a single direction occur due to anisotropic surface roughness. The experimental results were observed in terms of the relation among the water drop volumes, vibration frequency, and water drop speeds. Vibration frequency was found to be inversely proportional to the drop volume, which has top-speed in a specific frequency interval. Ultimately, water encapsulated microgels, coated by planar parylene, are smoothly transported along the nanofilm coated half-pipes. As a result, by controlling physicochemical properties of the nanofilm surface, a directed assembly of soft cargo (i.e., microgels) may be achieved on nanoscale surfaces. Transport water encapsulated microgels holds a great promise for medical and tissue engineering applications.

Different water droplet volumes can be transported on a nano-PPX coated half-pipe. Droplet volumes varying between 2 – 12 µL were experimented on a mechanical oscillator, which the frequency was adjusted with constant low amplitude. Smaller drop volumes were able to move at higher frequencies and bigger drop volumes were able to move at lower frequencies. Figure 3-11 demonstrates the frequency dependence of water droplets on a nano-PPX coated half-pipe surface.

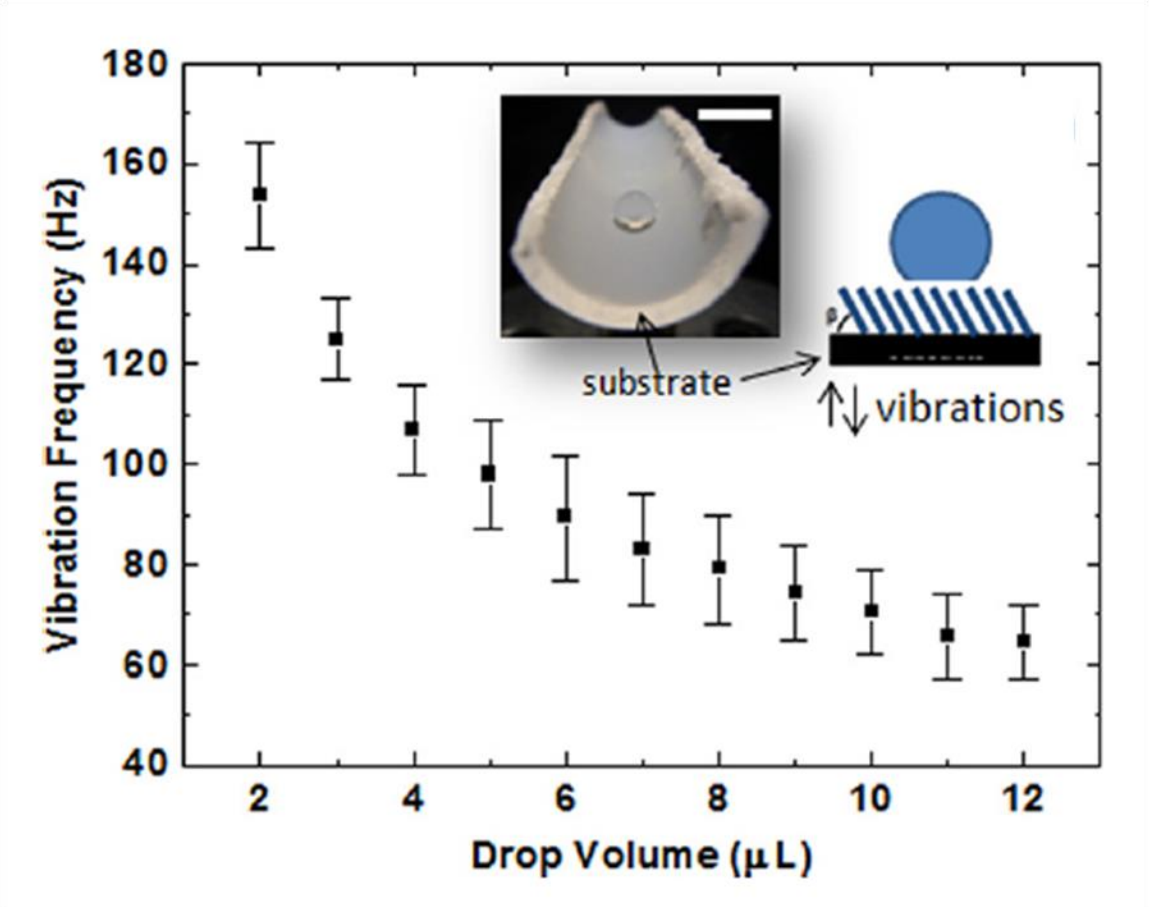


**Figure 3-11.** Vibration frequency dependence of water drop volume. Reproduced with permission from Sekeroglu *et al.*, *Applied Physics Letters* **99**, 063703 (2011) DOI: doi:10.1063/1.3625430. Copyright 2011 American Institute of Physics[23].

These results exhibited that every droplet volume requires a specific frequency interval to be transported on nano textured surfaces[24,25]. Furthermore, the droplet volumes on nano-PPX surface were found to be inversely proportional to the vibrational frequency ($\omega \sim 1/sqrt(V)$). This is supported by Rayleigh's spherical volumes theory[26] and can be

explained with $\omega = (\frac{3\pi\rho V}{8\gamma})^{0.5}$, where γ is surface tension of water and ρ is density of water.

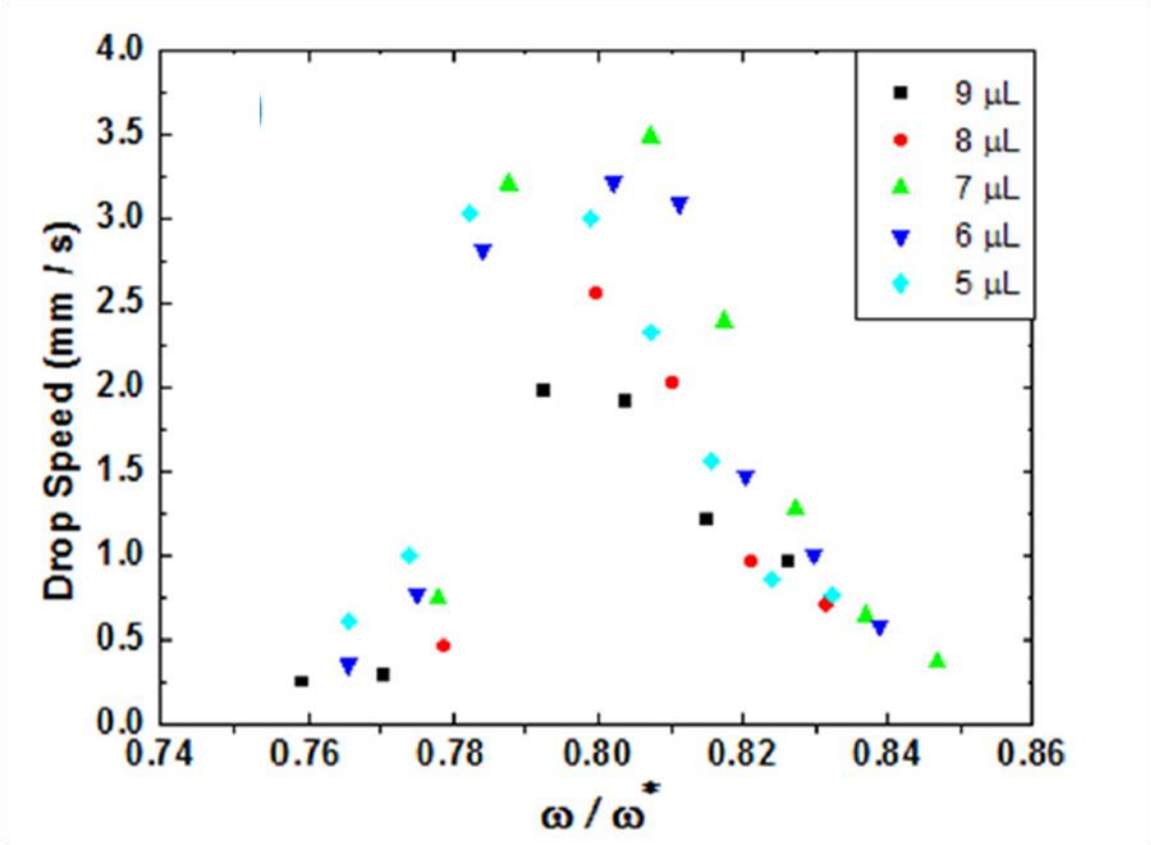


**Figure 3-12.** Droplet speed dependence on normalized vibration frequency that displays overlapping curves for all droplet volumes. Reproduced with permission from Sekeroglu *et al., Applied Physics Letters* **99**, 063703 (2011) DOI: doi:10.1063/1.3625430. Copyright 2011 American Institute of Physics[23].

Figure 3-12 shows drop speed dependence on normalized vibrational frequency. Normalization was done by dividing the vibrational frequency ($\omega$) by $\omega^*$, where $\omega^* = (\gamma/m)^{0.5}$, m is droplet mass, and γ is the surface tension of water. The curves for drop

speeds overlap each other even though the data was collected at different frequencies. This exhibits that these overlapping curves occur due to resonance effects caused by matching the forced vibrations and natural frequencies[27].

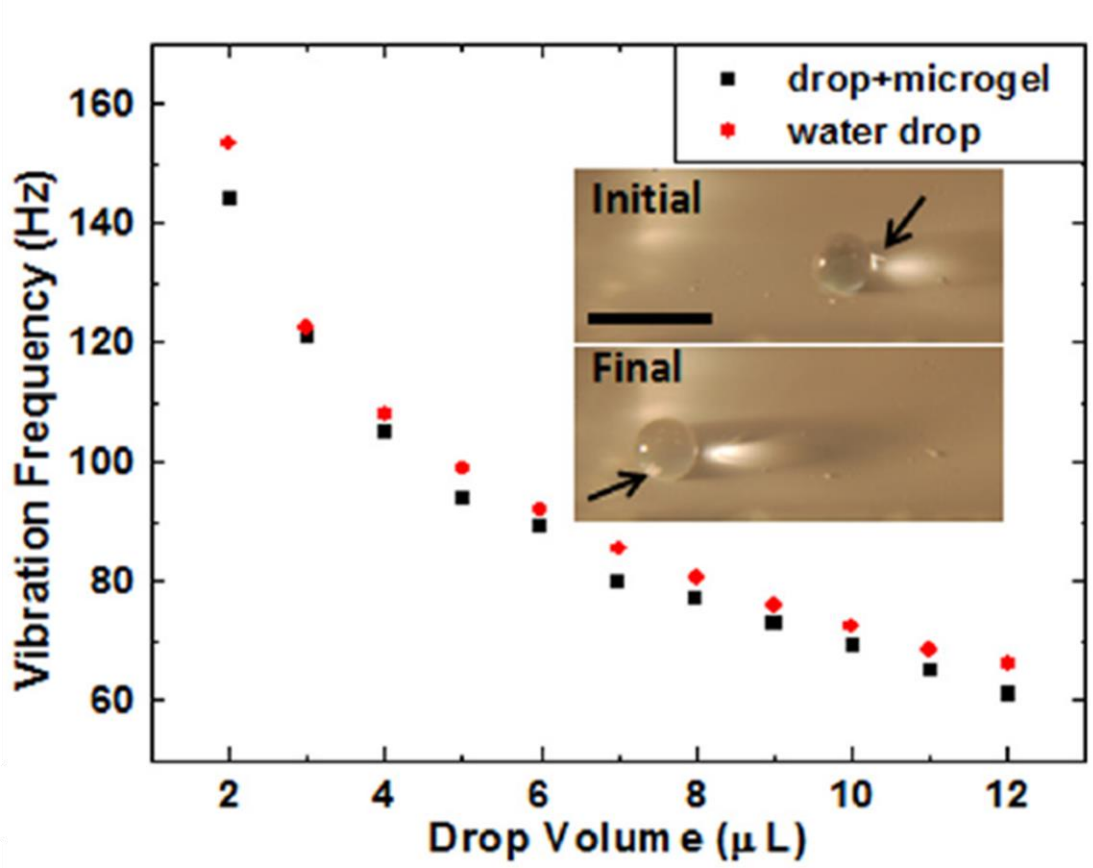


**Figure 3-13**. Comparison of water droplet and droplet encapsulated microgel transport on nano-PPX surface (scale bar: 5 mm). Reproduced with permission from Sekeroglu *et al.*, *Applied Physics Letters* **99**, 063703 (2011) DOI: doi:10.1063/1.3625430. Copyright 2011 American Institute of Physics[23].

The transport of water droplets can be employed to carrying cargo such as microgels. Microgels were prepared in order to experiment the ability of water droplets on a nano-PPX surface whether they can carry cargo materials. The microgel preparation procedure is explained in detail in the Materials and Methods chapter. Before the microgel experiments, the contact angle of water droplets were measured with and without microgel on a nano-PPX surface. The static contact angle of water droplets on a nano-PPX surface is $120^{o} \pm 3^{o}$, whereas the microgel reduces the contact angle of water droplets down to $88^{o} \pm 3^{o}$. This change from hydrophobic to hydrophilic region causes the water to penetrate in between the nanorods.

Therefore, the droplet transport with microgel does not seem to work as well. To overcome this problem, the microgels surfaces were coated with planar-PPX (~5 µm thick) using the parylene deposition system, mentioned in the Materials and Methods chapter. This planar-PPX coating makes the surface of the microgels hydrophobic. This prevents the microgels from sticking on the nano-PPX surface, while allowing the droplets to move[23].

A single microgel (500 $\mu m^3$) was placed into a 5 µl water droplet on a nano-PPX coated half-pipe surface (inset image in Figure 3-13) and the water encapsulated microgel was transported unidirectionally at 95 Hz frequency. Similar experiments were repeated for water droplets from 2 µl to 12 µl at their related frequencies. According to the results shown in Figure 3-13, water droplets encapsulated microgels exhibit similar transport behavior to water droplets in terms of required vibrational frequency (average) on the nano textured surface[23].

As the next step, multiple microgel particles were experimented on for merging and assembly purposes on nano-PPX coated half-pipe surfaces. In this case, two parallel experiments were performed as a sequential drop transport process (Figure 3-14). The first experiment has four water droplets aligned on nano-PPX surfaces that are approximately 2 - 3mm apart from each other (Figure 3-14.a). The first droplet on the right is 4 µL and the others are 2 µL each. This setup provides only one drop transport at a time. At 95 Hz frequency, the 4 µL droplet starts to move toward the next droplet. It merges with the next droplet becoming 6 µL. The frequency is dropped down to 85 Hz; therefore the 6 µL droplet starts to move towards the next one. As the droplets merge and get larger, the frequency required is dropped in order to provide transport.

The second experiment (Figure 3-14.b) was setup similar to the first one. In the second experiment, the microgels (500 um3) were added to the droplets using a micropipette before the sequential droplet transport started. The same frequencies were applied to the nano textured surface. As a result, microgels were merged into a single droplet indicating a stochastic assembly of microgels.

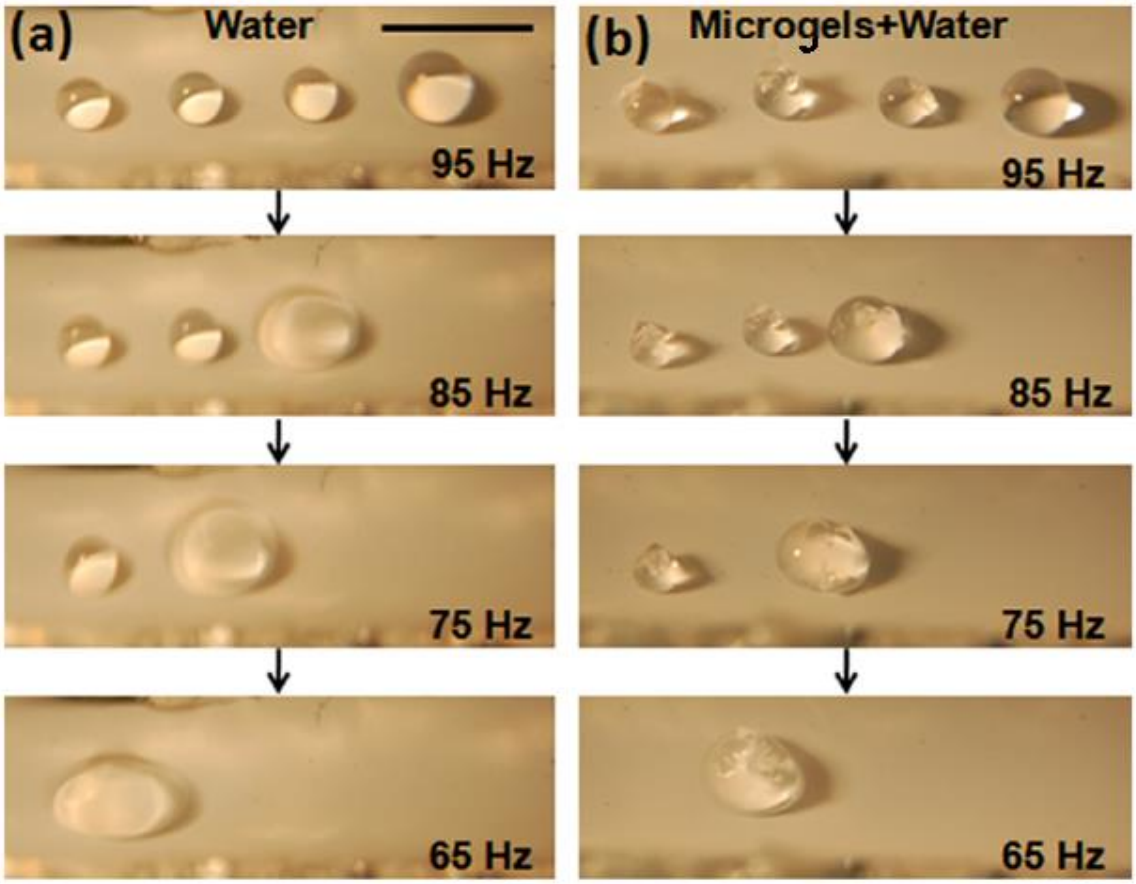


**Figure 3-14**. a. Merging droplets into a single drop. b. Merging multiple microgels into a single drop via droplet transport. Reproduced with permission from Sekeroglu *et al.*, *Applied Physics Letters* **99**, 063703 (2011) DOI: doi:10.1063/1.3625430. Copyright 2011 American Institute of Physics[23].

## 3.6. What Causes Anisotropy on the Nano-PPX Surface?

The water droplets on the nano-PPX are transported due to the surface anisotropy. It is beneficial to explain what causes the anisotropy, which is related to the hypothesis in this study. The anisotropy can be affected by either mechanical or interface contact.

Therefore, if the nano-PPX rods were rigid rather, would they still have the same transport properties? To answer this question, we performed an experiment by coating the nano-PPX surface (hydrophobic) with a thin gold layer (10-15nm). Gold coated nano-PPX composite film became more rigid in terms of elasticity of modulus. On the other hand, the gold coating changes the surface properties by making the surface hydrophilic. Fluorosilane was deposited on the surface to make the surface hydrophobic. The new surface (nano-PPX + gold layer) was tested with a 5 μL water droplet at 95 Hz frequency. Transport of the droplet was observed on the new surface, which is similar to bare nano-PPX surface. This suggests that the anisotropy is dominantly caused by interface contact rather than a mechanical effect.

## 3.7. Summary

In this chapter, the engineered nano textured surface (nano-PPX) was explored in terms of its wetting, adhesion, and transport properties. The nano-PPX surface has a pin-release ratchet mechanism for water droplets, which is derived from its nanoscale roughness. The nano-PPX ratchets, produced by Oblique Angled Polymerization (OAP) technique, have 80 μN differences between the pinning and release directions in terms of droplet retention forces[11]. The anisotropic structures on the surface have the ability to transport micro liter water droplets in one direction. This chapter also indicates that the droplets transport mechanism can be optimized by vibrational frequencies. Various droplet volumes can propel with vertical vibrations at frequency intervals. Furthermore, the water droplets can transport cargo materials (i.e., microgels) unidirectionally[23]. The ability of moving

various water droplet volumes at different frequencies is the key point to merge/assemble sequential drops into a single media as well as bringing microgels into close proximity.

This research is promising to overcome essential challenges such as assembly of microgels, bringing them into close proximity on nano textured platforms, and achieving assembly of three dimensional structures. The nano-PPX with unidirectional wetting property may be used for bio-architecture, digital fluidics, and anti-fouling surfaces in bioengineering and medicine fields[11,23].

## References

[1] Y.M. Zheng, X.F. Gao, and L. Jiang, Soft Matter **3**, 178 (2007).

[2] X. Gao and L. Jiang, Nature **432**, 36 (2004).

[3] K. Autumn, M. Sitti, Y.C.A. Liang, A.M. Peattie, W.R. Hansen, S. Sponberg, T.W. Kenny, R. Fearing, J.N. Israelachvili, and R.J. Full, Proceedings of the National Academy of Sciences USA **99**, 12252 (2002).

[4] A. Marmur, Soft Matter **9**, 7900 (2013).

[5] T. Young, Philosophical Transactions of the Royal Society of London A **95**, 65 (1805).

[6] D. Quéré, Annual Reviews of Materials Research **38**, 16.1 (2008).

[7] R.N. Wenzel, Industrial and Engineering Chemistry **28**, 988 (1936).

[8] A.B.D. Cassie and S. Baxter, Transactions of the Faraday Society **40**, 546 (1944).

[9] A.B.D. Cassie, Discussions of the Faraday Society **3**, 11 (1948).

[10] S. Boduroglu, M. Cetinkaya, W.J. Dressick, A. Singh, and M.C. Demirel, Langmuir **23**, 11391 (2007).

[11] N.A. Malvadkar, M.J. Hancock, K. Sekeroglu, W.J. Dressick, and M.C. Demirel, Nature Materials **9**, 1023 (2010).

[12] W. Lee, B.G. Park, D.H. Kim, D.J. Ahn, Y. Park, S.H. Lee, and K.B. Lee, Langmuir **26**, 1412 (2010).

[13] Z. Cheng, J. Gao, and L. Jiang, Langmuir **26**, 8233 (2010).

[14] D. Quéré, Annual Review of Materials Research **38**, 71 (2008).

[15] P.-G. de Gennes, F. Brochard-Wyart, and D. Quéré, *Capillarity and Wetting Phenomenon. Drops, Bubbles, Pearls, Waves.* (Springer, New York, USA, 2004), pp. 50–51.

[16] P.G. de Gennes, F. Brochard-Wyart, and D. Quéré, *Capillarity and Wetting Phenomenon. Drops, Bubbles, Pearls, Waves.* (Springer, Berlin, 2003).

[17] L. Gao and T.J. McCarthy, Langmuir **22**, 6234 (2006).

[18] E.B. Dussan V and R. Tao-Ping Chow, Journal of Fluid Mechanics **137**, 1 (1983).

[19] C.W. Extrand and Y. Kumagai, Journal of Colloid and Interface Science **170**, 515 (1995).

[20] D.H. Michael, Annual Review of Fluid Mechanics **13**, 189 (1981).

[21] L. Gao and T.J. McCarthy, Langmuir **25**, 14105 (2009).

[22] J. Zhang, Z. Cheng, Y. Zheng, and L. Jiang, Applied Physics Letters **94**, 144104 (2009).

[23] K. Sekeroglu, U.A. Gurkan, U. Demirci, and M.C. Demirel, Applied Physics Letters **99**, 63703 (2011).

[24] S. Dorbolo, D. Terwagne, N. Vandewalle, and T. Gilet, New Journal of Physics **10**, 113021 (2008).

[25] S. Courty, G. Lagubeau, and T. Tixier, Physical Review E **73**, 45301 (2006).

[26] J.W. Strutt and Lord Rayleigh, Trudy Moskovskogo Matematicheskogo Obshchestva 4 (1879).

[27] S. Daniel, M.K. Chaudhury, and P.G. de Gennes, Langmuir **21**, 4240 (2005).

# Chapter4. Theory

## 4.1. Introduction

Anisotropic wetting is an essential feature that nano-PPX surface exhibits when interacting with water droplets. This anisotropic wetting response may be explained theoretically by forming a basic ratcheting model for the nano-PPX rods. The theoretical model have parameters such as drop retention force, advancing contact angle, and receding contact angle, represented in Figure 4-1. In this theory, the anisotropic wetting behavior of nano-PPX is explained with the directional dependence of water droplets derived from advancing-receding contact angles with pin-release mechanism[1]. The theoretical calculations and predictions were performed in our research group by Matthew J. Hancock.

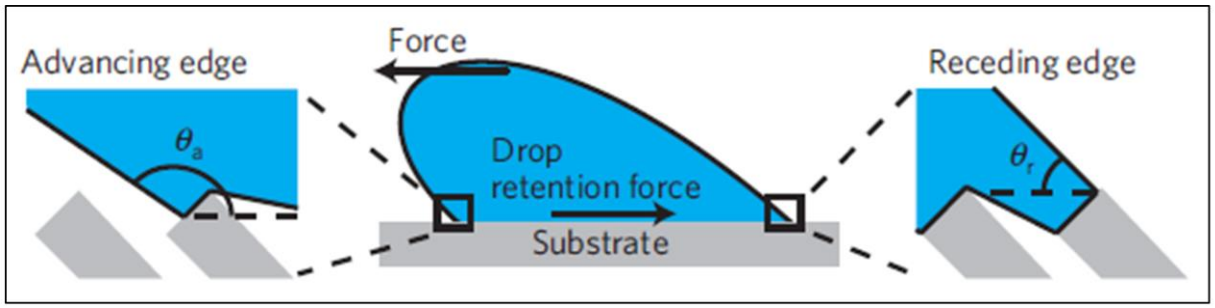


**Figure 4-1**. Schematic representation of drop retention force with advanced and receding contact angles at the edges. Reproduced with permission from Malvadkar *et al.*, *Nature materials* **12**, 1023-1028 (2010) DOI: 10.1038/NMAT2864. Copyright 2010 Macmillan Publishers Limited.[1]

Extrand has two approaches for modeling two dimensional ratchets[2] and three dimensional vertical rods[3]. According to Extrand, the net retention force on asymmetric asperities may be adjusted by increasing asymmetry and decreasing hysteresis of the surfaces. Also, he suggested

that the height of the asymmetric texture is less important than the shapes of the texture in terms of determining anisotropic wetting behavior.

## 4.2. Model Approach

According to Extrand's approach, the linear ratio of the advancing and receding contact line on the nano-PPX's rod ($\lambda$) structures is suggested. The advancing contact angle ($\Theta a$) and receding contact angle ($\Theta r$) were approximated as the averages of the meniscus contact angle at a rod and the 180$^o$ angle at air interface. Advancing meniscus or receding meniscus contact angles and rod surface are related by basic geometry. This relation includes parameters (Figure 4-2) such as the intrinsic advancing ($\Theta a_0$) and receding ($\Theta r_0$) contact angles of the material, nanorod diameter ($d$), nanorod tilt angle ($\beta$), and perpendicular nanorod spacing ($\delta$). Figure 4-2 represents release and pinning directions.

Advancing angle for release direction (Figure 4-2.a) is defined as:

$$\Theta_{aREL} = \lambda \min(\pi, \max(\Theta_{a1}, \Theta_{a2})) + (1-\lambda)\pi \qquad \text{Eq. 4-1}$$

For case 1:

$$\Theta_{a1} = \frac{3\pi}{2} - \beta - \arctan(\cot(\beta)/(1-s)) \qquad \text{Eq. 4-2}$$

For case 2:

$$\Theta_{a2} = \Theta_{a0} + \frac{\pi}{2} - \beta \qquad \text{Eq. 4-3}$$

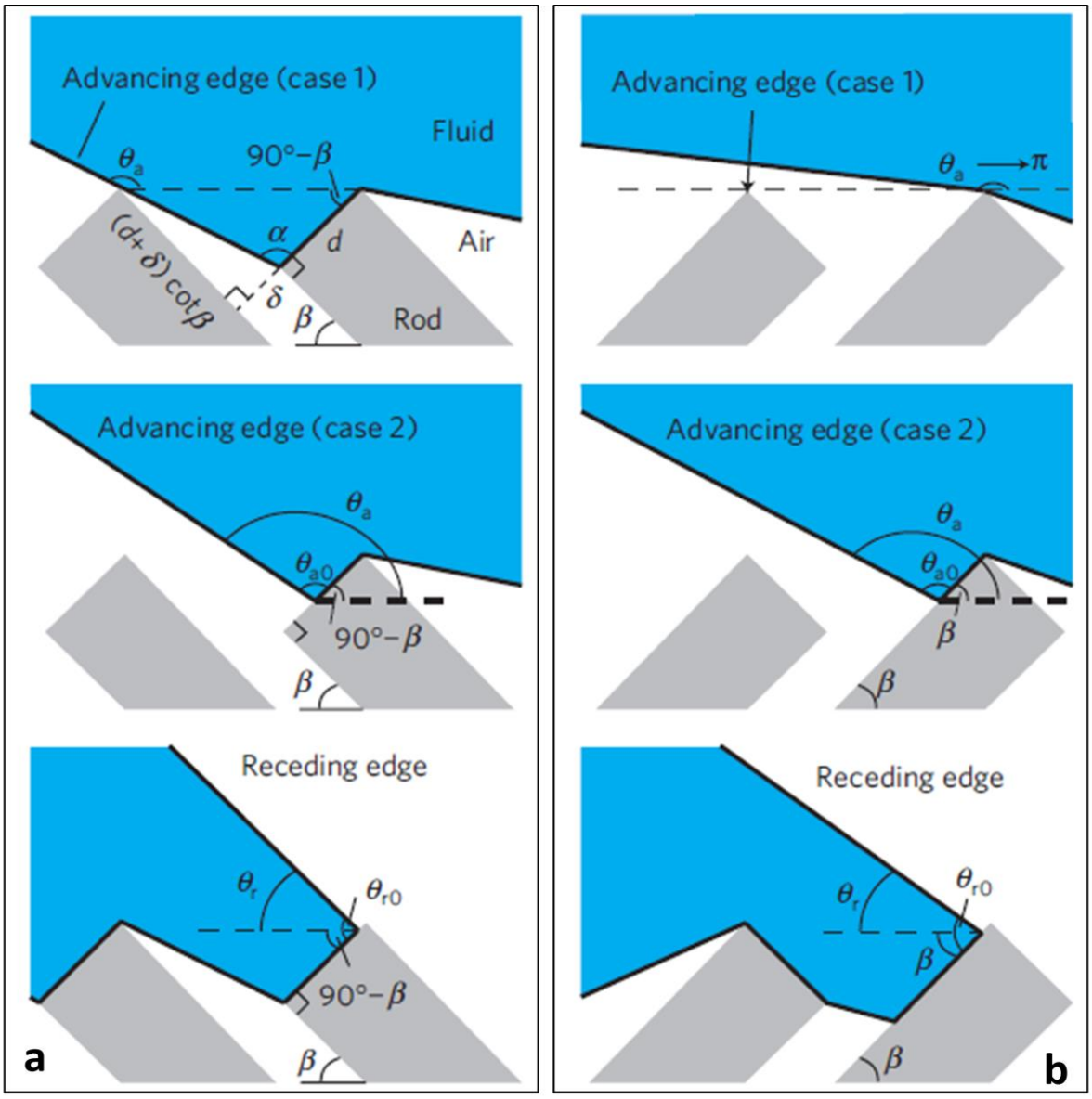


**Figure 4-2**. Schematic representation of theoretical models for water contact angles at the textured surface, a. Release direction b. Pinning direction. Reproduced with permission from Malvadkar *et al.*, *Nature materials* **12**, 1023-1028 (2010) DOI: 10.1038/NMAT2864. Copyright 2010 Macmillan Publishers Limited[1].

The receding angle for release direction is defined as:

$$\Theta_{rREL} = \lambda\left(\Theta_{r0} + \beta - \frac{\pi}{2}\right) + (1-\lambda)\pi \quad \text{Eq. 4-4}$$

The longitudinal nanorod spacing is defined as the solid fraction, $s = d/(d+\delta)$.

The advancing angle for pinning direction (Figure 4-2.b) is defined as:

$$\Theta_{aPIN} = \lambda \min(\pi, \Theta_{a0} + \beta) + (1-\lambda)\pi \quad \text{Eq. 4-5}$$

The receding angle for pinning direction is defined as:

$$\Theta_{rPIN} = \lambda(\Theta_{r0} - \beta) + (1-\lambda)\pi \quad \text{Eq. 4-6}$$

The fraction of retention force in the pinning direction and retention force in the release direction for one water droplet is calculated by:

$$\frac{F_{PIN}}{F_{REL}} = \frac{cos\theta_{rPIN} - cos\theta_{aPIN}}{cos\theta_{rREL} - cos\theta_{aREL}} \quad \text{Eq. 4-7}$$

If the water droplet is transported parallel to the ratcheted paths ($\delta = 0, s = 1$), then the ratio becomes

$$\frac{F_{PIN}}{F_{REL}} = \frac{\sin(\lambda(\beta + (1/2)\Delta\theta_0))}{\sin(\lambda(\frac{\pi}{2} - \beta + (1/2)\Delta\theta_0))} \quad \text{Eq. 4-8}$$

where $\Delta\theta_0$ is the difference of the intrinsic advancing ($\theta_{a0}$) and receding contact angles ($\theta_{r0}$). Eq. 4-8 can be simplified to Extrand's result[2], obtained from a geometrical aspect, for two-dimensional ratchets ($\delta = 0, s = 1, \lambda = 1$). If the rods are vertical on a substrate surface, the $\theta_a$ and $\theta_r$ can be reduced to Extrand's three-dimensional vertical rod model[3]. $\beta$, $\lambda$, $s$, and $\Delta\theta_0$ are constants and can be calculated for a nanofilm. Thus, Eq. 4-7 can be transformed in a constant

($C_0$), which represents the fraction of retention forces observed on a droplet at the surface. The constant $C_0$ is also estimated experimentally and represented as:

$$C_0 = \frac{cos\theta_{rPIN} - cos\theta_{aPIN}}{cos\theta_{rREL} - cos\theta_{aREL}} = \frac{V_{PIN}R_{REL}sin\alpha_{PIN}}{V_{REL}R_{PIN}sin\alpha_{REL}} \quad \text{Eq. 4-9}$$

In this equation, the gravitational force ($\rho V g sin\alpha$) has replaced the retention forces. The $R$ factors come from the retention force equation and the change in $k$ parameter is insignificant because of the droplet structure[1,4,5]. If the rod title angle ($\alpha$) is fixed and $R$ is proportional to$V^{1/3}$, then:

$$C_0 = (V_{PIN}/V_{REL})^{\frac{2}{3}} \quad \text{Eq. 4-10}$$

## 4.3. Comparison of Theoretical Model and Experiments

The nano-PPX rods have the following numbers: nanorod diameter ($d$) is ~ 150-200nm, nanorods spacing ($\delta$) is ~ 40nm, solid fraction ($s$) in nanorods is ~ 0.8, and the angle of nanorods ($\beta$) with substrate is 55 degrees. Intrinsic advancing ($\theta_{a0}$) and receding ($\theta_{r0}$) contact angles are measured as 95 and 75 degrees, respectively. Assuming the nano-PPX rods are a circular post, which combines into a square area, $\lambda$ is calculated ≅ 0.85. Also, Eq. 4-9 results into $C_0$ =1.22, which is close to $C_0 = (V_{PIN}/V_{REL})^{\frac{2}{3}} = (1.22 \pm 0.06)^{2/3} = 1.14 \pm 0.04$[1]

In the release direction, the measured advancing and receding contact angles of a drop on the nano-PPX surface are 128$^o$ and 60$^o$ $\pm$ 5$^o$ respectively, while the theoretical model suggests that, and receding contact angles should be 147$^o$ and 60$^o$ respectively. Similarly, the measured

advancing and receding contact angles in the pinning direction, are $137^o$ and $47^o \pm 5^o$ respectively, while the model suggests that, and receding contact angles should be $154^o$ and $43^o$ respectively[1].

According to these results, the receding contact angles are estimated closer than the advancing contact angles. The estimation should still be feasible since the differences in contact angle hysteresis are relatively cancelled while $C_0$ is calculated. While considering effects such as the simplifications in the theoretical model, non-uniform parts on the nano-PPX, evaporation in small droplets, and experimental errors, the experimental results approximately fit into the theoretical model[1].

The spacing of the nano-PPX rods can be deflected by the capillary force applied from the water droplets. At the drop perimeter, the nanorod spacing may become almost zero due to the bundling of single rods into clumps[6]. According to So *et al*., the clumping prediction agrees with a large capillary force to resistance of beam bending[7]. This is calculated by $h^2\gamma d/(EI)$~870, where nanorod height ($h$) is ~10 μm, nanorod diameter ($d$) is ~150-200 nm, surface tension of water ($\gamma$) is 72.8 dynes/cm, Young's modulus (E) is ~50-100MPa, and the moment of inertia (I) is $\pi d^4/64$. The theoretical model that was mentioned earlier exhibits close predictions in terms of calculating zero tip spacing ($s = 1$) at the receding contact angle point, where $C_0$ increases from 1.22 to 1.32. The $C_0$ value is still in the close proximity to the measure values[1].

The characterization and theoretical models exhibit that the unidirectional adhesion of the nano-PPX surface may be controlled by changing its parameters. The parameters, such as lateral nanorod spacing ($\lambda$), longitudinal ($s$) nanorod spacing, nano-PPX rod angle ($\beta$), and the advancing-receding ($\theta_{a0}$, $\theta_{r0}$) intrinsic contact angles, may be adjusted to control the $C_0$ constant

that is directly related to the unidirectional adhesion property. The dependence of $C_0$ constant on $\beta$ is shown in Figure 4-3.[1]

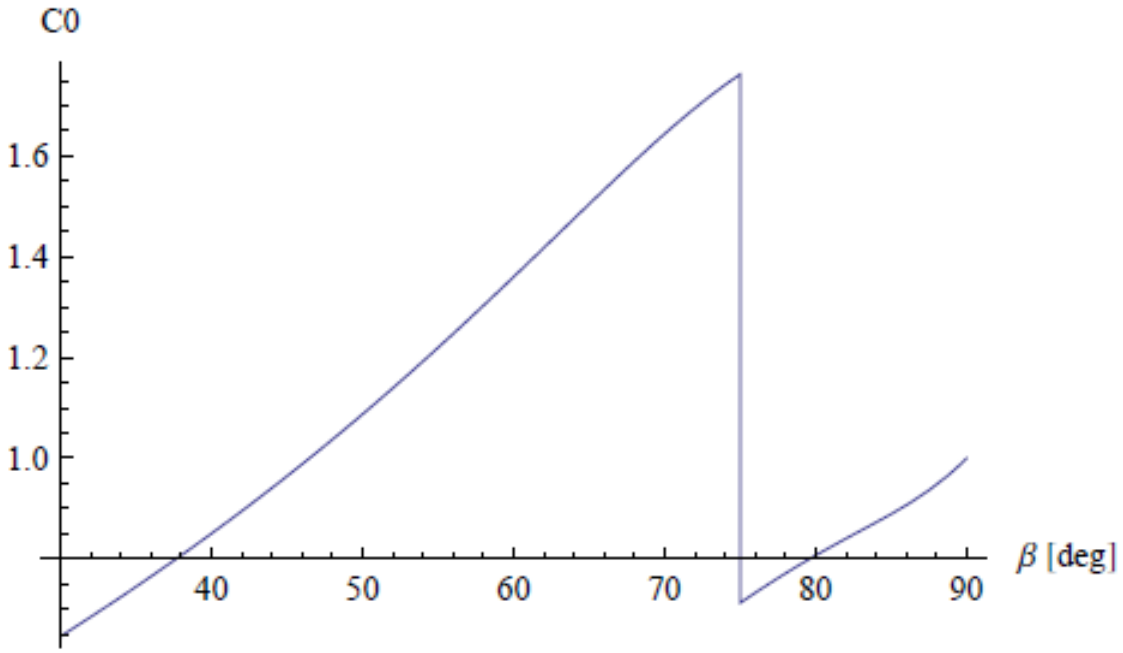


**Figure 4-3**. $C_0$ as a function of nano-PPX rod angle ($\beta$). Reproduced with permission from Malvadkar *et al.*, *Nature materials* **12**, 1023-1028 (2010) DOI: 10.1038/NMAT2864. Copyright 2010 Macmillan Publishers Limited[1].

According to the theory, if $\beta$ is increased up to 75 degrees, the $C_0$ will also linearly increase up to 1.8. After 75 degrees of angle ($\beta$), the $C_0$ shows a drastic drop below 0.8. Then from 75 to 90 degrees, a linear increase in $C_0$ continues until it reaches value of 1.0 . 90 degrees of nano-PPX is considered as isotropic and $C_0$=1.0.[1]

If $\beta$ is decreased below 45 degrees, the $C_0$ will also decrease linearly. In Chapter 5 (Applications and Devices), it is shown that the nano-PPX rod angle can be decreased down to 20 degrees

using mechanical shear. The theoretical model satisfies the experimental $C_0$ data. Different $C_0$ values for nano-PPX angles such as 32°, 24°, and 20° will be discussed in Chapter 5.

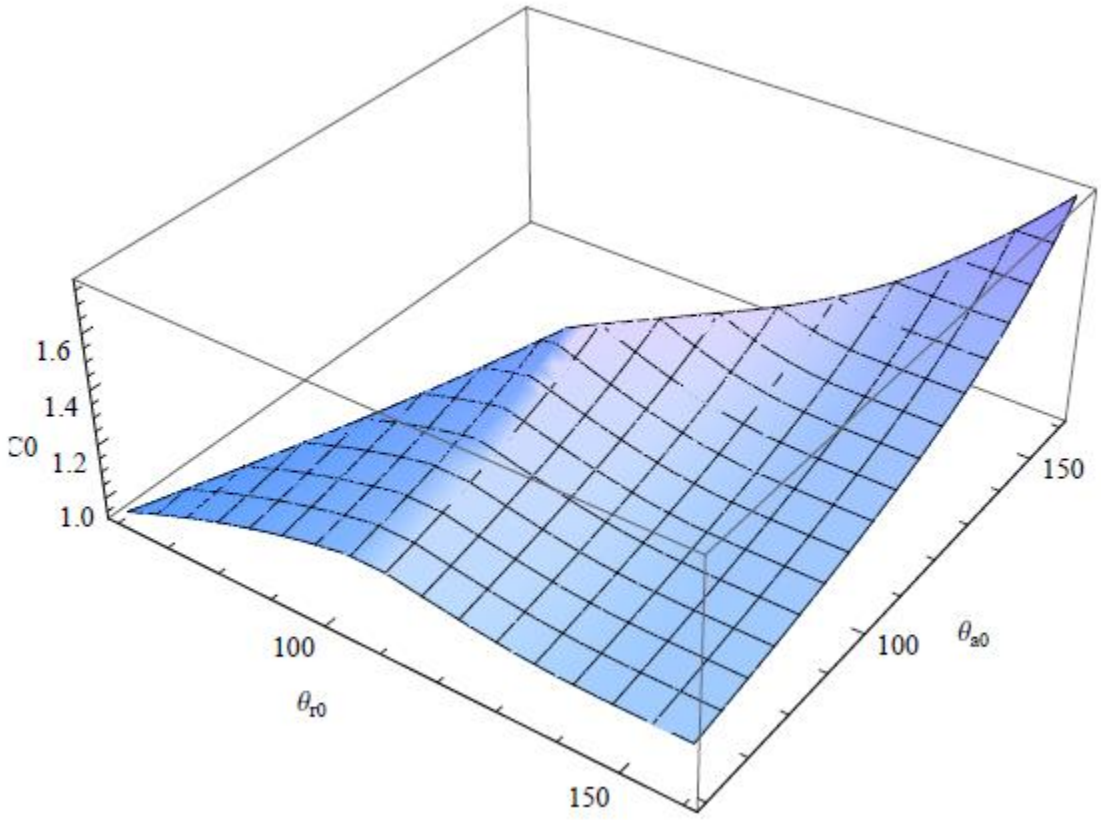


**Figure 4-4**. $C_0$ as a function of intrinsic advancing ($\theta_{a0}$) and receding ($\theta_{r0}$) contact angles. Reproduced with permission from Malvadkar *et al., Nature materials* **12**, 1023-1028 (2010) DOI: 10.1038/NMAT2864. Copyright 2010 Macmillan Publishers Limited[1].

Figure 4-4. demonstrates $C_0$ dependence on intrinsic advancing ($\theta_{a0}$) and receding ($\theta_{r0}$) contact angles. These contact angles may be adjusted by applying surface treatments to nano-PPX[8].

According to the theoretical model, both increasing $\theta_{a0}$ and $\theta_{r0}$ will make a definite increase in the $C_0$ constant. For instance, $C_0$ will increase from 1.22 to 1.31 when both $\theta_{a0}$ and $\theta_{r0}$ are increased from 75° and 95 ° to 85 ° and 105 °, respectively[1].

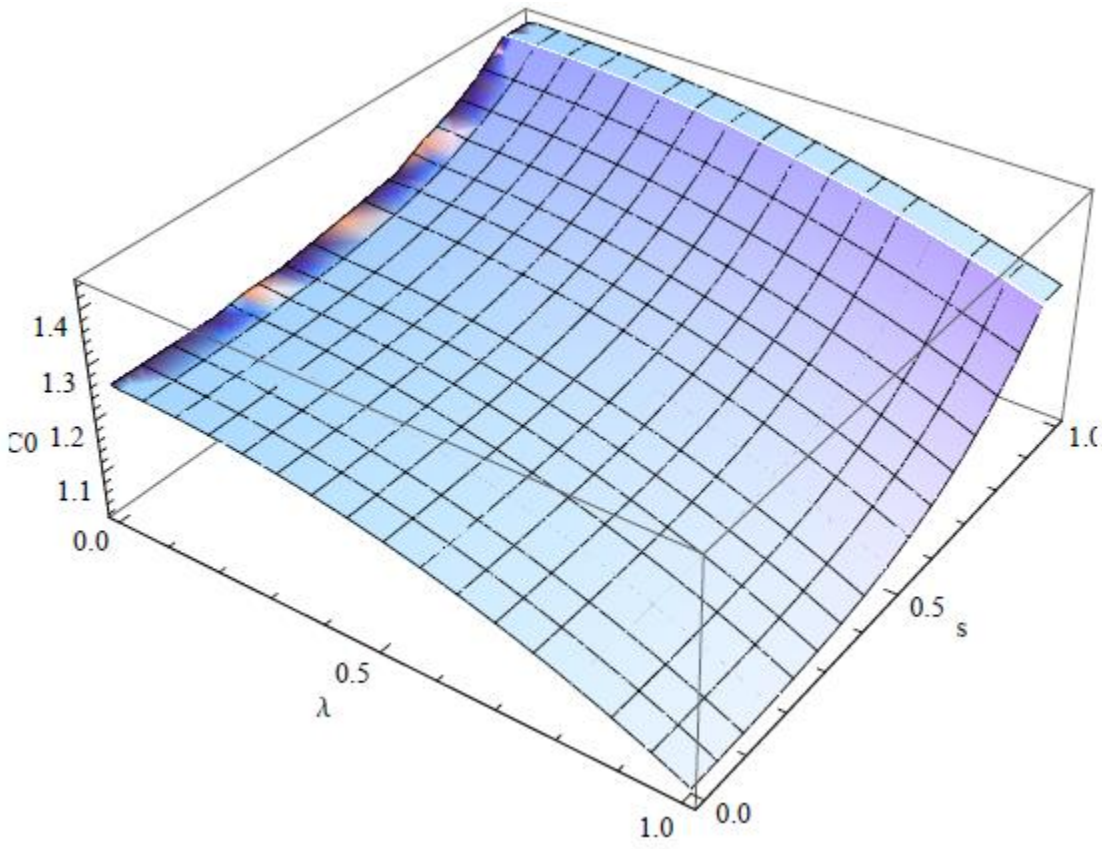


**Figure 4-5**. $C_0$ as a function of lateral ($\lambda$) and longitudinal ($s$) nanorod spacing. Reproduced with permission from Malvadkar *et al.*, *Nature materials* **12**, 1023-1028 (2010) DOI: 10.1038/NMAT2864. Copyright 2010 Macmillan Publishers Limited[1].

Figure 4-5. shows $C_0$ dependence on lateral ($\lambda$) and longitudinal ($s$) nanorod spacing. According to the theoretical model, increasing longitudinal ($s$) nanorod spacing from 40 nm to 100 nm will increase $C_0$ by 0.27. Similarly, decreasing lateral ($\lambda$) nanorod spacing will slightly increase the $C_0$ constant.

## 4.4. Summary

In summary, the adhesive wetting properties of nano-PPX rods may be controlled by changing the design parameters. During the oblique angle deposition procedure of nano-PPX on substrates, different variations such as changes in rod diameter can occur due to defects or flux fluctuations. These changes directly affect the adhesive wetting behavior. Moreover, self-shadowing during nanorod growth may produce non-uniform rod tips and nanorods at different heights. Despite all of the possible non-uniformities and defects, the adhesive force between the nano-PPX surface and water droplets is always explicitly bigger than the release and other isotropic directions. Thus, the unidirectionality and the adhesive wetting behavior of nano-PPX are always applicable in terms of serving the applications of wetting, adhesion, and transport. Yet, the $C_0$ constant varying properly over all the parameters indicates consistency for the directional wetting and adhesion behavior of nano-PPX.

It should be emphasized that the surface properties of nano-PPX are unique, similarly to natural creatures from animal and plant kingdoms. The theoretical model and the reasonable assumptions on design predictions state that the nano-PPX surface may be enhanced to have a variety of anisotropic wetting and adhesion behaviors. Using surface treatments and adjusting the design parameters, nano-PPX could be used for a variety of applications as a transport/assembly platform for digital fluidics field.

## References

[1] N.A. Malvadkar, M.J. Hancock, K. Sekeroglu, W.J. Dressick, and M.C. Demirel, Nature Materials **9**, 1023 (2010).

[2] C.W. Extrand, Langmuir **23**, 1867 (2007).

[3] C.W. Extrand, Langmuir **18**, 7991 (2002).

[4] C.W. Extrand and Y. Kumagai, Journal of Colloid and Interface Science **170**, 515 (1995).

[5] A. ElSherbini and A. Jacobi, Journal of Colloid and Interface Science **299**, 841 (2006).

[6] M.C. Demirel, M. Cetinkaya, A. Singh, and W.J. Dressick, Advanced Materials **19**, 4495 (2007).

[7] E. So, M.C. Demirel, and K.J. Wahl, Journal of Physics D: Applied Physics **43**, 45403 (2010).

[8] S. Boduroglu, M. Cetinkaya, W.J. Dressick, A. Singh, and M.C. Demirel, Langmuir **23**, 11391 (2007).

# Chapter5. Device Applications

## 5.1 Introduction

Recent studies indicate that assembly of microgels has become an essential topic in micro-architecture[1–3]. Merging microgels into close proximity is managed using water as the carrier media. For instance, microliter droplets are able to carry microgels on surfaces with nano roughness[4]. If water transport is properly controlled on the nano surface, directed assembly/merging of particles may be possible. Accordingly, simple devices can be built to introduce microgels into close proximity for building blocks. The water droplets exhibit propulsion using external forces (i.e. mechanical vibrations [4–6]) to propel on surfaces. To understand the droplet motion on directional surfaces, their characteristics such as wetting and transport properties must be clearly understood. The wetting and transport properties of various surfaces were investigated in the field of digital microfluidics. In recent publications droplet motion on engineered directional surfaces have been achieved using forces such as capillary[7], electrowetting[8], focused acoustic waves[9], surface tension[10], transistor based actuation[11], Leidenfrost ratchets[12], and chemical gradient[13]. Apart from these techniques, the idea of vibrating droplets[4,5] on surfaces brings a new approach to droplet motion on surfaces due to its simplicity in use and avoidance of complex manufacturing steps. Applying mechanical vibration to the surface enables water droplet propulsion on asymmetric textured surfaces overcoming forces (e.g. adhesion and gravitational) directional transport. The geometry of the surface ratchets causes the unidirectional droplet motion via vibration. Adjusting physical properties of nanotextured surfaces such as changing the angle of nanorods and

fabricating tracks on the directional surfaces provided the control of droplet motion. The ability of droplet manipulation opens up new aspects for device applications. Device platforms may provide droplet transport to specific targets as well as carrying cargo.

## 5.2 Studies on Directional Water Droplet Transport

Directional droplet propulsion on micro and nano surfaces have been investigated by a number of research groups. Sandre *et al*., created directional micro ratchets that are parallel to each other. These parallel surfaces moved water droplets using breathing motion[14]. Shastry *et al*., produced microstructures with a superhydrophobic gradient, which can propel water droplets when mechanical vibration is applied to the surface[6]. Linke *et al*., investigated the propulsion of water droplets on micro ratcheted surface at Leidenfrost state. The directional movement of the water droplets was due to the vapor flow occurring between liquid (boiling water) and solid surface (anisotropic ratchets)[15]. Zhang *et al*., proposed a similar method by transporting water droplets on directional micro ratchets using actuation by magnetic field[16]. Recently, Daniel *et al*.,[17] and Mettu *et al*.,[18] displayed that water droplets on non-wetting flat surfaces can be guided directionally by vibrating the surface asymmetrically. Duncombe *et al*., engineered a surface with directional tracks to transport droplets on round pathways; however water droplets can only move on single channels[19]. Chu *et al*., demonstrated a directional surface where liquids are able to spread on tilted nanorods. Self-propagation of the liquid and wetting properties were controlled by changing the angle of hydrophilic nano structures[20].

Our research group showed that microliter water droplets move unidirectionally on a polymeric nanorod system (nano-PPX) using mechanical vibrations. The pin-release mechanism on asymmetric nano-PPX provides the water droplets with a unidirectional propulsion on the surface[5]. We reported that moving water droplets on a nanotextured surface can be used as a soft cargo (i.e. microgels) carrier. The velocity of the droplet transport depends on the frequency of vertical vibrations and the droplet volume[4].

Having considered the latest studies for liquid droplet transport technologies, it is apparent that manufacturing directional surfaces to guide water droplets for transport and assembly purposes are limited. Also, some of the manufacturing processes require photolithography and cleanroom facilities, which are expensive and time consuming. Emergent technologies are required to produce inexpensive and easy-to-use platforms for assembly applications. Nano-PPX surface is one of the better surfaces that can guide water droplets via vertical vibrations. In Chapter 3, it was demonstrated that nano-PPX coated half-pipe surfaces have been able to transport droplets unidirectionally[4,5].

## 5.3 Aim of Fabricating Tracks on Nano-PPX

Textured nano-PPX surfaces have hydrophobicity and high hysteresis. Water droplets can move on the nanorods (i.e. nano-PPX) with minimal drop deformations. During the vertical vibrations, water droplets follow straight paths on the surface. Droplets may also travel on paths towards the sides due to having equal forces in forward, right, and left directions. Only the force in the reverse direction is smaller than the forces in the other directions.

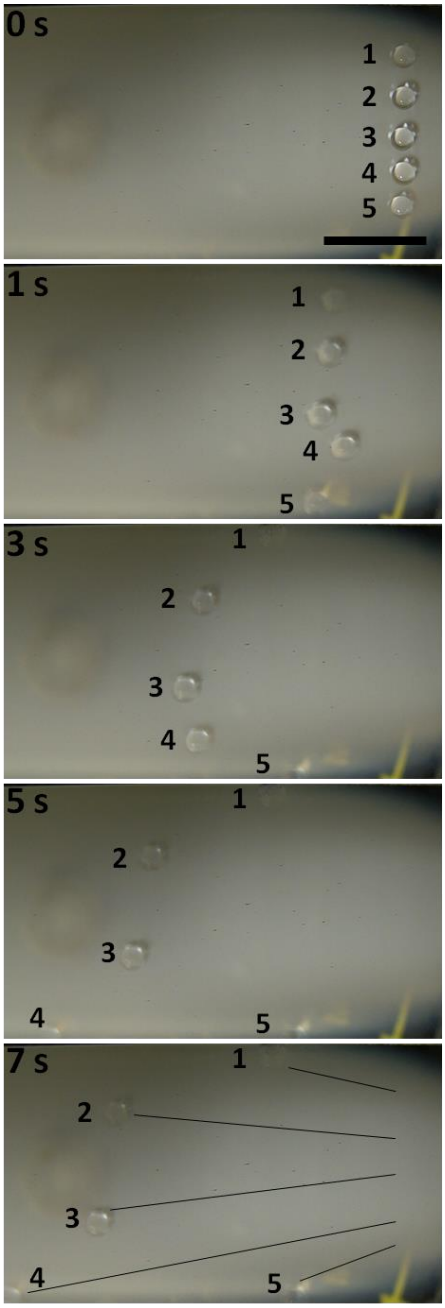


**Figure 5-1**. 5 μL droplets on nano-PPX surface following straight paths during vibrational frequency of 95 Hz. Numbers are located in front of the drop at each scene. Lines in the final scene ($7^{th}$ second) represent the straight paths followed by droplets (Scale bar: 1cm).

Figure 5-1 displays a simple experiment to present the possible movements of water droplets on the directional nano-PPX surface. Five water droplets (5μL each) were lined up side-by-side on the nano-PPX coated glass substrate. The surface was vibrated at 95 Hz frequency with low amplitude. During the vibrations, the droplets started ($t = 0$) to move from left to right, unidirectionally. Even though they all followed straight paths on the surface, three of the water droplets (numbers 1, 4, and 5) traveled to the edges of the substrate.

The other drops (numbers 2 and 3) followed straight paths towards the other end on the surface. As a result droplets may travel to the sides, following straight paths, due to the edge effects and the nanorod having lower density closer to the side of the substrate. Half-pipes were used to transport droplets on perfect straight paths in the earlier experiments in Chapter 3.

Water droplets and cargo materials (e.g. microgels) are required to follow certain paths to reach desired targets. Transport of water droplets should be reproducible and assembly/merging activity needs to be in an ordered manner. Thus, a platform with certain pathways to guide droplets is necessary. This problem can be solved by fabricating tracks on the nano-PPX surface, inspired from trains moving on rails; therefore the water droplets follow the straight tracks to reach the desired points. A track-assisted nano-PPX surface is a quick solution to overcome this challenge.

Nano-PPX is a soft material (Young's Modulus ~ 100 MPa[21]) that can deform with applied pressure. A rubber strip was used to deform the nano-PPX surface. Figure 5-2.a demonstrates a simple way to create a track line on the nano-PPX surface. The rubber

strip applies pressure on the surface along the nanorod direction. The pressure between the rubber and the surface forces the nano-PPX rods to deform. The applied stress simply causes the polymeric nanorods to switch into the plasticity region. The angle of nanorods changes from $45^{o}$ to lower angles (Figure 5-2.a-b). By deforming the nano-PPX rods, a track line was created on the nanorods. This track is expected to assist the droplet transport action by preventing the droplet from traveling to sides.

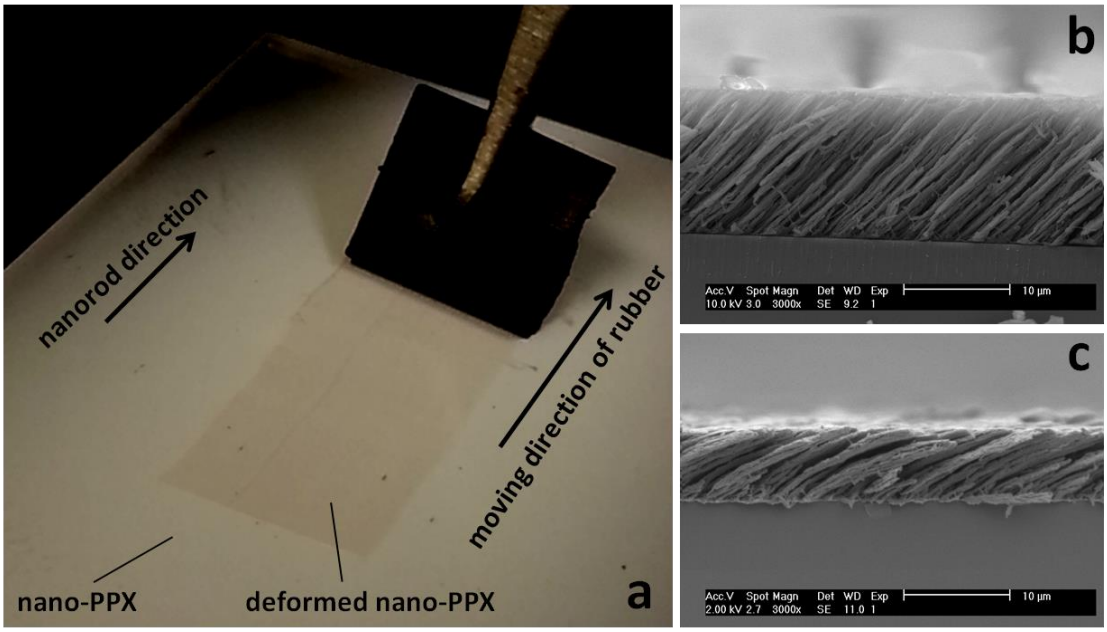


**Figure 5-2**.a. Nano-PPX surface is deformed by a rubber strip along the nanorod direction, b. Cross sectional SEM of nano-PPX without deformation, c. Cross sectional SEM of deformed nano-PPX.

Figure 5-3.a-b demonstrates the topographic surface images of nano-PPX and deformed nano-PPX. The roughness of the surface changes after the deformation and the spacing among nanorods get smaller. The nano-PPX deformation only exhibits physical changes,

the FTIR peaks of both cases demonstrate that no chemical changes occurred via deformation procedure (Figure 5-3.c).

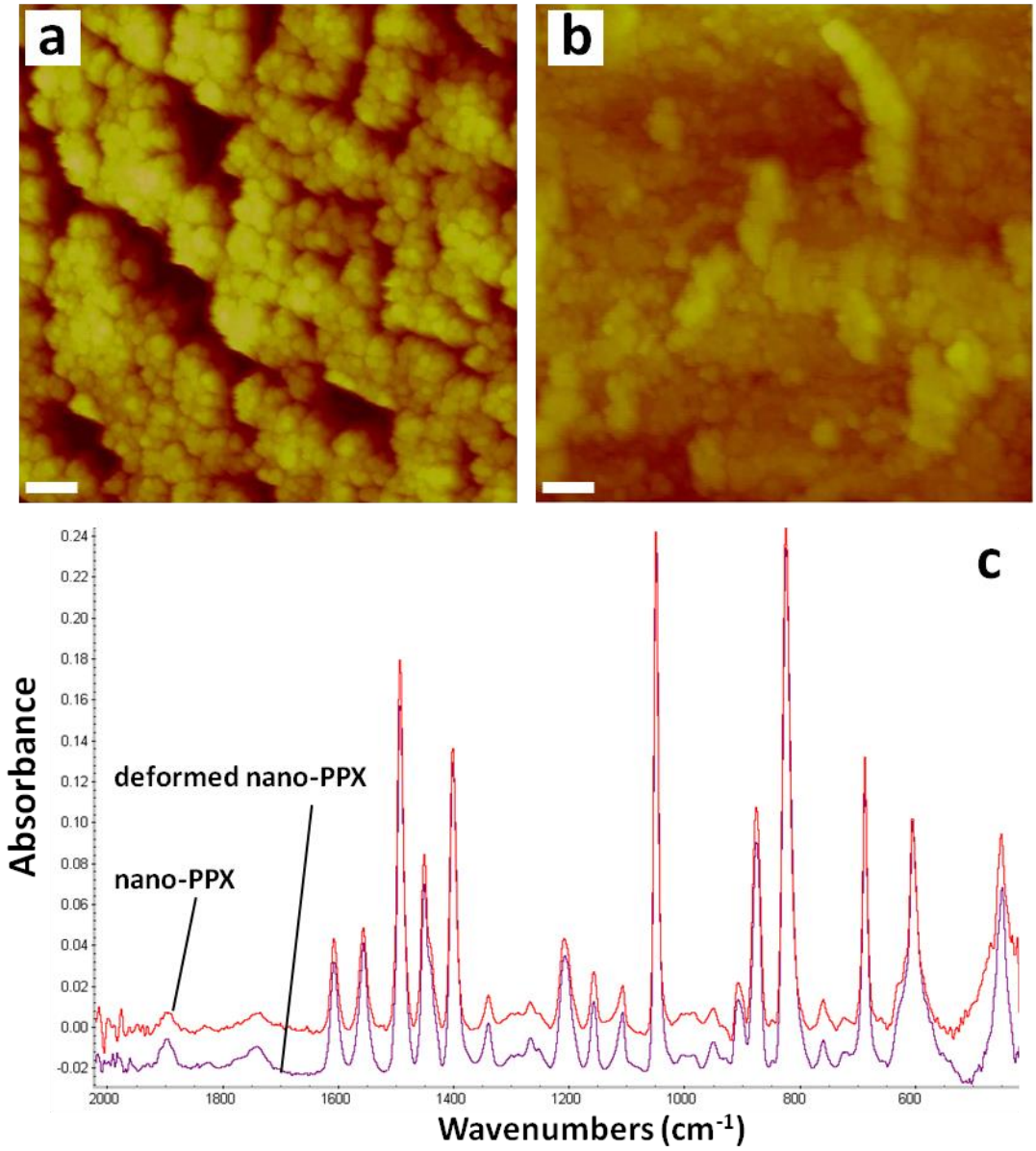


**Figure 5-3**. a. AFM image of nano-PPX with no deformation, b. AFM image of nano-PPX with no deformation, c. Comparison of FTIR peaks between deformed and undeformed nano-PPX surfaces.

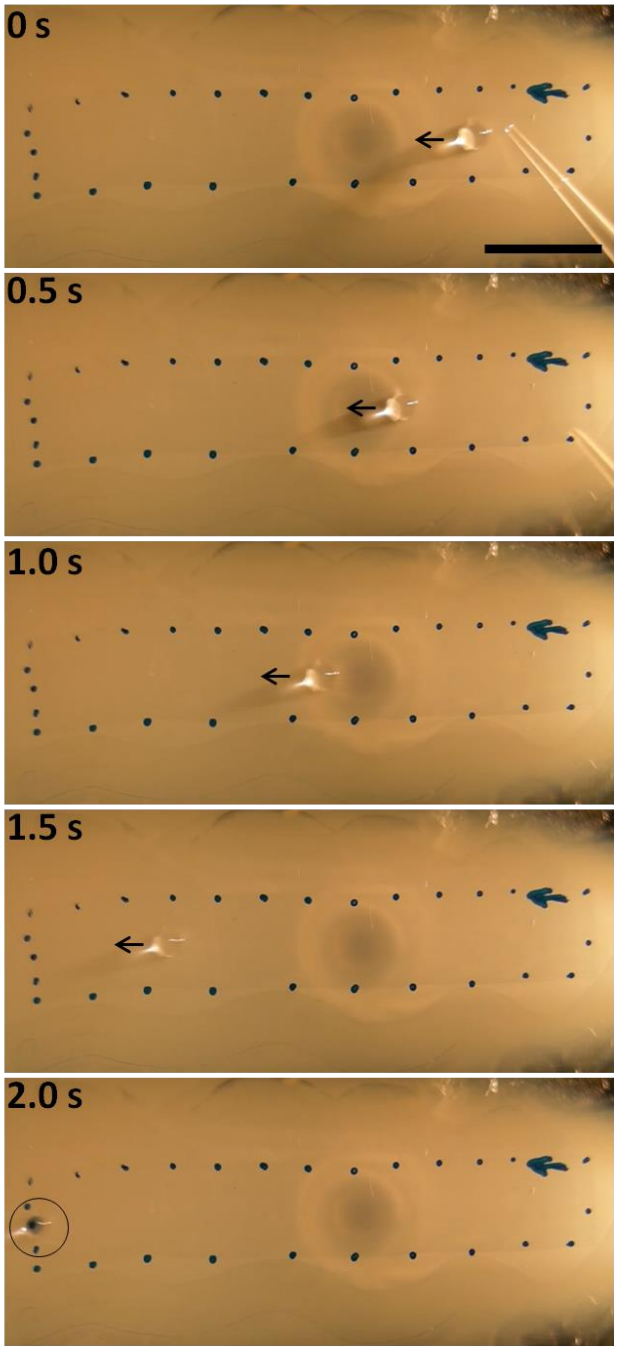


**Figure 5-4**. 5 µL droplets on nano-PPX surface following random paths during vibrational frequency of 95 Hz. Numbers are located in front of the drop at each scene. Dots were placed to indicate the deformed part of the surface (Scale: 1cm).

Figure 5.4 demonstrates a nano-PPX surface with a deformed track using the rubber strip. 5 μL was placed on the surface and vibrational frequency was applied at 95 Hz. The droplet followed a complete straight path from the start until the end of the track. This showed that the pathways for the droplets transport can be manipulated by deforming nano-PPX surface into tracks. To manipulate and guide droplets on the nano-PPX surface, multiple tracks should be fabricated. In this method, additional tracks are also possible during or after the fabrication process. Controlling the angle of the nano-PPX may demonstrate different wetting properties as well as providing various droplet velocities, which is discussed in the further sections.

## 5.4 Deforming Nano-PPX into Angles

We have developed a unidirectional transport system for water droplets with microgel cargo[4]. The transport had to be performed in a half-pipe in order to prevent droplets going to the sides due to the edge effects. Duncombe *et al*., took the directional transport system to a further point where droplets can move directionally on circular paths. However droplet propulsion is limited to single channels and a rapid addition of tracks is not possible[19].

To overcome these challenges, droplet transport may be performed on track-assisted nano-PPX surface where droplets move along the tracks to desired targets. Merging several droplets using multiple tracks can be defined as basic devices. These devices can be designed to sort and mix water droplets. Deforming the nano-PPX and controlling the final nanorod angles will provide the flexibility of creating desired tracks. The details of the deposition process have been described in Chapter 2, Materials and Methods.

Figure 5-5.a and e shows cross sectional and top view of the nano-PPX rods deposited on a glass substrate. The growth of nanorods is anisotropic with a 45 degree angle from the substrate plane.

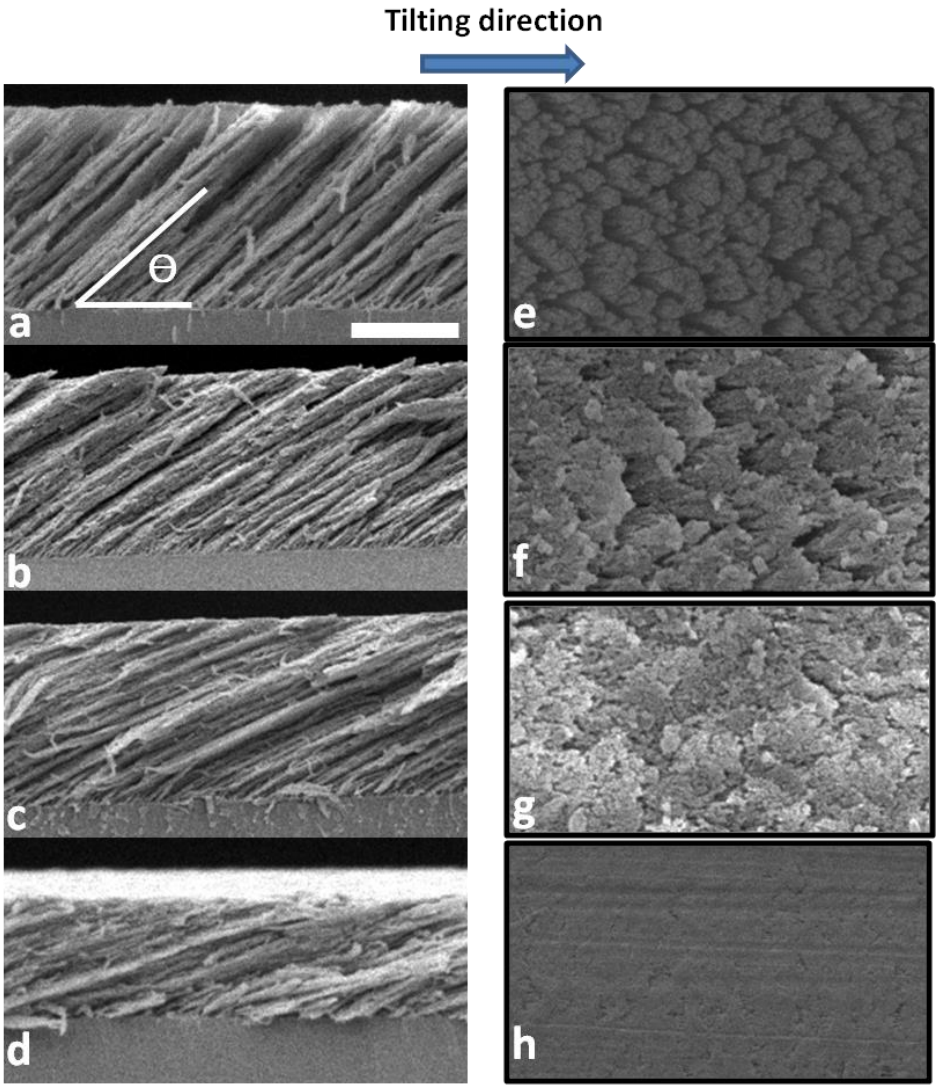


**Figure 5-5**. a - d. Cross sectional SEM images of nano-PPX ($\Theta = 45^{o}$) and tilted nano-PPX ($\Theta = 32^{o}$, $24^{o}$, $20^{o}$ respectively), e - h. Top images of SEM images of nano-PPX ($\Theta = 45^{o}$) and tilted nano-PPX ($\Theta = 32^{o}$, $24^{o}$, $20^{o}$ respectively), (Scale bar: 5 µm).

In Figure 5-5, the cross sectional and top view couples; b-f, c-g, and d-h represent the tilted nano-PPX rods, with $32^{o}$, $24^{o}$, and $20^{o}$ angles, respectively. Pressure was applied on the nano-PPX surface to obtain the various angles. The nano-PPX coated substrate was moved horizontally and the applied force was kept still during the deforming process of nano-PPX rods. Applying higher pressure caused nanorods to be tilted into smaller angles. The pressure dependence of nano-PPX tilt angle is shown in Figure 5-6. The tilt angle is inversely proportional to the applied pressure. As more pressure is applied, spacing between nanorods gets smaller. The required pressure to increase the tilt angle exponentially increases due to very small spacing between the nanorods.

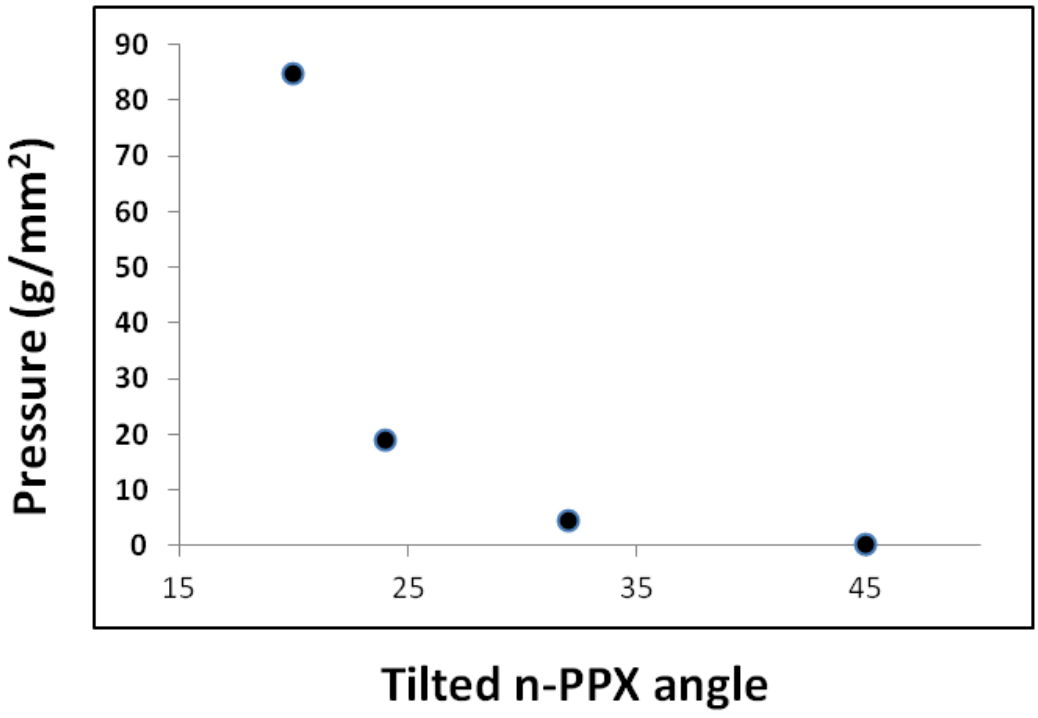


**Figure 5-6**. Nano-PPX angle variation dependence on the applied pressure on the surface.

## 5.5 A Setup for Fabricating Tracks on Nano-PPX

The rubber strip was used to deform the nano-PPX rods in the earlier sections in this chapter. To be able to create multiple tracks, a smaller soft tip was necessary. This tip can be used to simply draw tracks on the nano-PPX surface. A silicone tip pen was built using a glue gun and a regular pen (Figure 5-7). The tip of the pen is flexible enough to draw the desired tracks (e.g. straight lines and curves) and it is stiff enough to deform the nano-PPX.

The pen with the soft silicone tip was attached to an electronic cantilever device where the vertical distance to the substrate can be controlled by a computer (Figure 5-7.a). The stage where the nano-PPX controlled substrate lays can be moved along the x and y axis. The pen can also be moved in the z direction to apply the required force. These movements in the x-y-z coordinate system provide the ability to draw a variety of tracks on the nano-PPX surface. After the tracks are drawn, the deformed and the non-deformed parts are distinguished by the white contrast difference (Figure 5-7.b). A top SEM image demonstrates the difference between the inside and outside of the track channels (Figure 5-7.c).

This method to draw tracks will be encountered to create simple devices to sort and mix droplets in future sections of this chapter.

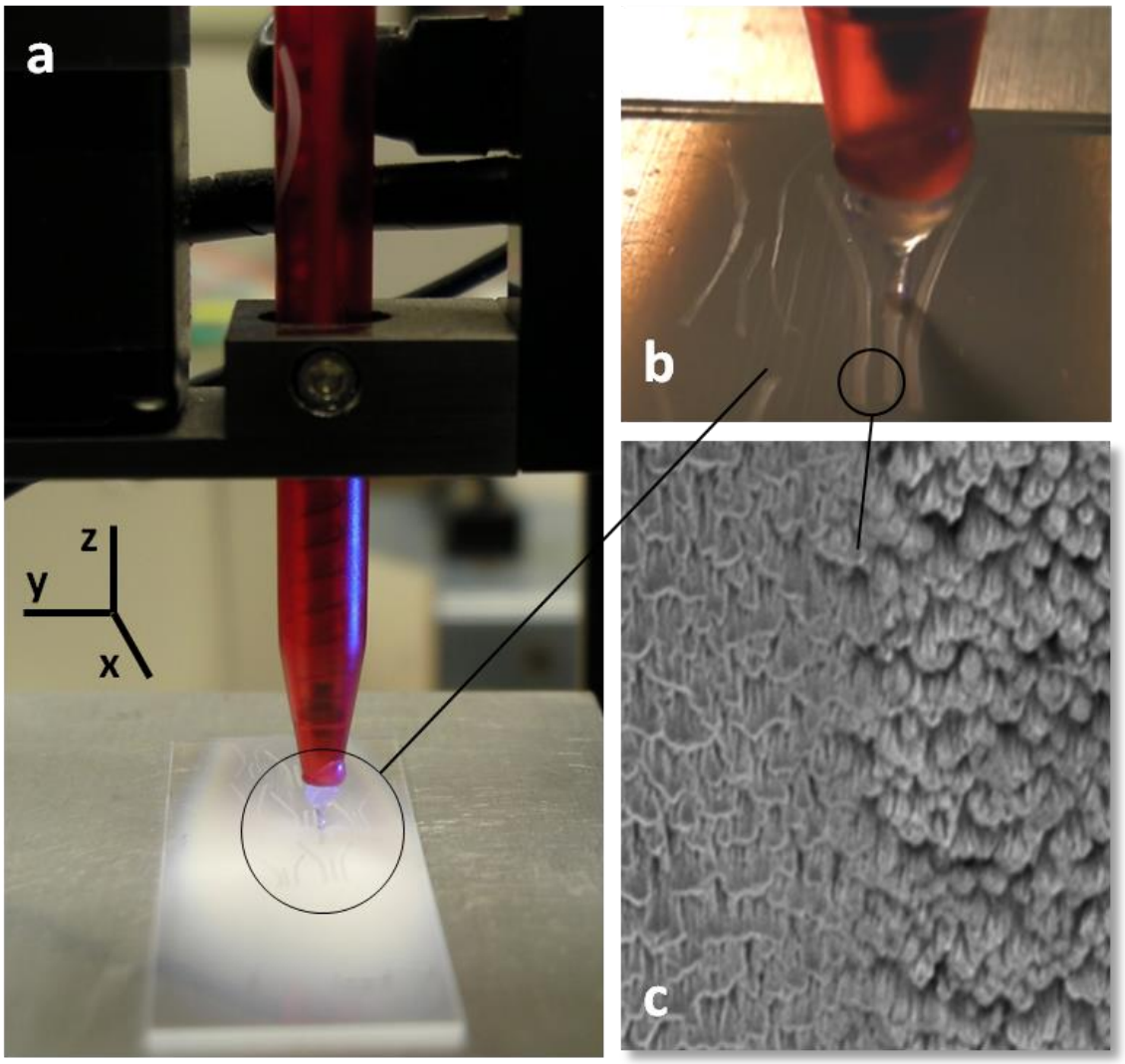


**Figure 5-7**. a. Image of the track drawing setup, b. Close-up image of the silicone tip on tracks, c. Top view SEM image of the inside and outside of the track on nano-PPX surface.

## 5.6 Wetting Properties of Tilted Nano-PPX

The tilted nano-PPX may exhibit different wetting and transport properties from nano-PPX. Typically, a nano-PPX surface has anisotropic and isotropic directions in terms of the ability of water adhesion and wetting. This ability can be expressed with critical droplet volume (*V*), which is the maximum amount of water the surface can adhere to itself at a certain stage angle. Droplet volumes that are larger than V will not adhere; they will slide off the surface. The critical droplet volume varies depending on the stage tilting angle, anisotropic, and isotropic directions.

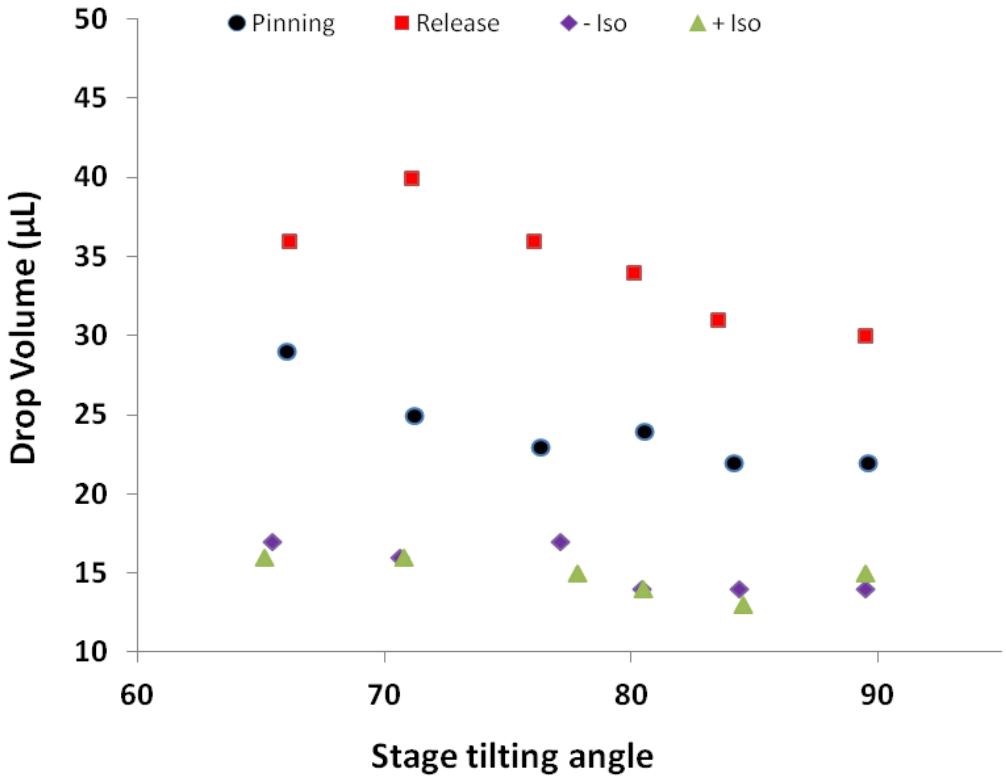


**Figure 5-8**. Critical drop volume dependence on stage tilting angle for anisotropic (pinning, release) and isotropic (+, −) directions.

Figure 5-8 demonstrates $V$ dependence on stage tilting angles between 65 and 90 degrees for the tilted ($25^{o}$) nano-PPX sample. The nano-PPX and the tilted nano-PPX surfaces carry more water volumes at the pinning and release (anisotropic) directions than the $+$ and $-$ (isotropic) directions due to the pinning-release mechanism on the film surface[5].

Both isotropic directions $(+,-)$ approximately carry the same amount of droplet volumes. The tilted nano-PPX demonstrated a new wetting behavior for the anisotropic directions. The critical drop volumes for the release direction are larger than the pinning direction (Figure 5-8). This result is also confirmed for the $C_0$ calculations for the tilted nano-PPX surface (Figure 5-9).

While measuring the critical volumes at certain stage angles, advancing and receding angles at droplet edges are calculated. Critical volumes at pinning and release directions (*Vrel*, *Vpin*) generate $C_0$ constant for the anisotropic axis. Similarly, $C_0$ constant at isotropic axis is formed by droplet volumes in + and – directions (*Viso+*, *Viso–*). $C_0$ constant is a predicted ratio of the retention forces for a water droplet volume on nano-PPX.

According to the $C_0$ calculations, isotropic axis values revolve around 1. Unlike the nano-PPX surface, the $C_0$ numbers for the anisotropic axis of tilted nano-PPX that are lower than 1 revolve around 0.75. This result agrees with the theoretical model mentioned in Chapter 4.

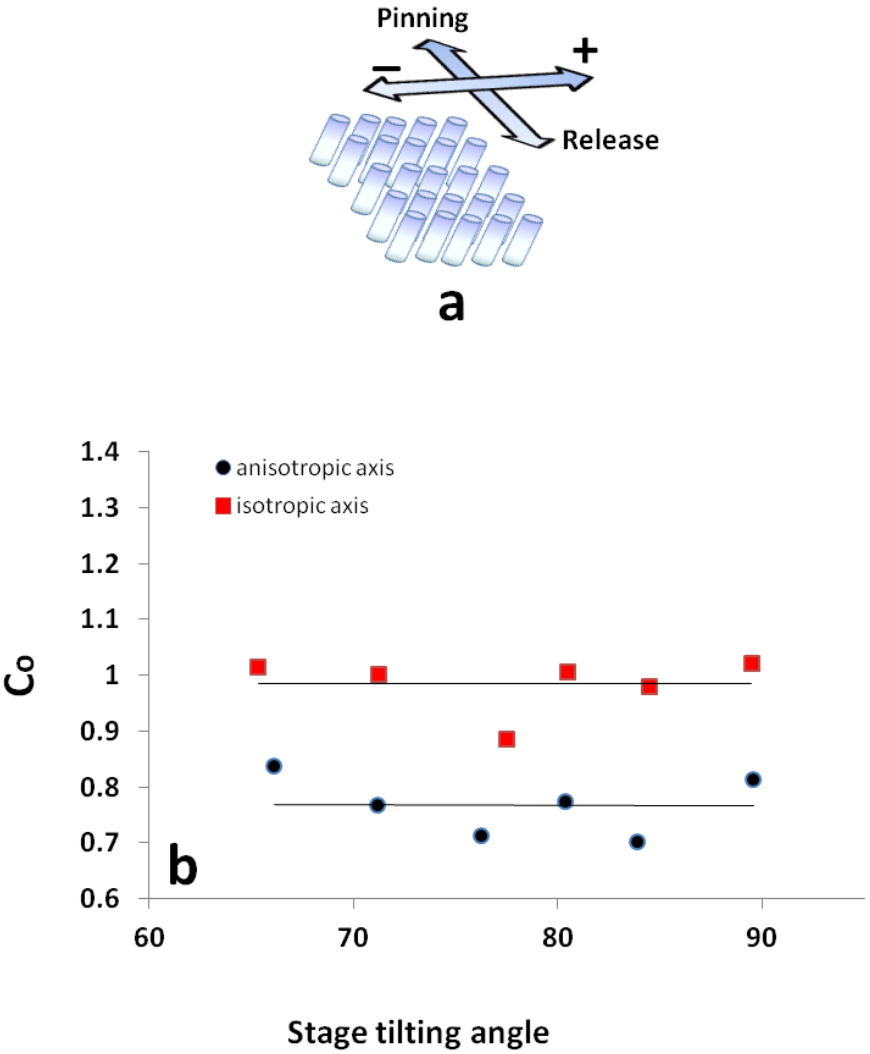


**Figure 5-9**.a. Pinning, release, + and – directions on nano-PPX surface, b. Co vs. stage tilting angle for anisotropic and isotopic directions.

The tilted nano-PPX was also tested to investigate the vibrational frequency dependence on water droplet volumes. The substrate with tilted nano-PPX was horizontally glued on a mechanical vibrator (PASCO SF 9324). Various frequencies were applied with constant amplitude (~0.5mm).

Figure 5-10 displays the results for various droplet sizes (2-12 µL). The tilted nano-PPX surface is able to transport water droplets at lower and wider frequency intervals comparing to the nano-PPX surface due to having larger contact angles hysteresis.

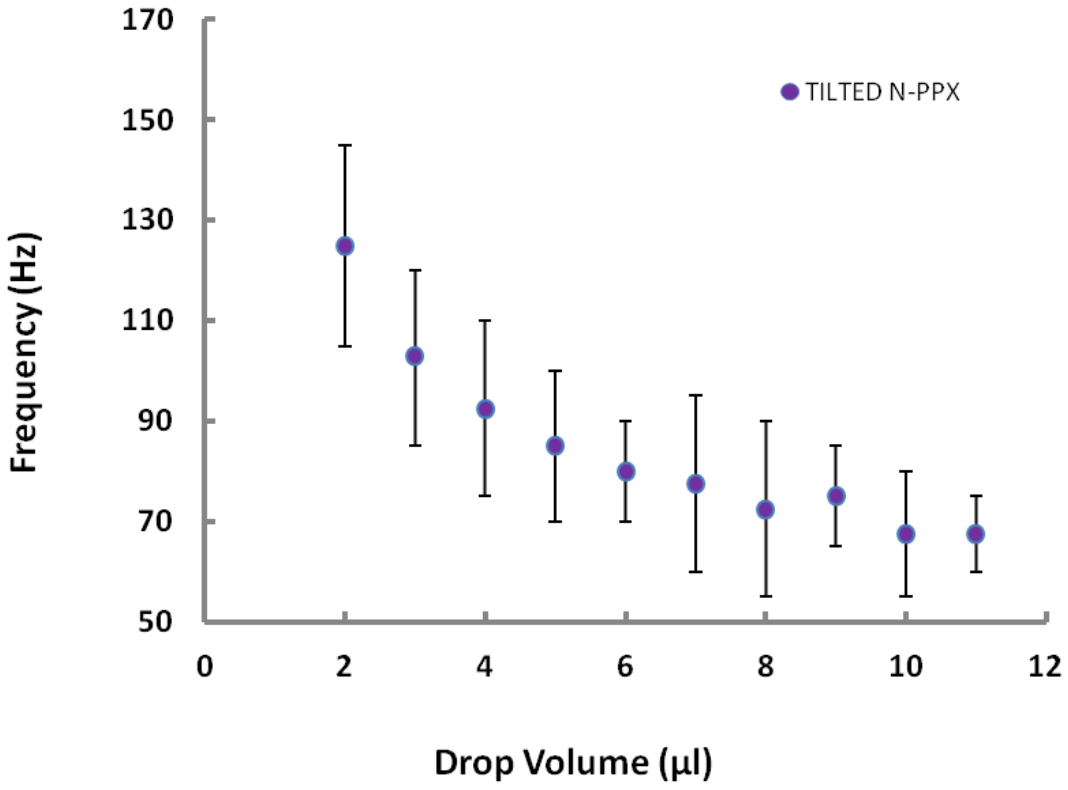


**Figure 5-10**. Frequency dependence as a function of drop volume on tilted nano-PPX.

According to Rayleigh[22] for spherical volumes the scaling ($w$) is inversely proportional to Sqrt($V$), that is $w = (3\pi\rho V/(8\gamma))^{0.5}$ , (water surface tension: $\gamma$ and water density: $\rho$). This scaling function was applied to the drop speed data collected for volumes between 4ul to 10ul (Figure 5-11).

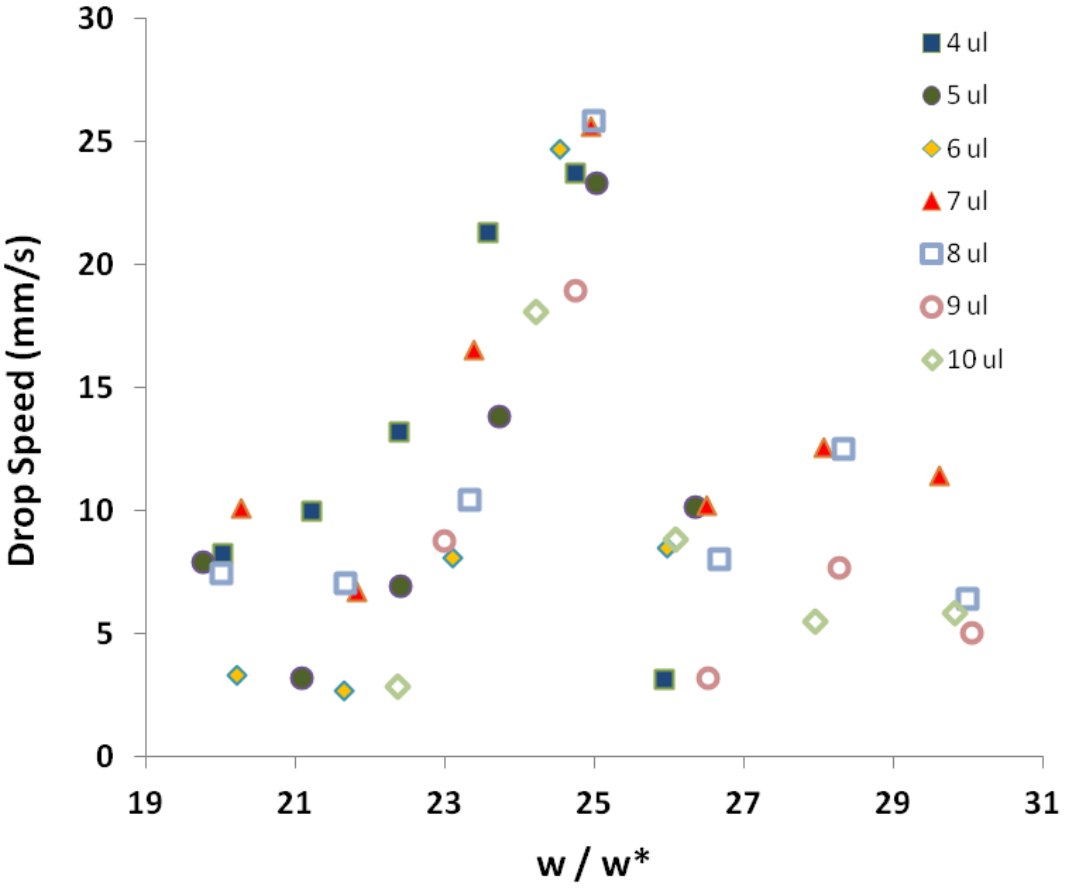


**Figure 5-11**. Drop speed as a function of normalized vibrational frequency.

When the normalization of the vibrational frequency ($^{w}/_{w^*}$) is calculated for the experimental data, the drop speed curves approximately overlap on each other. This behavior is both observed for nano-PPX and tilted nano-PPX, showing that different drop volumes demonstrates similar behavior due to their resonance effects related to the vibrational frequencies[4,17].

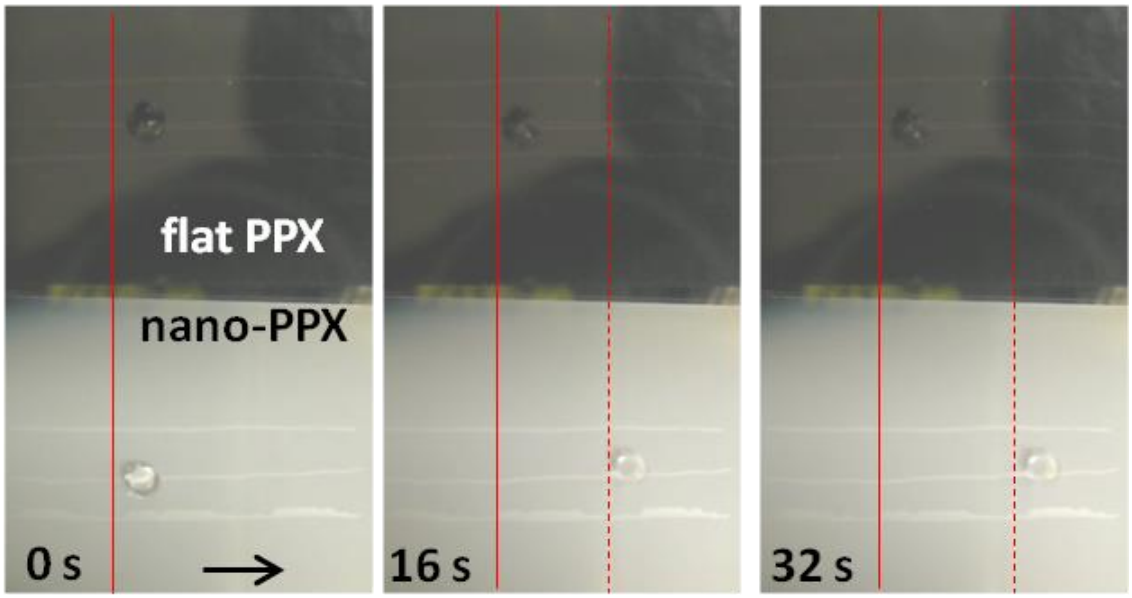


**Figure 5-12**. Control experiment on tilted nano-PPX and planar-PPX, red line shows the start point for the droplets. Red arrows indicate the direction of the propulsion.

A control experiment was performed to investigate whether water droplets move on planar-PPX surfaces (Figure 5-12). Straight tracks were fabricated on both nano-PPX and planar-PPX coated surfaces. 5µl droplets were placed on the surfaces. Mechanical vibrations were applied at 95 Hz frequency (~ 0.5mm amplitude). The water droplet on nano-PPX surface was transported through the track whereas the droplet on the planar-PPX surface did not move from its initial place.

This indicates that the directional transport only happens on PPX when vibrational frequency is applied to the anisotropic nano-PPX. Mechanical vibrations with low amplitudes do not propel droplets on surfaces if there is no anisotropic texture.

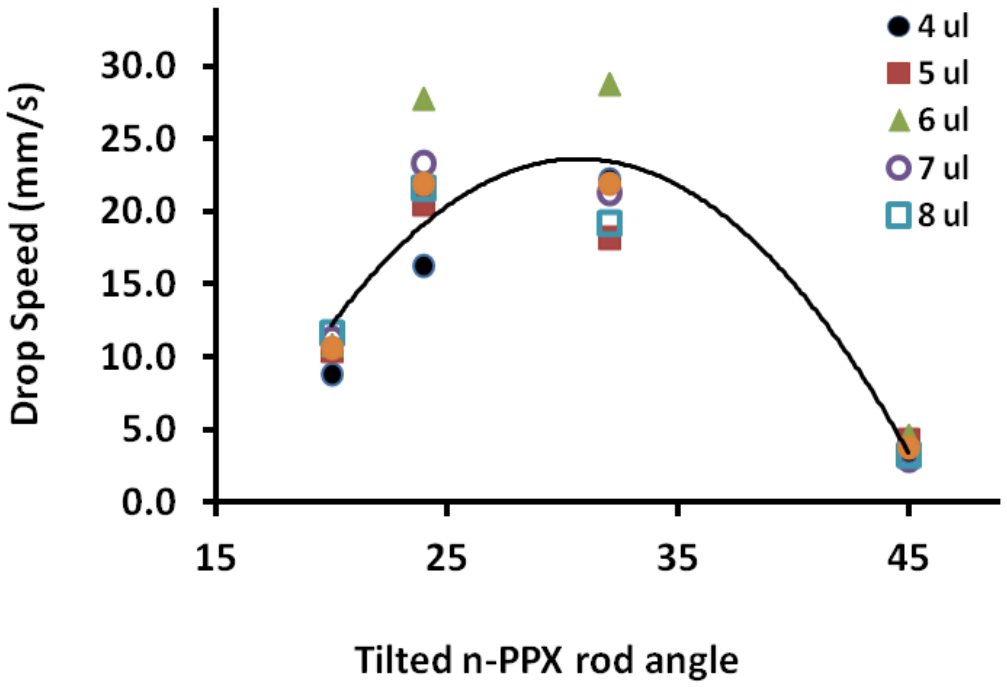


**Figure 5-13**. Droplet speed dependence on tilted nano-PPX angle for various droplet sizes.

Figure 5-13 shows the drop speeds of various droplets volumes (4 – 8 μL) that were measured on the tilted nano-PPX surface for all the angles ($\Theta$ = 45$^o$, 32$^o$, 24$^o$, 20$^o$). It was observed that tilted surfaces propel droplets at higher speeds than the nano-PPX (45$^o$) due to the new wetting properties. Among the tilted surfaces, 24 and 32 degree angles exhibited higher velocities. The curvature in the plot indicates that if the tilting angle goes higher than 45$^o$ or lower than 20$^o$, the droplet speed will reach close to zero. Correspondingly, it was tested that a flat (planar-PPX, 0$^o$) parylene surface will not transport droplets. Moreover, the theoretical model in Chapter 4 stated that nano-PPX with 90$^o$ will exhibit isotropic behavior which will not provide unidirectional droplet motion.

## 5.7 Simple Devices by Fabricating Multiple Tracks on Nano-PPX

Fabricating tracks on the nano-PPX surface can guide water droplets on desired pathways. We used a pen with a soft silicone tip to draw tracks along the nanorod directions to obtain tilted nano-PPX paths. When water droplets are placed on the tracks, they are in contact with both nano-PPX and deformed nano-PPX. It is important to investigate how the track width of the deformed nano-PPX affects the droplet speed on the surface.

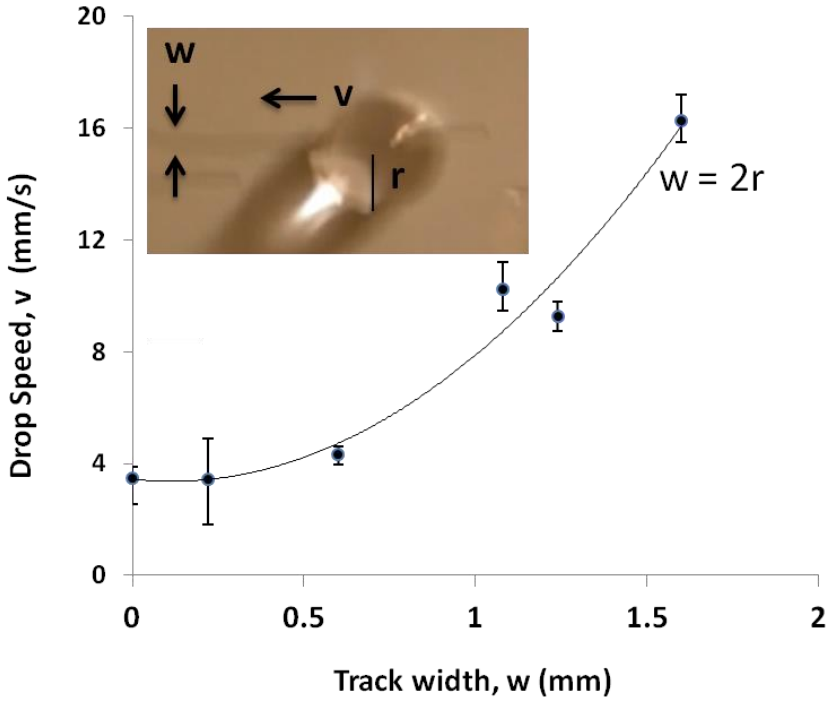


**Figure 5-14**. Droplet speed dependence on track width of deformed nano-PPX (w: track width, v: drop speed, 2r: drop diameter that is in contact with the surface).

Figure 5-14 represents the relation between the droplet speed and the track width of deformed nano-PPX. When the track width is increased, the water droplets travel faster on the surface, reaching 16mm/s. This is four times faster than the droplets moving on nano-PPX surface.

We designed simple devices to unidirectionally transport water droplets on the nano-PPX surface with fabricated tracks. Figure 5-15 demonstrates a volume-dependent sorting device. A water droplet (0.8 μl) was placed on Track 1 (Figure 5-15.a). This droplet was transported along Track 1 without switching to other tracks on the surface. Similarly, the next droplet (5 μl) is added on Track 1 (Figure 5-15.b). The contact diameter of the droplet is fairly larger than the sum of track widths. Therefore, it switches to Tracks 2 and 3, which provides the volume dependent sorting activity.

The preference of droplets to move on a path may be dependent on drop diameter at contact (2r), track width (w), and the distance between fabricated tracks (a). Simply, if the track width is larger than the drop diameter, the water droplet does not switch to the other track. If the drop diameter is larger than the sum of the distance between the tracks and track width, then the water droplet switches to the other channel.

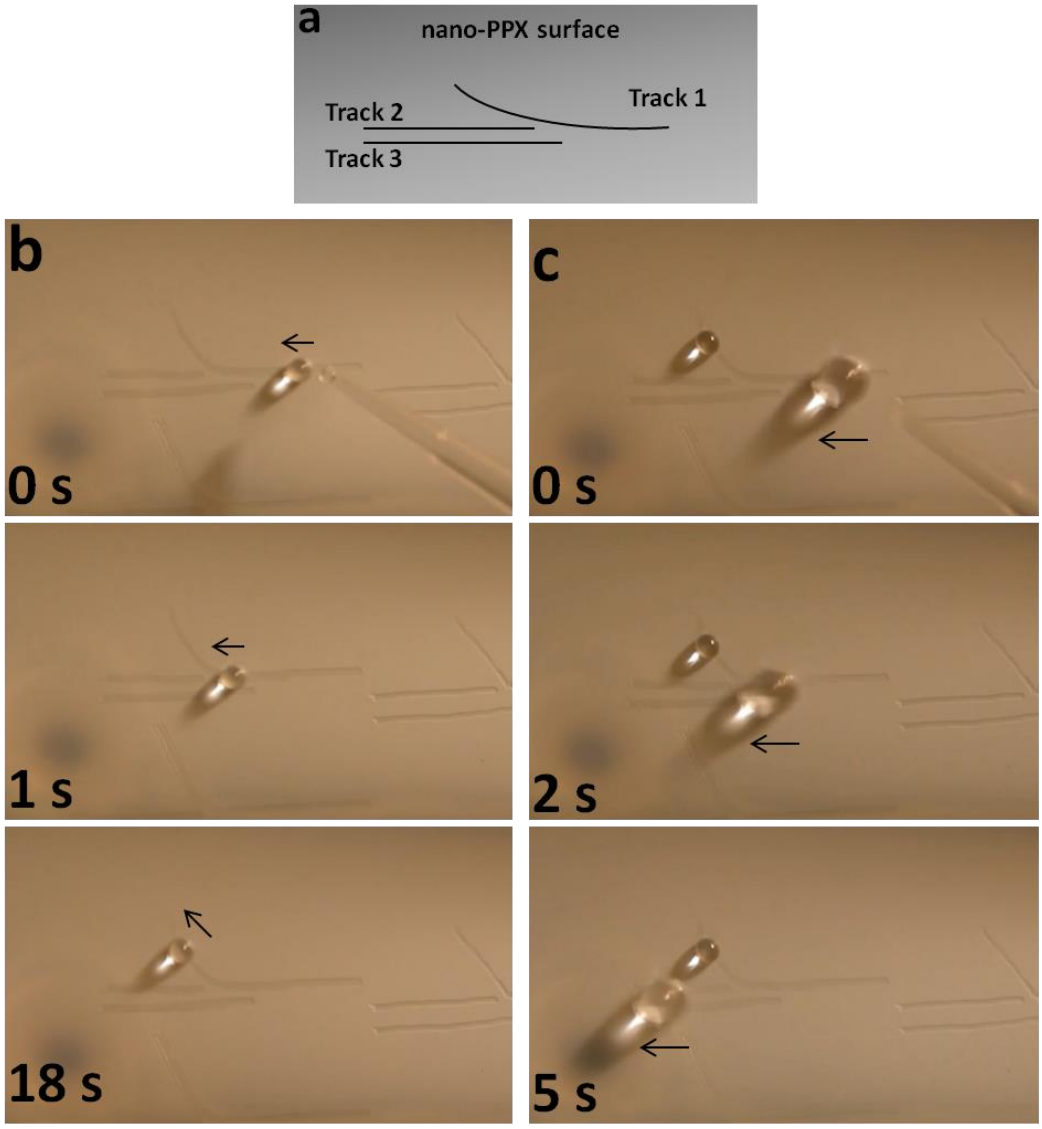


**Figure 5-15**. a. Schematic of volume dependent sorting device with three fabricated tracks, b. 0.8 µL drop passes the junction towards the curved track (Frequency: 212 Hz), c. 5 µL drop continues straight to the double channel ahead (Frequency: 95 Hz).

Figure 5-16 demonstrates a volume-dependent mixing device. The droplets (2 µl) were placed on Tracks 1 and 3. They were transported on the tracks from the beginning to the end without any mixing (Figure 5-16.a). On the same surface, larger droplets (4 µl) were placed on Tracks 1 and 3. They started to move from the beginning of the tracks to the

junction where Track 2 starts. At the junction, the droplets mix and form a larger droplet (Figure 5-16.b). The large drop (8 µl) was transported to the end of the device. Thus, volume dependent mixing occurs on the device.

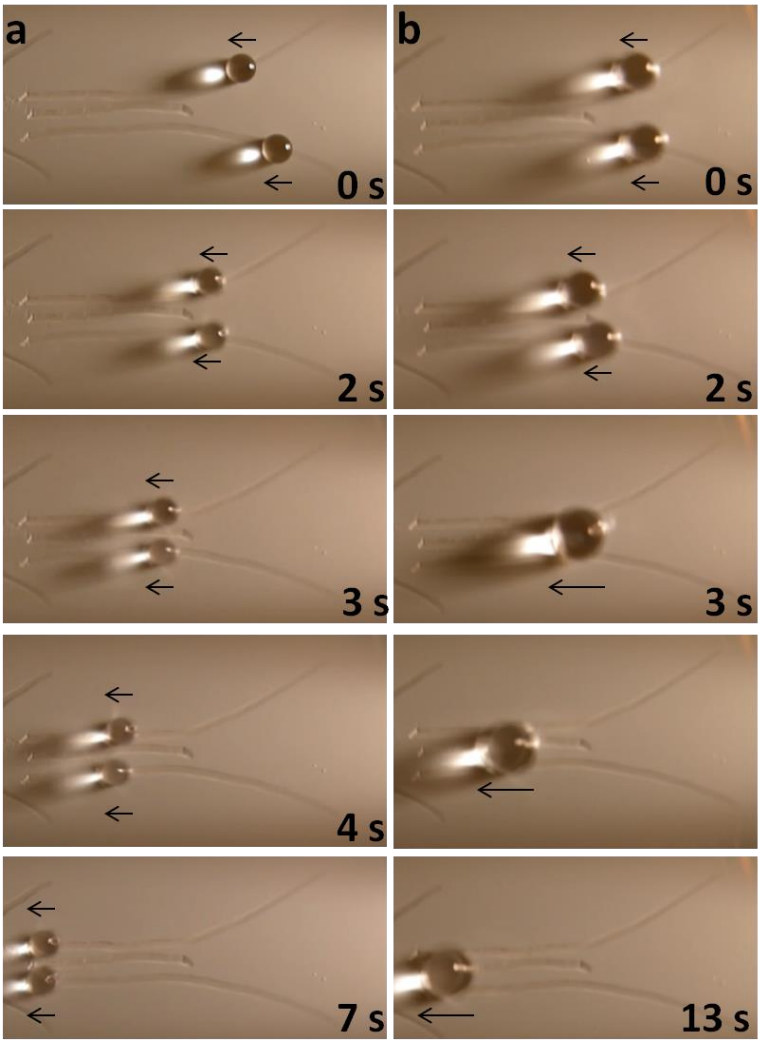


**Figure 5-16**. Volume dependent mixing device, a. 2 µL droplets move on tracks and continue without mixing (Frequency: 133 Hz), b. 4 µL drop move forward, mix at the junction (8 µL) and continue moving through the end of the channels (Frequency: 95 Hz, then 75 Hz).

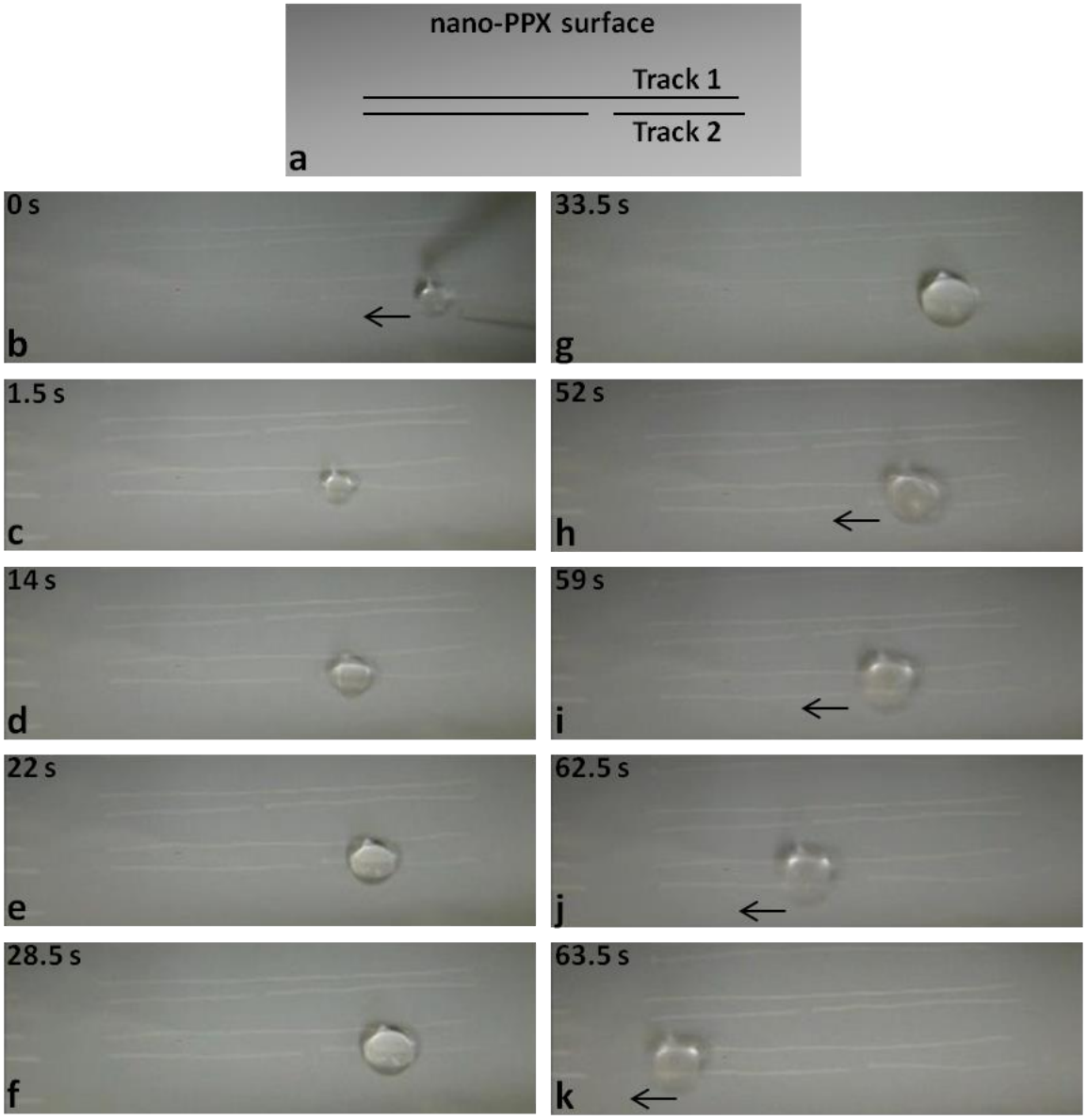


**Figure 5-17**. Schematic of gate device, b-c. 2µl drop is moving forward, d. 4 µl drop (no propulsion), e. 6 µl drop (no propulsion), f. 8 µl drop (no propulsion), g. 10 µl drop, h-k. 10 µl drop moves forward (65 Hz frequency) by passing the gate in the tracks.

Figure 5-17 displays a gate device where only certain volume of droplets can complete the tracks. The gate device consists of two parallel tracks. One of the tracks is discontinued (no track is fabricated). This provides the volume dependent transport on the nano-PPX surface. A 2 µl drop travels to the gate, which cannot move further due to the discontinued track. More drop volumes are added to the initial drop, by increasing 2 µl at a time. When the drop volume reaches 10 µl, it is in contact with both tracks. Therefore, it passes through the gate and continues the directional transport on the nanotextured surface.

These presented devices may be fabricated in many ways. Since water droplets are able to transport microgels[4] on nano-PPX surfaces, these devices may be used for merging/assembling microgels. Transporting cargo to specific targets can be achieved via droplet transport on the nanotextured surfaces.

## 5.8 Summary

Droplet transport on flat nano-PPX surfaces exhibit several complications. Water droplets may travel straight pathways toward the side of nano-PPX surface. Due to edge effects during the growth of nanorods, the droplets tend to slide towards the side of the substrate. This may prevent droplets from going to the desired targets. Tracks on nano-PPX surfaces are fabricated to overcome this challenge. The process of fabricating tracks is basically applying mechanical pressure on the nanorods and tilting them into lower angles. The tilt angle is controlled by the applied pressure on the surface.

The nano-PPX with tilted tracks exhibits a similar anisotropic wetting behavior to the regular nano-PPX rods. On the other hand, water droplets move with fairly higher speeds and at larger frequency intervals. Being able to control the tilting angle and freely drawing tracks on the surface inspired the idea of creating basic devices.

These basic devices can function in terms of various volume dependent devices (i.e. sorting and mixing). The sorter device is able to separate two different droplet volumes into separate tracks. The mixer device is able to merge certain droplet volumes into a single drop. The gate device only lets certain drop volumes to continue the transport action on the tracks.

## References

[1] Y. Du, M. Ghodousi, E. Lo, M.K. Vidula, O. Emiroglu, and A. Khademhosseini, Biotechnology and Bioengineering **105**, 655 (2010).

[2] Y. Du, E. Lo, M.K. Vidula, M. Khabiry, and A. Khademhosseini, Cellular and Molecular Bioengineering **1**, 157 (2008).

[3] B. Zamanian, M. Masaeli, J.W. Nichol, M. Khabiry, M.J. Hancock, H. Bae, and A. Khademhosseini, Small **6**, 937 (2010).

[4] K. Sekeroglu, U.A. Gurkan, U. Demirci, and M.C. Demirel, Applied Physics Letters **99**, 63703 (2011).

[5] N.A. Malvadkar, M.J. Hancock, K. Sekeroglu, W.J. Dressick, and M.C. Demirel, Nature Materials **9**, 1023 (2010).

[6] A. Shastry, M.J. Case, and K.F. Böhringer, Langmuir **22**, 6161 (2006).

[7] A. Ahmadi, K.D. Devlin, H. Najjaran, J.F. Holzman, and M. Hoorfar, Lab on a Chip **10**, 1429 (2010).

[8] M.G. Pollack, A.D. Shenderov, and R.B. Fair, Lab Chip **2**, 96 (2002).

[9] U. Demirci and G. Montesano, Lab Chip **7**, 1139 (2007).

[10] E. Berthier and D.J. Beebe, Lab on a Chip **7**, 1475 (2007).

[11] A. Perl, A. Gomez-Casado, D. Thompson, H.H. Dam, P. Jonkheijm, D.N. Reinhoudt, and J. Huskens, Nature Chemisty **3**, 317 (2011).

[12] G. Lagubeau, M. Le Merrer, C. Clanet, and D. Quéré, Nature Physics **7**, 395 (2011).

[13] M.K. Chaudhury and G.M. Whitesides, Science **256**, 1539 (1992).

[14] O. Sandre, L. Gorre-Talini, A. Ajdari, J. Prost, and P. Silberzan, Physical Review E **60**, 2964 (1999).

[15] H. Linke, B.J. Alemán, L.D. Melling, M.J. Taormina, M.J. Francis, C.C. Dow-Hygelund, V. Narayanan, R.P. Taylor, and A. Stout, Physical Review Letters **96**, 154502 (2006).

[16] J. Zhang, Z. Cheng, Y. Zheng, and L. Jiang, Applied Physics Letters **94**, 144104 (2009).

[17] S. Daniel, M.K. Chaudhury, and P.G. de Gennes, Langmuir **21**, 4240 (2005).

[18] S. Mettu and M.K. Chaudhury, Langmuir **27**, 10327 (2011).

[19] T.A. Duncombe, E.Y. Erdem, A. Shastry, R. Baskaran, and K.F. Boehringer, Advanced Materials **24**, 1545 (2012).

[20] K.-H. Chu, R. Xiao, and E.N. Wang, Nature Materials **9**, 413 (2010).

[21] E. So, M.C. Demirel, and K.J. Wahl, Journal of Physics D: Applied Physics **43**, 45403 (2010).

[22] J.W. Strutt and Lord Rayleigh, Trudy Moskovskogo Matematicheskogo Obshchestva 4 (1879).

# Chapter6. Conclusions and Future work

## 6.1. Conclusions

In this thesis, a bio-inspired nanotextured polymer (nano-PPX) was employed to create an asymmetric surface[1,2]. It was proved that the asymmetry in nanoscale causes droplet transport. The hysteresis of the water droplets provides the unidirectional motion. The wetting and transport properties of the asymmetric nano-PPX nanorods were observed throughout the study. These properties were employed for applications such as transporting water encapsulated microgels, water droplet sorting, and mixing devices. These applications are possible pathways to fulfill the necessity of emergent technologies in bioengineering and medicine fields for directed assembly lines and 3D architecture.

Our research group has developed the oblique angle polymerization (OAP) technique to convert the generic bulk parylene coating into functional coatings with nanostructures such as helical, convex, and columnar (nano-PPX) shapes. Among these nanostructures, the engineered nano-PPX has exhibited great functions that already exist in nature. Functions such as butterfly wings shedding droplets[3,4], water strider limbs staying on water[5,6], beetles applying directional friction[7], and plants with anisotropic pin-release mechanisms[6,8] have been mimicked using the nano-PPX surface.

The bio-inspired research of our group has brought the OAP technique and the nano-PPX surface to fabricating digital fluidics devices. The nano-PPX coated surface has several advantages over other textured surfaces that exist in literature. Nano-PPX surface is manufactured using the OAP method that is a template-free and lithography-free

technique. The nano-PPX production process does not require any clean room facilities and the necessary vacuum conditions are in the mid range. Therefore, nano-PPX surface is an inexpensive, easy-to-produce, and a multi-functional surface.

The contributions of this thesis to science are proving that asymmetry in nanoscale causes droplet transport, managing the transport of micro liter water droplets on a nanotextured surface unidirectionally, merging microgels into a single media via directional droplet transport on nano-PPX, deforming the nano-PPX surface to create tracks that provide droplet delivery to desired targets, and opening a new pathway to engineer assembly platforms for soft cargo materials (i.e. microgel) into close proximity for assembly processes.

## 6.2. Future work

A future aspect on nano-PPX research is transporting other liquids apart from water droplets. Since other liquids will display different contact angles on the nanotextured rods, the surface properties of nano-PPX should be adjusted. Lowering the surface energy may provide a less adhesive non-wetting surface for more viscous materials such as glycerol and oil. With liquids facing high surface energies such as hexane and ethanol, the nano-PPX surface may require a layer of fluorosilane to decrease the surface energy. Besides surface energy modifications, adjusting the nanorod arrangement in terms of their lateral and longitudinal spacing will provide higher anisotropic wetting conditions.

Neuron cells have been cultured on the directional nano-PPX surface to investigate biased axonal growth[9]. The anisotropic texture provides the cells to grow unidirectionally affected by biomechanical cues. As a future work, the neuron cells may be grown on nano-PPX surface with different angles. The growth speed and dominance of chemical or mechanical cues can be investigated. Controlling the cell growth and direction may be promising for neuro-regeneration applications[9].

Another aspect for nano-PPX is providing a new platform for microgel assembly purposes. Deforming the nano-PPX rods and changing their angle to create tracks has been a promising solution for merging microgels. Microgels encapsulated cells may be assembled into close proximity by making accurate assembly lines on the nano-PPX surfaces. As devices types were proposed in this thesis, a cell assembly device would be a great start for bioengineering and medicine fields.

## References

[1] N.A. Malvadkar, M.J. Hancock, K. Sekeroglu, W.J. Dressick, and M.C. Demirel, Nature Materials **9**, 1023 (2010).

[2] K. Sekeroglu, U.A. Gurkan, U. Demirci, and M.C. Demirel, Applied Physics Letters **99**, 63703 (2011).

[3] Y.M. Zheng, X.F. Gao, and L. Jiang, Soft Matter **3**, 178 (2007).

[4] H. Kusumaatmaja and J.M. Yeomans, Soft Matter **5**, 2704 (2009).

[5] X. Gao and L. Jiang, Nature **432**, 36 (2004).

[6] H. Wu, R. Zhang, Y. Sun, D.D. Lin, Z.Q. Sun, W. Pan, and P. Downs, Soft Matter **4**, 2429 (2008).

[7] T. Eisner and D.J. Aneshansley, Proceedings of the National Academy of Sciences USA **97**, 6568 (2000).

[8] P. Guo, Y. Zheng, C. Liu, J. Ju, and L. Jiang, Soft Matter **8**, 1770 (2012).

[9] R. Beighley, E. Spedden, K. Sekeroglu, T. Atherton, M.C. Demirel, and C. Staii, Applied Physics Letters **101**, (2012).

# Appendix A. Representative Publications

[1] K. Sekeroglu, U.A. Gurkan, U. Demirci, and M.C. Demirel, Applied Physics Letters **99**, 63703 (2011).

[2] M.J. Hancock, K. Sekeroglu, and M.C. Demirel, Advanced Materials **22**, 2223 (2012).

[3] N.A. Malvadkar, M.J. Hancock, K. Sekeroglu, W.J. Dressick, and M.C. Demirel, Nature Materials **9**, 1023 (2010).

[4] C. Staii, E. Spedden, T. Atherton, K. Sekeroglu, and M. Demirel, Bulletin of the American Physical Society **58**, (2013).

[5] K.Sekeroglu and M. Demirel, "A Digital Fluidic Device with Texttured Rachets"Advanced Functional Materials, 2013 (Submitted).

# Appendix B. Nontechnical Abstract

Bio-inspiration at the nanoscale from animal and plant kingdoms has been an important research topic in recent years. Butterfly wings, water strider limbs, and rye grass leaves have essential wetting, adhesion, and transport functions. Observing the nature and biomimicking its functions by synthetically producing them in laboratory scale introduces new pathways for solving problems (i.e. assembly) in bioengineering field. A vapor phase method has been used to fabricate a textured polymer. The polymer surface has directional wetting properties similar to butterfly wings, which guides rain droplets away from its body. These properties are employed to guide water droplets unidirectionally and transport cargo. Assembling objects at the microscopic length scale has been an essential challenge due to its difficulty to bring small cargo into close proximity. This problem can be solved by making assembly lines where small objects are carried to certain targets by using water drops. Drawing simple tracks on a textured polymer surface is a simple method to produce fluidics devices for guiding droplets that can carry cargo. This new method is a promising step to overcome the assembly challenge in multiple fields in engineering and medicine.

# VITA

## Koray Sekeroglu

Koray Sekeroglu was born on July 5, 1981 in Izmir, Turkey. He graduated from Izmir Institute of Technology in Turkey in 2006. He completed a TUBITAK research project in Turkey in 2008. He started his PhD studies in the Department of Engineering Science and Mechanics at The Pennsylvania State University in 2009 joining Dr. Melik Demirel's research group as a graduate student. Koray has worked in multiple projects and published several journal papers. His research interests are directional polymers, bio-inspired micro-nano textured thin films and low-cost polymer-based devices. He also worked as a teaching assistant for three semesters in the Department of Engineering Science and Mechanics while pursing his PhD studies.